Investigation of femtosecond fiber laser systems with respect to low repetition rates, pulse energy scaling, and all-fiber-integrability

Von der Fakultät für Mathematik und Physik

der Gottfried Wilhelm Leibniz Universität Hannover

zur Erlangung des Grades

Doktor der Naturwissenschaften

Dr. rer. nat.

genehmigte Dissertation

von

Dipl.-Phys. Dirk Mortag

geboren am

17. August 1980 in Celle

2012

Referent: Prof. Dr. Uwe Morgner
Korreferent: Prof. Dr. Detlev Ristau
Tag der Promotion: 26. Juni 2012

Kurzzusammenfassung

Auf ytterbiumdotierten Fasern basierende Ultrakurzpuls-Lasersysteme wurden in den letzten Jahren intensiv untersucht. Dies liegt unter anderem an ihren attraktiven Eigenschaften wie dem justagefreien Betrieb, der guten Wärmeableitung sowie der Möglichkeit, günstige Diodenlaser mit großer Ausgangsleistung zum optischen Pumpen zu verwenden. Sie besitzen eine große Verstärkungsbandbreite, was sie ideal für die Erzeugung von Femtosekundenpulsen im nahinfraroten Wellenlängenbereich bei 1 µm macht. Die von Faserlasern erreichten Pulsparameter konnten bis heute beachtlich gesteigert werden, so dass sie nun mit etablierten Festkörperlasern auf Kristallbasis, speziell dem sehr gut funktionierenden, aber komplexen und voluminösen Titan-Saphir-Laser, konkurrieren können. Jedoch ist weitere Entwicklungsarbeit nötig, um die Leistung von Faserlasern weiter zu steigern sowie die Vorteile des Fasermediums vollständig auszunutzen und dadurch neue Anwendungsfelder auch außerhalb des Labors zu eröffnen. Gegenstand dieser Arbeit sind deshalb Untersuchungen hinsichtlich der vollständigen Faserintegration dieser Lasersysteme sowie der Pulsenergieskalierung. Des Weiteren wurden Oszillatoren mit geringen Pulsrepetitionsraten untersucht, um teure und komplexe optische Modulatoren für die Senkung der Repetitionsrate in nachfolgenden Verstärkern potentiell unnötig zu machen. In dieser Arbeit wurden mehrere Oszillatoren sowie Verstärker aufgebaut und untersucht. Der erste Aufbau besteht aus einem dispersionsgesteuerten Solitonlaser, der hinsichtlich einer geringen Pulswiederholrate untersucht wurde. Bei einer Wiederholfrequenz von 1,8 MHz konnten 93 fs lange Pulse durch den Einsatz eines Grismkompressors im Resonator zur Kompensation der Dispersion dritter Ordnung erreicht werden. Da eine weitere Pulsenergieskalierung mit diesem Konzept nicht möglich war, wurde das Pulsregime der dissipativen Solitonen hinsichtlich großer Resonatorlängen und maximaler Ausgangspulsenergie untersucht. Bei einer Wiederholrate von 2,1 MHz konnten Pulsenergien von 50 nJ und, separat, Pulsdauern von 492 fs erzeugt werden. Um kürzere Pulse zu generieren, wurde die Gesamtdispersion des Resonators verringert, was ebenfalls die Pulsenergie reduzierte. Es stellte sich heraus, dass das Erzeugen minimaler Pulsdauern eine minimale Resonatordispersion erfordert. In diesem Fall waren die Pulsenergien limitiert durch die Pumpleistung der vorhandenen einmodigen Laserdioden. Deshalb wurde das Doppelmantelpumpkonzept auf einen dissipativen Solitonlaser angewendet. Dieser emittierte eine mittlere Leistung von 1,2 W sowie 139 fs lange Pulse mit Energien von 25 nJ. Die gewonnenen Erkenntnisse wurden dann benutzt, um einen vollständig faserintegrierten Laser hinsichtlich minimaler Pulsdauer zu entwickeln. Die damit erzeugten 76 fs langen Pulse wurden anschließend durch Realisierung von zwei unterschiedlichen Konzepten verstärkt. Beide Konzepte waren auf die vollständige Faserintegration, mit Ausnahme des Kompressors, ausgelegt. Der erste Aufbau nutzte eine speziell entwickelte Streckerfaser in Kombination mit einem Gitterkompressor, wodurch Pulsenergien von 2,2 µJ und Pulsdauern von 189 fs erzeugt werden konnten. Der zweite Aufbau verwendete eine Standardfaser zur Pulsstreckung zusammen mit einem Grismkompressor. Damit konnten 152 fs lange Pulse mit Energien von 0,6 µJ erzeugt werden.

Schlagwörter: Faserlaser, Femtosekundenpuls, Faserintegration

Abstract

Ultrashort pulse ytterbium-doped fiber laser systems have been intensively studied in the last decade due to their attractive properties like alignment-free operation, good heat dissipation, and the availability of low-cost high-power diode lasers for optical pumping. They offer a large amplification bandwidth, which is ideal for the generation of femtosecond pulses in the near infrared wavelength region at 1 µm. Their output pulse parameters such as pulse duration and energy have been considerably increased in the last years. Thus, ytterbium-doped fiber lasers can now compete with well-established solid-state systems in terms of the achievable pulse parameters and especially with the well performing but complex and bulky Ti:sapphire laser. However, more work is needed to further improve the performance of fiber lasers and to fully profit from the advantages of the fiber medium like alignment-free operation and robustness against environmental disturbances to open up new application areas also outside the laboratory. The subject of this thesis was thus the study of femtosecond fiber laser systems with respect to all-fiber-integrability and pulse energy scaling. Also, fiber oscillators with low pulse repetition frequencies were analyzed to potentially render costly and complex pulse picking units unnecessary in fiber amplifier systems for further pulse energy scaling. Several femtosecond oscillators and amplifiers were studied in this thesis. The first setup describes a stretched-pulse fiber laser, which is investigated with respect to low pulse repetition frequencies. At 1.8 MHz repetition rate, 93 fs long pulses could be generated by incorporating a specially designed grism compressor for third-order dispersion compensation. As pulse energy scaling was not possible within the stretched-pulse regime, the dissipative-soliton mode-locking scheme was investigated with respect to long resonators and maximum achievable pulse energies. At 2.1 MHz repetition frequency, pulse energies up to 50 nJ could be generated and, separately, pulses as short as 492 fs. To generate shorter pulses, the total resonator dispersion was reduced, which also reduced the output pulse energies. It turned out that the minimum achievable pulse duration required a minimum intracavity dispersion but the pulse energy was then limited by the available pump power of single-mode laser diodes. To overcome this, the double-cladding pumping scheme was applied to a dissipative-soliton oscillator, which emitted 1.2 W average power and 139 fs long pulses with energies of 25 nJ. The gained knowledge of dissipative-soliton fiber lasers was then used to build a completely fiber-integrated laser with respect to a minimum output pulse duration. For that, the intracavity dispersion was minimized to achieve compressed pulse durations of 76 fs. The pulses were subsequently amplified using two different amplifier concepts, which were both designed to be all-fiber-integrated except for the pulse compressor. The first setup featured third-order dispersion compensation by incorporating a specially designed fiber stretcher. After compression with a grating arrangement, 189 fs long pulses with energies of 2.2 µJ were achieved. The second amplifier setup used a standard fiber stretcher in combination with a grism compressor for third-order dispersion compensation to generate pulse energies of 0.6 µJ and pulse durations of 152 fs.

Key words: fiber laser, femtosecond pulse, fiber-integration

Selbst wenn man alle diese Schritte tadellos ausgeführt hat, kann es immer noch dazu kommen, dass die Ursprungsidee unzureichend war oder dass ein wichtiges Teil, das für den Aufbau vorgesehen war, nicht vorhanden ist. Ist dies der Fall, bleibt einem meist nur der völlige Neustart. Um dies zu verhindern, zeigen die Mitarbeiter großes Geschick im Bereich der Improvisation, so wird beispielsweise eine nicht vorhandene Optik im Notfall auch mal durch eine Scherbe ersetzt.

aus dem Bericht eines Schülerpraktikanten

Even if every step was carried out correctly, it can still turn out that the original idea was insufficient or one important part, that was designated for the experiment, is not available for any reason. If this is the case, one is often left to a complete re-start. To avoid this, the employees show great improvisation skills, so for instance, in an emergency, a not available optics is sometimes replaced even by a glass cullet.

from the report of a high school student intern

Contents

1 Introduction **1**

2 Mode-locked fiber lasers **5**
- 2.1 Glass fibers 5
- 2.2 Nonlinear polarization evolution 9
- 2.3 Stretched-pulse regime 10
- 2.4 Dissipative solitons 12

3 Ultrashort pulse fiber amplifiers **13**
- 3.1 Fiber chirped-pulse amplification 13
- 3.2 Compensation of third-order dispersion 15

4 Low-repetition rate stretched-pulse fiber laser **23**
- 4.1 Experimental setup 24
- 4.2 Characteristics of the grism compressor 25
- 4.3 Results at 1.8 MHz repetition frequency 26
- 4.4 Conclusion 29

5 Low-repetition rate dissipative-soliton fiber laser **31**
- 5.1 Birefringent filter characteristics 31
- 5.2 Experimental setup 33
- 5.3 Results at 2.1 MHz repetition frequency 34
- 5.4 Results at 5.4 MHz repetition frequency 38
- 5.5 Results at 29 MHz repetition frequency 41
- 5.6 Conclusion 42

6 High-average power dissipative-soliton laser **43**
- 6.1 Experimental setup 43
- 6.2 Results at 48 MHz repetition frequency 44
- 6.3 Conclusion 47

7 All-fiber dissipative-soliton laser **49**
- 7.1 Experimental setup 50
- 7.2 Results at 71 MHz repetition frequency 51
- 7.3 Influence of pulse energy variation 55
- 7.4 Conclusion 57

8 All-fiber amplifier with fiber-based third-order dispersion compensation **59**
- 8.1 Experimental setup 60
- 8.2 Stretcher and compressor dispersion 62
- 8.3 Temporal pulse stretching 64

8.4 Results at 4.5 MHz repetition frequency 66
8.5 Limitations 68
8.6 Conclusion 70

9 All-fiber amplifier with grism-based third-order dispersion compensation **73**
9.1 Experimental setup 73
9.2 Characteristics of the grism compressor 74
9.3 Results at 5.9 MHz repetition frequency 76
9.4 Conclusion 79

10 Conclusion **81**

Appendices **85**
A References used for pulse parameter comparison in Figure 1.1 85
B Easy-to-implement grism compressor 90
C Intracompressor parallel plate for dispersion tuning 91

List of acronyms and abbreviations **95**

List of figures **97**

List of tables **101**

References **103**

List of publications **115**

Curriculum vitae **117**

Acknowledgment **119**

1 Introduction

Ultrashort pulse fiber laser systems have been in the focus of intense research in the last decades. Their unique properties like alignment-free operation, good heat dissipation due to a large surface to volume ratio, and the availability of low-cost high-power diode lasers for optical pumping offer great potential for applications in science as well as in industry. Possible application areas of femtosecond high-energy pulses range from wavelength conversion, the generation of high-harmonics [Cor93], ultra-precise material processing [Chi96, Li11], general nonlinear optics [Boy03], to ophthalmology and especially the treatment of refractive errors of the eye [Sug02, Pla10], the generation of terahertz radiation [Cha06], frequency metrology [Ude99], and femtosecond laser spectroscopy [Han05].

For pulse durations above 30 fs, state-of-the-art fiber lasers can nowadays compete with well-established solid-state crystal-based systems, e.g. Ti:sapphire lasers, concerning pulse energy, pulse duration, and average power. While Ti:sapphire oscillators typically exhibit a complex cooling scheme and have to be optically pumped by gas lasers or frequency-doubled solid-state lasers, fiber laser systems can be very compact, robust, as well as air-cooled. Another advantage is the possibility of optical pumping with a small quantum defect by low-cost semiconductor laser diodes. Due to the confinement of the light in the fiber core, the usually good beam quality is determined by the fiber properties, which is insensitive to environmental disturbances. Additionally, ytterbium-doped fibers exhibit a large spectral gain bandwidth, which is due to the amorphous structure of the fused silica glass. These properties make them ideal for the generation and amplification of broadband femtosecond pulses.

Because the fiber laser systems demonstrating record pulse energies and shortest pulse durations incorporate free-space optics, they do not fully profit from the advantages of the fiber medium as a waveguide device. Although it is possible to generate high average powers as well as high pulse energies with large-diameter rod-type fibers, these lasers are far away from a compact, environmentally stable, and all-fiber-integrated system. However, the robustness of fiber laser systems against environmental disturbances would be largely increased by using exclusively fiber-based components. One aim of this thesis was thus to study femtosecond fiber laser systems regarding all-fiber-integrability.

As for many applications, the pulse peak intensities generated by laser oscillators are not large enough, the pulse energies are often increased in a subsequent amplifier. Because of the limited average power capabilities of the amplifier, the pulse repetition frequency is typically reduced by an optical pulse picker to achieve energies in the microjoule range. In this respect, using a seed oscillator with a low repetition frequency would render costly and complex pulse picking units unnecessary and would simplify the overall setup. The development of oscillators with low repetition rates was thus also an aim of this thesis together with the maximization of the output pulse energies.

To avoid higher-order mode issues of large-mode area fibers and challenges of splicing photonic crystal fibers, all fibers used in this work had a solid fused silica-based core with core diameters ≤ 10 µm. The laser systems presented in this thesis are based on ytterbium-doped fibers and therefore emit radiation at around 1 µm wavelength.

To compare the results achieved in this work with recently published research results, an overview of the pulse parameters of state-of-the-art ytterbium fiber laser systems is shown in Figure 1.1. The parameters achieved in this thesis are marked in red and demonstrate inter alia record pulse parameters for all-fiber-integrated fiber laser systems. A comprehensive overview of the actual status of high-power fiber lasers is also given in Reference [Ric10].

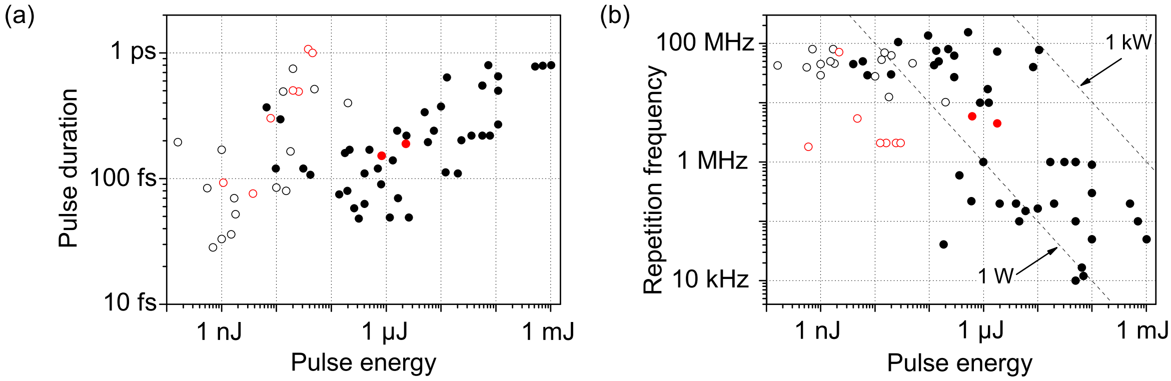

Figure 1.1: Pulse parameters of state-of-the-art ytterbium-doped fiber oscillators (open circles) and amplifiers (full circles). The parameters achieved in this thesis are depicted in red. The references are listed in Appendix A.

Organization of the thesis

This thesis is organized as follows. Chapter 2 and 3 give a brief introduction to mode-locked fiber lasers and ultrashort pulse fiber amplifiers. In Chapter 4, a stretched-pulse fiber laser is investigated with respect to low pulse repetition frequencies. At 1.8 MHz repetition rate, 93 fs long pulses could be generated by incorporating a specially designed grism compressor for third-order dispersion compensation into the cavity. As pulse energy scaling was not possible within the stretched-pulse regime, the dissipative-soliton mode-locking scheme was investigated with respect to long resonators and maximum achievable pulse energies in Chapter 5. It revealed that for a large total resonator dispersion, corresponding to 2.1 MHz repetition frequency, pulse energies up to 50 nJ could be generated and, separately, pulses as short as 492 fs. To generate shorter pulses, the total resonator dispersion was reduced, which also reduced the output pulse energies. It turned out that the minimum achievable pulse duration required a minimum intracavity dispersion but the pulse energy was then limited by the available pump power of single-mode laser diodes. To overcome this, the double-cladding pumping scheme was applied to a dissipative-soliton oscillator in Chapter 6. 1.2 W average power and pulse energies of 25 nJ at the repetition frequency of 48 MHz could be demonstrated, while the pulses were compressed to durations of 139 fs.

In the following Chapter 7, the gained knowledge of dissipative-soliton fiber lasers was used to build a completely fiber-integrated laser with respect to a minimum output pulse duration. For that, the intracavity dispersion was minimized to achieve compressed pulse durations of 76 fs. As the used fiber components did not allow for high-power double-cladding pumping, the pulse energy was limited to about 3 nJ. To further show the potential of these laser systems, the pulses were subsequently amplified using two different amplifier concepts, which were both designed to be all-fiber-integrated except for the pulse compressor. First, Chapter 8 demonstrates a fiber chirped-pulse amplifier, which featured third-order dispersion compensation by incorporating a specially designed fiber stretcher. After compression with a grating arrangement, pulse energies of 2.2 µJ and pulse durations of 189 fs were achieved. In Chapter 9, a second amplifier setup is investigated, which used a standard fiber stretcher in combination with a grism compressor for third-order dispersion compensation. After dechirping, pulse energies of 0.6 µJ and durations of 152 fs were measured. Both oscillator-amplifier systems were characterized by incorporating exclusively fiber-integrated components except for the pulse compressors, which make them attractive for applications also outside the laboratory. The thesis closes with a conclusion in Chapter 10.

2 Mode-locked fiber lasers

In this chapter, the underlying basics of the studied passively mode-locked fiber oscillators are presented. The properties of optical fibers including the group delay dispersion and spectral characteristics of ytterbium-doped fibers are covered. Mode-locking via nonlinear polarization evolution in optical fibers is introduced as well as the studied dispersion-managed and dissipative-soliton pulse regimes.

2.1 Glass fibers

Fused silica optical fibers offer several advantages when applied to fiber lasers and amplifiers. They are robust against environmental disturbances and alignment-free due to the confinement of the electrical field inside the fiber core. Fibers allow for very compact laser and amplifier setups, are low-cost, and, furthermore, the attenuation of typically less than 1.5 dB/km at a wavelength around 1 µm can be neglected [Nuf06].

Step-index fibers were used in the laser systems studied in this thesis. Figure 2.1 shows the cross section and refractive index profile of a typical step-index fiber. The core with refractive index n_1 is surrounded by a cladding with a slightly lower index n_2, such that the condition for wave-guiding $n_1 > n_2$ is fulfilled [Agr07]. If the V parameter

$$V = \frac{2\pi a}{\lambda}\sqrt{n_1^2 - n_2^2}, \tag{2.1}$$

where a stands for the core diameter and λ for the wavelength [Mit05], is below the critical value of $V_c = 2.4045$, the fiber supports only one transversal mode for wavelengths larger than the cutoff wavelength λ_c. The latter is defined by

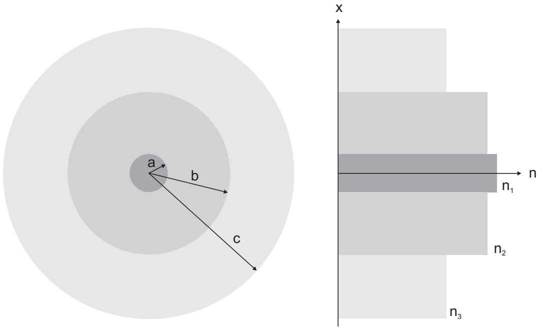

Figure 2.1: Cross section and corresponding refractive index profile of a step-index fiber.

$$\lambda_c = \frac{2\pi a}{V_c}\sqrt{n_1^2 - n_2^2}. \tag{2.2}$$

If the V parameter is only slightly above V_c, higher-order modes can efficiently be suppressed by coiling the fiber to introduce mode-dependent loss [Kop00]. In the studied laser systems, exclusively single-mode or effectively single-mode fibers with $V \leq 2.44$ and fiber core diameters of ≤ 10 µm were used to avoid modal dispersion and beam profile issues of large-mode area fibers.

Group delay dispersion

In ultrashort pulse fiber lasers, temporal pulse broadening due to group delay dispersion (GDD) plays a significant role. A mathematical description of the GDD uses a Taylor series expansion of the wavenumber $\beta(\omega)$ around the center frequency

$$\beta(\omega) = \sum_{k=0}^{\infty} \frac{1}{k!} \left.\frac{d^k\beta(\omega)}{d\omega^k}\right|_{\omega_0} (\omega - \omega_0)^k \tag{2.3}$$

$$= \beta_0 + \beta_1(\omega - \omega_0) + \frac{1}{2}\beta_2(\omega - \omega_0)^2 + \frac{1}{6}\beta_3(\omega - \omega_0)^3 + ... \tag{2.4}$$

with the dispersion coefficients of kth order $\beta_k = \left.\frac{d^k\beta(\omega)}{d\omega^k}\right|_{\omega_0}$ and $k \in \mathbb{N}$ [Agr07]. While β_1 represents the inverse of the group velocity, the terms β_k with $k \geq 2$ contribute to temporal pulse broadening with typically decreasing impact with increasing k. For pulse durations larger than 200 fs, it is usually sufficient to compensate for the second-order dispersion β_2. However, when considering pulses durations of 100 fs, it becomes necessary to additionally take the third-order dispersion (TOD) β_3 of the amplifier system into account, especially when using long fiber lengths. The topic of TOD compensation in fiber laser systems is covered in detail in Section 3.2.

In optical fibers, not only the material dispersion, expressed by $\beta(\omega) = n(\omega)\frac{\omega}{c}$ with the wavelength-dependent refractive index $n(\omega)$, contributes to the GDD. Because the radial coordinate of the electrical field w, where its power decreased to 1/e of its maximum value, is given by $w = a\left(0.65 + 1.619\,V^{-3/2} + 2.879\,V^{-6}\right)$, the field is not only confined to the core with index n_1 but also extends to the cladding region with lower refractive index n_2 if the V parameter of the fiber is below $V_c = 2.4045$ [Mar77]. In step-index fused silica fibers, this waveguide dispersion usually results in a larger β_2 value at 1 µm wavelength and, simultaneously, the zero-dispersion wavelength λ_0, where $\beta_2(\lambda_0) = 0$ holds, increases compared to the dispersion of bulk fused silica [Mit05].

As the dispersion is an important parameter when working with femtosecond fiber lasers, the GDD of the applied fibers was calculated. The calculation was based on the material dispersion of fused silica and the contribution of the waveguide dispersion as described by the Gloge model [Glo71]. The numerical aperture (NA) and the core radius were adjusted to match the cutoff wavelength $\lambda_c = 920$ nm of the mostly used Nufern 1060-XP single-mode fiber as given in Reference [Nuf06]. Having a numerical aperture of 0.14 and a mode field diameter (MFD) of 6.2 µm at 1060 nm wavelength, the approximated NA and MFD values were 0.139 and 6.06 µm, respectively. For the calculation of the index of refraction $n(\lambda)$ of fused silica, the Sellmeier equation

$$n^2(\lambda) = 1 + \frac{B_1\lambda^2}{\lambda^2 - C_1} + \frac{B_2\lambda^2}{\lambda^2 - C_2} + \frac{B_3\lambda^2}{\lambda^2 - C_3} \tag{2.5}$$

was used with coefficients C_i and B_i taken from Reference [Sch07]. The calculated dispersion coefficients at the wavelength of 1030 nm are listed in Table 2.1 together with the material dispersion of fused silica for comparison.

Parameter	Unit	Fused silica	Nufern 1060-XP (modeled)
β_2	ps^2/km	19.0	24.5
β_3	ps^3/km	0.041	0.024
β_3/β_2	fs	2.169	0.968

Table 2.1: Group delay dispersion of fused silica and Nufern 1060-XP fiber at 1030 nm wavelength.

It is notable that the second-order dispersion β_2 increased to 24.5 ps^2/km and the third-order dispersion β_3 decreased to 0.024 ps^3/km compared to bulk fused silica due to the waveguide contribution. Figure 2.2 (a) and (b) show the corresponding dispersion curves for a wide and a narrow wavelength range. These calculated dispersion values were used when considering the total dispersion of the studied laser systems in the following chapters.

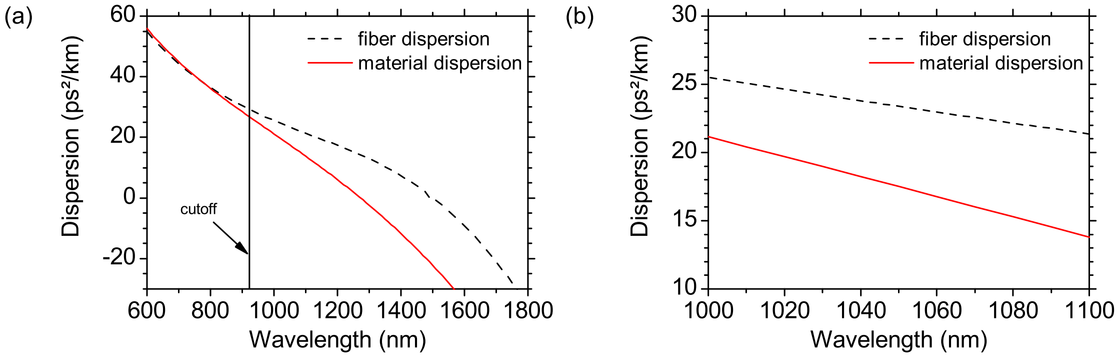

Figure 2.2: (a) Material and fiber dispersion. (b) Detail of graph (a).

Ytterbium-doped fibers

To achieve gain in optical fibers, the fiber core can be doped with rare earth ions like ytterbium, erbium, or thulium, which differ in their spectral characteristics. In this work, ytterbium-doped fibers were used, which allow for the generation and amplification of radiation at wavelengths around 1030 nm. They offer a large gain per unit length and a large spectral gain bandwidth, which can be used to generate and amplify ultrashort broadband pulses. The large bandwidth is caused by Stark splitting of the ytterbium energy levels due to different local electric fields in the amorphous glass matrix [Des94]. Figure 2.3 (a) shows typical emission and absorption cross sections of ytterbium-doped glass fibers. They exhibit an absolute maximum at the wavelength of 976 nm, while the emission cross section features a local maximum at a wavelength of 1030 nm. It has to be noted that the characteristic of the emission cross section is dependent on the energy level inversion. For small inversion levels, one can obtain a flatly distributed gain at wavelengths larger than 1030 nm, while for large inversion levels, the gain bandwidth at 1030 nm is reduced.

A diagram of the three-level structure of ytterbium-doped glass is shown in Figure 2.3 (b). Although several wavelengths can be used for optical pumping, the oscillators and amplifiers studied in this thesis were pumped by fiber-coupled laser diodes at the wavelength of 976 nm. This wavelength offers a small quantum defect and the maximum absorption per unit length when considering emission at 1030 nm.

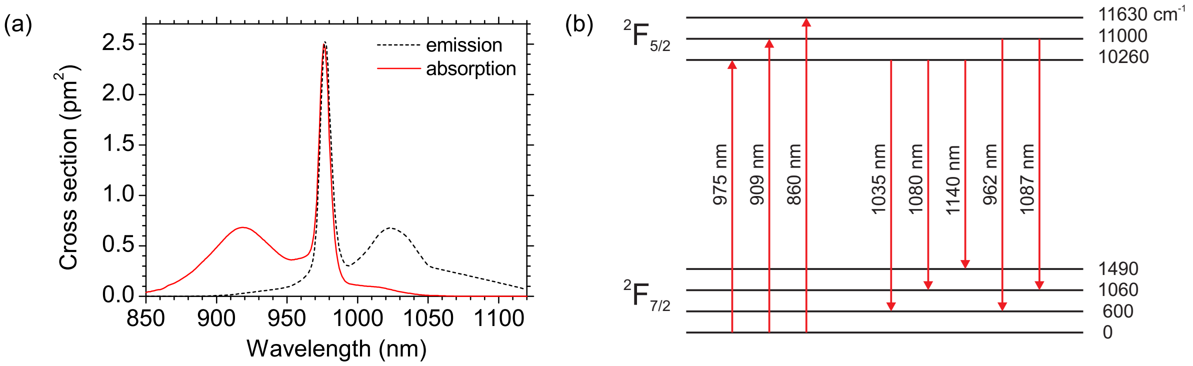

Figure 2.3: (a) Typical emission and absorption cross sections of ytterbium-doped glass and (b) energy level diagram of ytterbium [Pas95].

2.2 Nonlinear polarization evolution

In ultrashort pulse fiber lasers, the occurring high peak powers in presence of a nonlinear material response can induce an intensity-dependent phase shift of the pulse. It is called self-phase modulation (SPM) if the phase change is induced by the pulse itself, and cross-phase modulation in case another electrical field alters the phase. According to Reference [Boy03], the nonlinearity can be described by an intensity-dependent refractive index assuming an essentially instantaneous response of the medium $n(t) = n_0 + n_2^I I(t)$, where $I(t) = n_0 c\,(2\pi)^{-1}|\mathcal{A}(z,t)|$ and $\mathcal{A}(z,t)$ is the slowly varying pulse envelope and c the speed of light. The self-phase change of a pulse traveling through a medium with length L is then described by

$$\phi_{nl}(t) = -n_2^I I(t)\omega_0 L/c \tag{2.6}$$

with the central angular frequency ω_0. The change of the instantaneous frequency is given by the derivative of the nonlinear phase

$$\omega(t) = \omega_0 + \frac{d}{dt}\phi_{nl}(t), \tag{2.7}$$

which leads to a modified and typically broader output spectrum. This intensity-dependent phase shift can be used in fiber oscillators to favor pulsed over continuous-wave operation and thus to achieve passive mode-locking for the generation of ultrashort pulses [Smi70, Hau00].

The mechanism of mode-locking by nonlinear polarization evolution (NPE) is depicted in Figure 2.4. The linear polarized electric field of a short pulse propagates through a birefringent medium—the optical fiber—and the polarization changes from linear to elliptical. When the pulse passes the nonlinear Kerr medium, the axis of the polarization ellipse rotates due to the nonlinear accumulated phase. Because the amount of rotation is intensity-dependent, this mechanism can be used to discriminate low-intensity wings by placing a polarizer in the beam behind the Kerr medium [Hau95].

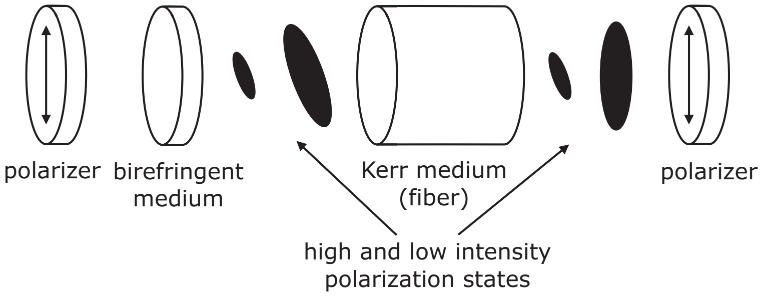

Figure 2.4: Schematic of the mode-locking mechanism using nonlinear polarization evolution (from Reference [Hau95]).

2.3 Stretched-pulse regime

The pulse regime, i.e. the spectral and temporal evolution of the pulse inside the resonator, plays an important role in mode-locked oscillators as it determines the achievable output pulse parameters. First femtosecond fiber lasers used the generation of solitons in anomalously dispersive fibers, where the pulse duration is close to the Fourier limit almost everywhere in the cavity [Mol84, Mit87]. These oscillators were able to generate pulse energies in the range of 0.1 nJ, but further power scaling was constrained by the soliton area theorem [Lam80].

This limitation was overcome by the invention of the stretched-pulse or dispersion-managed soliton laser, which uses temporal breathing of the pulse to lower the average peak power. For this reason, segments with normal and anomalous group delay dispersion were incorporated into the cavity, so the circulating pulses undergo twofold stretching and compression during one round-trip.

Figure 2.5 shows the group delay dispersion, the pulse duration, and the frequency modulation, also called chirp, of the pulse along the resonator position for a stretched-pulse oscillator. The pulse duration has two minima in the resonator and the chirp changes twice its sign [Nij98].

With this scheme, pulse energies in the range of 2 nJ could be demonstrated, which is about 20 times larger than that of soliton fiber lasers [Nel96].

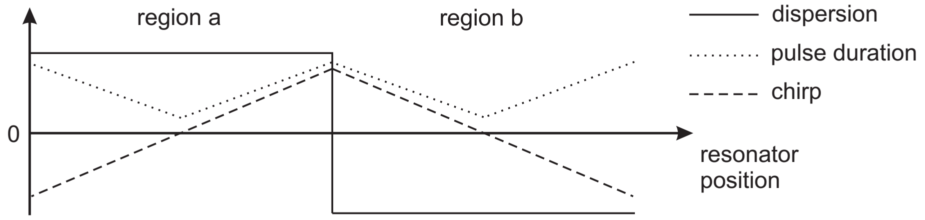

Figure 2.5: Dispersion, pulse duration, and chirp along the stretched-pulse resonator (from Reference [Wis08]).

Typically, the sections with normal and anomalous dispersion are designed such that the total second-order dispersion is around zero, i.e. $\beta_{2,a} L_a + \beta_{2,b} L_b \approx 0$. A common scheme uses normally dispersive fibers in combination with gratings having anomalous dispersion to generate pulse energies of 2.2 nJ and durations well below 100 fs at 1 µm wavelength [Lim03].

Applying this scheme to larger cavity lengths—to reduce the repetition rate and thus eliminate the need for a pulse picker in a successive amplification system—is challenging, as the third-order dispersion contributions of the fiber and the grating compressor have the same sign and, therefore, add up and corrupt the pulse quality. Hence, the condition $\beta_{3,a} L_a + \beta_{3,b} L_b = 0$ needs to be fulfilled to achieve the shortest possible pulses. For this reason, an appropriate pulse compressor was designed and implemented in the oscillator studied in Chapter 4 [Say09]. It is based on gratings and prisms and thus allowed for the compensation of third-order dispersion. The details of TOD compensation are covered in Section 3.2.

The application of dispersion-managed solitons led to a considerable improvement of the output pulse parameters, but further power scaling had been very challenging, as the maximum achievable energy is limited by the tolerable SPM induced nonlinear phase as well as pulse breakup due to optical wave-breaking in normally dispersive fibers [Tom85, Rot89, And92]. Newer concepts try not to avoid the fiber nonlinearity but to exploit it in order to further scale the pulse parameters. Parabolic pulses, first predicted to appear in fiber amplifiers with normal dispersion, nonlinearity, and a uniform gain, found application also in fiber oscillators [Fer00, Ild04b]. With this scheme, 100 fs long pulses with energies of 14 nJ could be demonstrated [Buc05].

Although it was possible to scale the pulse energy by intracavity parabolic pulse generation, the focus of the actual research lies on the dissipative-soliton pulse regime, which allows for even larger pulse energies. It is applied to the oscillators described in Chapter 5 and 6 and will thus be described in the next section.

2.4 Dissipative solitons

Further scaling of the pulse parameters was initiated by the invention of the dissipative-soliton laser, which is characterized by the absence of anomalously dispersive elements [Cho06]. Hence, it is also called all-normal dispersion fiber laser.

The evolution of dissipative solitons is based on nonlinear propagation under the influence of normal dispersion and spectral broadening by SPM as depicted in Figure 2.6 (a). The fiber dispersion in combination with SPM leads to a monotonic stretching of the circulating pulses. Thereby, the spectral width of the broadened pulses can even exceed the gain bandwidth of the ytterbium-doped fiber. Successive spectral filtering of the strongly chirped pulses leads to a temporal shortening and to a consistent intracavity pulse evolution as sketched in Figure 2.6 (b). Although the pulses undergo excessive self-phase modulation, the resulting spectral phase of the output pulses can typically be compensated for by a grating compressor. With that, pulse durations below 50 fs from dissipative-soliton oscillators have been demonstrated [Chi10, Chi12]. Reference [Wis08] gives an overview of all-normal dispersion fiber lasers. A general overview of dissipative solitons, not solely restricted to laser physics, is given in Reference [Akh05].

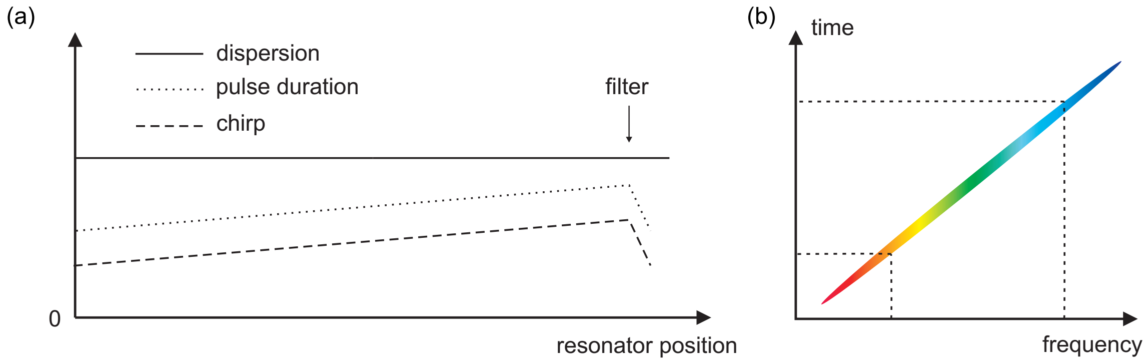

Figure 2.6: (a) Dispersion, pulse duration, and chirp along the dissipative-soliton resonator (from Reference [Wis08]). (b) Spectral filtering of chirped pulses leads to a temporal shortening.

3 Ultrashort pulse fiber amplifiers

In this chapter, the basics of femtosecond fiber amplifiers are covered. The fiber chirped-pulse amplification scheme is presented as well as two different approaches for third-order dispersion compensation, which were applied to the laser systems described in Chapter 8 and 9.

3.1 Fiber chirped-pulse amplification

The achievable maximum pulse energy in ultrashort fiber amplifiers is inter alia limited by the nonlinear response of the medium. For that reason, a common way to avoid high peak intensities is to temporally stretch the pulses before amplification. Figure 3.1 shows a schematic of such a chirped-pulse amplification (CPA) system. After stretching and amplification, the pulses are subsequently compressed by an appropriate pulse compressor [Str85].

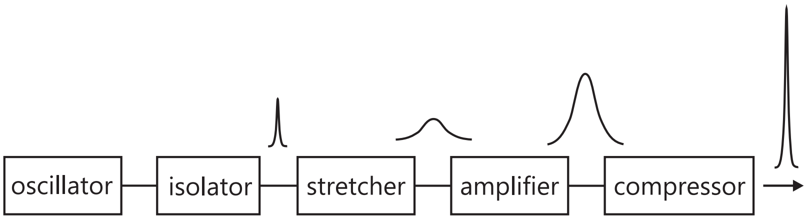

Figure 3.1: Schematic of a chirped-pulse amplification system.

Generally, there are many different types of optical pulse stretchers and compressors having both advantages and disadvantages. Considering femtosecond pulses, the dispersion terms β_2, β_3, and for the shortest pulses even β_4 of stretcher and compressor should be matched in order to achieve the shortest possible pulse durations. On the other hand, using fiber-based stretchers and compressors would greatly reduce the system complexity and, when the fiber components are spliced together, would make the CPA system alignment-free as well as more robust against environmental disturbances.

For spectral bandwidths of smaller than 3 nm and pulse durations of larger than 500 fs, it is usually sufficient to compensate for the second-order dispersion of the stretcher. Higher-order dispersion terms do not have a large impact on the pulse quality and can thus be omitted. Typically, a grating compressor having anomalous dispersion is used in this case, which can compensate for the normal dispersion of the stretcher [Tre69]. However, for shorter pulses and broader spectra, it becomes more important to consider also higher-order dispersion terms of stretcher and compressor.

Perfect dispersion matching can be achieved by using optical gratings both for stretching and compression [Tre69, Mar87, Pes87]. Small amounts of residual third-order dispersion can then be compensated for with different line densities of the gratings [Squ98] or tuning the angle of incidence of the grating compressor. This approach together with aberration-free reflective type stretcher designs have been the common CPA basis for many years [Che96, Ban00, Jia02]. As angular dispersion always results in anomalous group delay dispersion, prism arrangements can, in principle, also be used for pulse compression [Die06]. However, they typically exhibit only small dispersion values and are, therefore, applied almost exclusively inside laser resonators [Die83, For84].

Not every stretcher type can also be used for compression of ultrashort pulses with large energies. This is caused by the large peak power, which can lead to pulse breakup or even damage of the compressor. For these reasons, fiber-based compressors have not yet been able to compress femtosecond pulses with microjoule energies. However, fused silica transmission gratings can withstand very high peak intensities combined with very high diffraction efficiencies of larger than 95 % and are for these reasons often used in fiber CPA systems [Cla03, Cla08]. Another approach uses high-energy pulse compression inside bulk material in down-chirped pulse amplification [Gau04, Gau06], while chirped volume Bragg gratings recently offered great potential [Lia07, Cha09]. In both schemes, the peak power can easily be reduced by using an appropriate beam diameter.

Because of the smaller pulse energy before amplification, optical fibers can be used for pulse stretching. There are several fiber-based stretchers, which can in principle be integrated in fiber CPA systems. Possible candidates are chirped fiber Bragg gratings, written in step-index fibers [Oue87, Ime04] as well as standard fused silica step-index fibers with normal dispersion at 1 µm wavelength [Nuf06]. The transverse refractive index profile of the fiber can also be designed to achieve specific dispersive properties. This is utilized in so-called triple-cladding fibers (see also Section 3.2) to achieve a defined ratio of third-order to second-order dispersion [Grü00, Grü10]. Anomalous group delay dispersion can be achieved in solid fused silica fibers by the usage of higher-order modes in combination with long period Bragg gratings for mode-conversion [Ram06]. Apart from these examples, hollow core photonic bandgap fibers may be a candidate for high-energy fiber-based pulse compression [Cry11, Smi03, Rob05]. As about 95 % of the guided optical power is located in air filled regions, the nonlinearity is highly reduced compared to solid-core fibers. However, splicing these fibers is challenging and dispersion fine tuning is possible only by cutting back the fiber.

For long, fiber-based stretchers have not been applied to ultrashort pulse CPA systems due to the cumulative third-order dispersion of the fiber stretcher and the grating compressor, which degrades the pulse quality. However, the next section covers different schemes for the successful implementation of fiber stretchers in CPA systems even for output pulse durations in the range of 100 fs.

3.2 Compensation of third-order dispersion

In this thesis, two concepts for third-order dispersion compensation were pursued. One includes a standard step-index fiber stretcher in combination with a grism compressor (synonym for grating prism compressor), the other one uses a specially designed triple-cladding fiber stretcher in combination with a grating compressor. These schemes were applied to the fiber oscillator described in Chapter 4 and the amplifiers covered in Chapter 8 and 9.

Before going into technical detail, the impact of TOD in fiber CPA systems is analyzed. For that, the temporal pulse broadening of two Gaussian pulses at 1030 nm wavelength is studied. They initially have temporal full widths at half maximum (FWHM) of 100 fs and 500 fs, respectively. The corresponding root mean square (RMS) widths are 42 fs and 212 fs. Concerning the temporal dispersive broadening, it can be shown that the RMS width σ of an initially unchirped Gaussian pulse evolves under the influence of fiber dispersion with coefficients β_2, β_3, and length L according to

$$\sigma(\beta_2, \beta_3, L) = \sigma_0 \sqrt{1 + \left(\frac{\beta_2 L}{2\sigma_0^2}\right)^2 + \frac{1}{2}\left(\frac{\beta_3 L}{4\sigma_0^3}\right)^2}, \tag{3.1}$$

where σ_0 is the initial RMS width [Agr07]. Figure 3.2 (a) shows the RMS width of the stretched pulse as a function of fiber length assuming $\beta_2 = 24.5\ \mathrm{ps}^2/\mathrm{km}$ and $\beta_3 = 0.024\ \mathrm{ps}^3/\mathrm{km}$ as calculated in Section 2.1. As a result, stretching the pulses with 500 fs FWHM to the same duration compared to the 100 fs pulses requires about five times the fiber length. The influence of residual TOD on the two pulses after compression is shown in Figure 3.2 (b). Compression is achieved by a grating arrangement having a line density of 1500/mm, which resulted in a third-order to second-order dispersion ratio of $\beta_3/\beta_2 = -6.5$ fs. Because the signs of the TOD coefficients of stretcher and compressor are the same, the TOD is cumulative and leads to larger compressed pulse durations for larger stretcher fiber lengths.

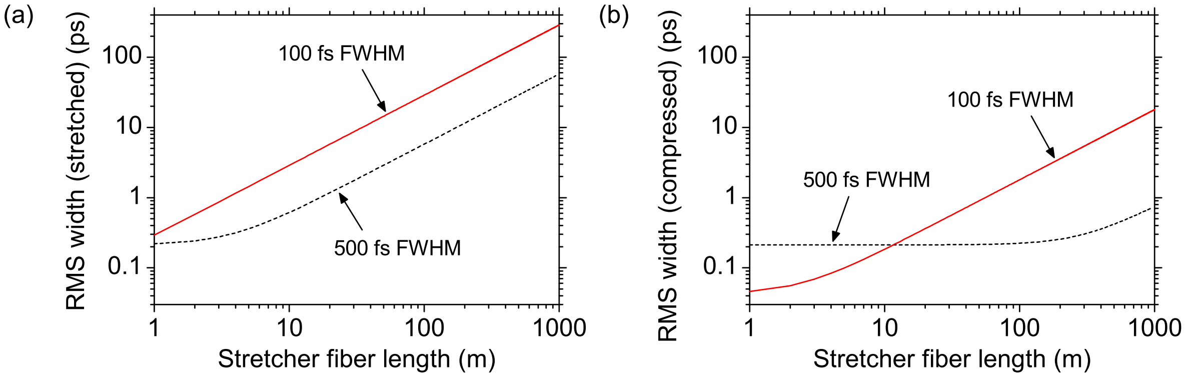

Figure 3.2: (a) Stretched pulse duration due to second- and third-order dispersion. (b) Residual TOD leads to increased RMS widths after compression.

It is notable in Figure 3.2 (b) that for fiber lengths larger than 12 m, the compressed pulse RMS width of the initially 100 fs long pulse is always larger than that of the initially 500 fs long pulse. For example, stretching the pulses to RMS widths of 57 ps requires about 200 m fiber for the 100 fs pulse and about 1 km for the 500 fs long pulse. However, the corresponding RMS widths after compression are 3.6 ps for the 100 fs pulse but only 0.7 ps for the initially 500 fs long pulse. This corroborates the importance of TOD compensation in fiber CPA systems when working with pulse durations in the range of 100 fs.

To estimate the influence of the fiber dispersion on the pulse propagation, dispersion lengths are used. For the dispersion terms of second and third order, one defines $L_D = T_0^2/|\beta_2|$ and $L'_D = T_0^3/|\beta_3|$ with the pulse duration T_0 [Agr07]. After propagating through a second-order dispersive medium with length L_D, the duration of a Gaussian pulse increased by a factor of $\sqrt{2}$. Table 3.1 shows the dispersion lengths for pulse durations of 50 fs, 100 fs, and 500 fs and a standard step-index fiber with a dispersion of $\beta_2 = 24.5\,\mathrm{ps}^2/\mathrm{km}$ and $\beta_3 = 0.024\,\mathrm{ps}^3/\mathrm{km}$ at 1030 nm wavelength. For the pulse duration of 100 fs, the dispersion lengths L_D and L'_D corresponding to β_2 and β_3 are 0.4 m and 42 m, respectively. Hence, working with 100 fs long pulses and fiber lengths of several ten meters requires consideration of both the system's second- as well as third-order dispersion.

In practice, TOD compensation can be achieved in different ways when using a fiber-based stretcher. While linearly chirped fiber Bragg gratings lack in performance due to residual TOD [Oue87], the dispersion of a nonlinearly chirped fiber grating can be matched to that of a grating compressor [Ime04]. However, the limited spectral bandwidth of fiber Bragg gratings have to be considered when stretching broadband femtosecond pulses. Also, an optical circulator has to be used as the fiber grating is a reflective device.

T_0	L_D	L'_D
500 fs	10.2 m	5208 m
100 fs	0.4 m	42 m
50 fs	0.1 m	5 m

Table 3.1: Dispersion lengths for Gaussian pulses with different pulse durations.

Another approach uses nonlinearly chirped volume Bragg gratings for compression, whose dispersion inversely matches that of a fiber stretcher. Pulse compression is then realized by simple Bragg reflection inside a bulk glass material. Although offering great potential, this scheme has not been realized so far.

Soon after the demonstration of the first CPA system, prisms were incorporated into grating compressors for cubic phase compensation [For87, Pes89, Kan94, Zao07]. It was demonstrated that gratings, that are directly applied to prisms, show a very linear dispersion curve [Tou93]. These grating prism compressors—also termed grism compressors—offer more flexibility in terms of their dispersive properties compared to grating arrangements. The compressor can be designed to simultaneously achieve anomalous second-order dispersion < 0 ps^2 and a positive ratio of third- to second-order dispersion ($\beta_3/\beta_2 > 0\,\mathrm{fs}$) as required when using a standard fiber stretcher at 1 µm wavelength [Kan95, Kan97, Gib06, Dur08]. Figure 3.3 shows typical dispersion curves of grism and grating compressors for grating line densities of 600/mm and 1500/mm. The slopes of the curves of grisms and gratings are opposite in sign due to a different sign of their TOD value.

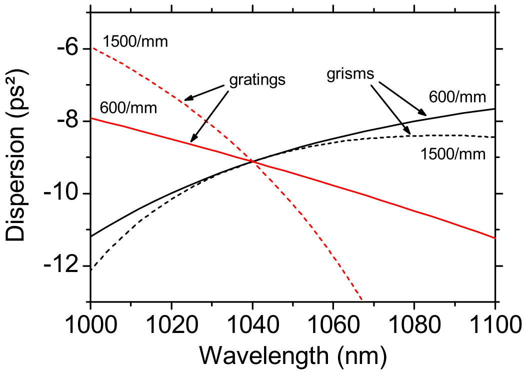

Figure 3.3: Typical dispersion curves of grating and grism compressors with the indicated grating line densities.

Figure 3.4 shows a schematic of such a grism compressor, which was used for TOD compensation both in the experiments described in Chapter 4 and 9. The beam is refracted at the surface of the transmission grating in point P_1, travels through the material with refractive index n_1, and is then diffracted at the grating surface in point P_2. The insertion of a prism results in the refraction in points P_3 and P_4 as well as propagation through material with refractive index n_2. Subsequently, the beam passes through a corresponding second prism grating arrangement, which is point symmetrically arranged. The spatially widened parallel beam in point P_9 is then back reflected by a retroreflector with a height displacement and passes the compressor in backward direction. It is notable that the optical phase and, therefore, the dispersion doubles when the beam passes the components twice.

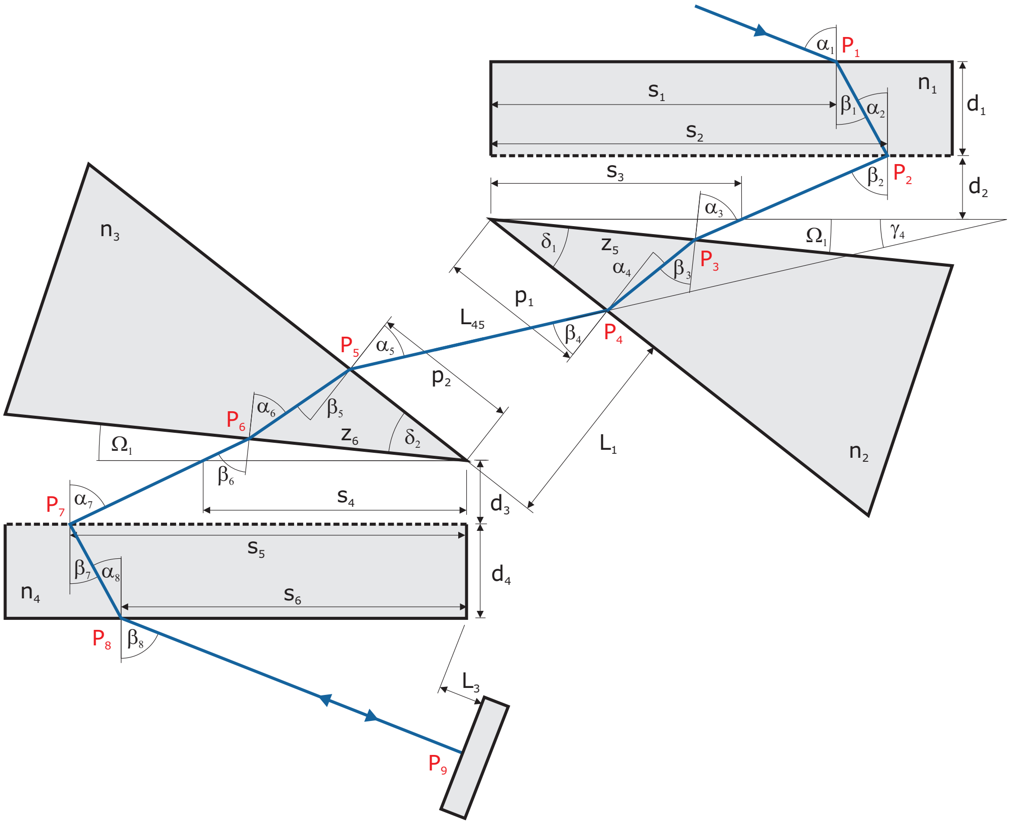
α_1
P_1
n_1
s_1
β_1
α_2
d_1
s_2
β_2
P_2
s_3
d_2
α_3
Ω_1
γ_4
n_3
δ_1
z_5
α_4
β_3
P_3
p_1
L_{45}
β_4
P_4
P_5
α_5
p_2
P_6
α_6
β_5
z_6
δ_2
Ω_1
L_1
n_2
β_6
s_4
d_3
P_7
α_7
s_5
d_4
β_7
α_8
n_4
s_6
P_8
β_8
L_3
P_9

Figure 3.4: Sketch of the grism compressor. A ray through the device is depicted in blue.

In the points P_2 and P_7, the beam is diffracted in accordance to the grating equation $\sin(\gamma) + n\,\sin(\theta) = \lambda/d$, where γ is the angle of incidence, θ the angle of the diffracted beam, n the material refractive index, and $d = 1/g$ the grating line separation [Pal05]. The characteristic of gratings is that they introduce an additional phase shift of 2π per ruling [Tre69, Hua11], which has to be included manually in the model. In points P_1, P_3 to P_6, and P_8, the beam is refracted according to Snell's law $\sin\theta_1/\sin\theta_2 = n_2/n_1$, where θ_1 is the incidence angle in the medium with refractive index n_1 and θ_2 the angle of the refracted beam in the medium with refractive index n_2.

In general, the properties of a dispersive system can be calculated using a matrix formulation [Mar88] or operators [Dru08]. Within the scope of this work, a program for the calculation of the grism compressor dispersion was developed. It calculates the spectral phase of the beam $\phi(\lambda)$ based on straight ray propagation according to the diffraction and refraction laws as described above. In doing so, beam divergence was neglected. This was acceptably fulfilled for the beams in the corresponding experiments described in Chapter 4 and 9, which stayed collimated over distances of several meters. The group delay is then calculated by taking the derivative of the spectral phase to

$$\beta_1(\lambda) = -\frac{\lambda^2}{2\pi c}\frac{d}{d\lambda}\phi(\lambda) \tag{3.2}$$

and the dispersion terms of higher order accordingly to

$$\beta_n(\lambda) = -\frac{\lambda^2}{2\pi c}\frac{d}{d\lambda}\beta_{n-1}(\lambda) \quad \text{for} \quad n \geq 2. \tag{3.3}$$

The practical implementation was realized by using C++ as programming language in combination with Qt for the graphical user interface. The program's user interface is shown in Figure 3.5. It accepts the grism compressor parameters as depicted in Figure 3.4 as input parameters. The program includes a geometrical consistency check to ensure that the optical elements do not overlap and their size is large enough for a given spectral bandwidth. Also, the beam size on each element is calculated. When optimizing the dispersive properties of the compressor by changing the input parameters, the dispersion gradients are helpful. They indicate, how the grism compressor dispersion alters, when the prism separation L_{45}, the prism apex angle δ, the prism grating angle Ω, the angle of incidence $\alpha = \alpha_1$, and the prism grating separation $D_2 = d_2$ are varied.

The compressor complexity and, therefore, the alignment needs are drastically reduced by using a second retroreflector as depicted in Figure 3.6. With that, the beam is reflected with a horizontal displacement and travels through the compressor in backward direction [Lai94, Cha10]. This allows using a single grating and a single prism covering only approximately half the space and, furthermore, reducing the overall costs. Such an assembly was used in both the experiments described in Chapter 4 and 9.

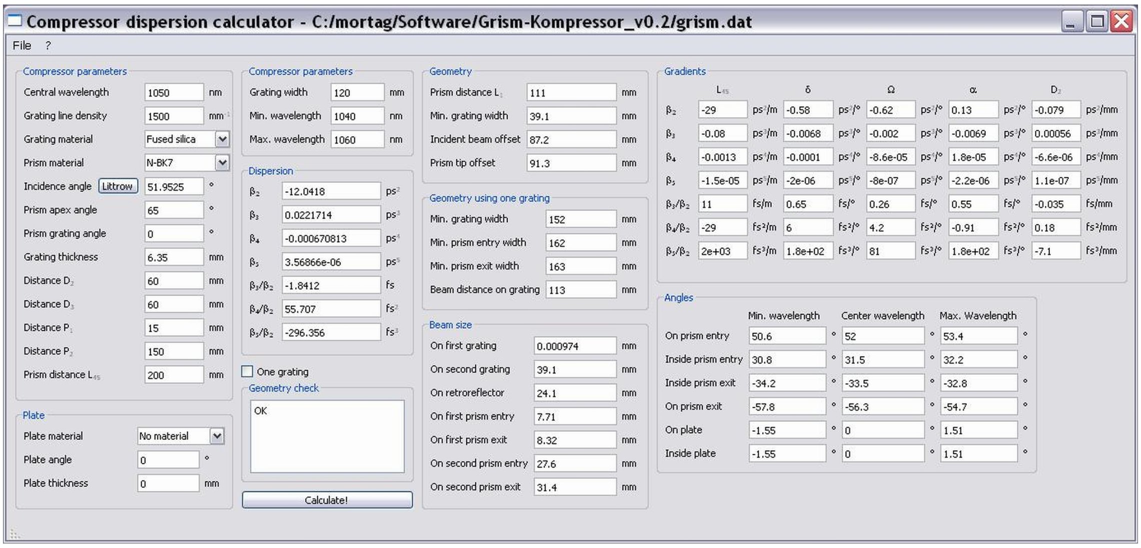

Compressor dispersion calculator - C:/mortag/Software/Grism-Kompressor_v0.2/grism.dat

Compressor parameters

Central wavelength 1050 nm
Grating line density 1500 mm^{-1}
Grating material Fused silica
Prism material N-BK7
Incidence angle 51.9525 °
Prism apex angle 65 °
Prism grating angle 0 °
Grating thickness 6.35 mm
Distance D_2 60 mm
Distance D_3 60 mm
Distance P_1 15 mm
Distance P_2 150 mm
Prism distance L_{45} 200 mm

Plate

Plate material No material
Plate angle 0 °
Plate thickness 0 mm

Compressor parameters

Grating width 120 mm
Min. wavelength 1040 nm
Max. wavelength 1060 nm

Dispersion

β_2 -12.0418 ps^2
β_3 0.0221714 ps^3
β_4 -0.000670813 ps^4
β_5 3.56866e-06 ps^5
β_3/β_2 -1.8412 fs
β_4/β_2 55.707 fs^2
β_5/β_2 -296.356 fs^3

☐ One grating

Geometry check

OK

Geometry

Prism distance L_1 111 mm
Min. grating width 39.1 mm
Incident beam offset 87.2 mm
Prism tip offset 91.3 mm

Geometry using one grating

Min. grating width 152 mm
Min. prism entry width 162 mm
Min. prism exit width 163 mm
Beam distance on grating 113 mm

Beam size

On first grating 0.000974 mm
On second grating 39.1 mm
On retroreflector 24.1 mm
On first prism entry 7.71 mm
On first prism exit 8.32 mm
On second prism entry 27.6 mm
On second prism exit 31.4 mm

Gradients

	L_{45}		δ		Ω		α		D_2	
β_2	-29	ps^2/m	-0.58	ps^2/°	-0.62	ps^2/°	0.13	ps^2/°	-0.079	ps^2/mm
β_3	-0.08	ps^3/m	-0.0068	ps^3/°	-0.002	ps^3/°	-0.0069	ps^3/°	0.00056	ps^3/mm
β_4	-0.0013	ps^4/m	-0.0001	ps^4/°	-8.6e-05	ps^4/°	1.8e-05	ps^4/°	-6.6e-06	ps^4/mm
β_5	-1.5e-05	ps^5/m	-2e-06	ps^5/°	-8e-07	ps^5/°	-2.2e-06	ps^5/°	1.1e-07	ps^5/mm
β_3/β_2	11	fs/m	0.65	fs/°	0.26	fs/°	0.55	fs/°	-0.035	fs/mm
β_4/β_2	-29	fs^2/m	6	fs^2/°	4.2	fs^2/°	-0.91	fs^2/°	0.18	fs^2/mm
β_5/β_2	2e+03	fs^3/m	1.8e+02	fs^3/°	81	fs^3/°	1.8e+02	fs^3/°	-7.1	fs^3/mm

Angles

	Min. wavelength		Center wavelength		Max. Wavelength	
On prism entry	50.6	°	52	°	53.4	°
Inside prism entry	30.8	°	31.5	°	32.2	°
Inside prism exit	-34.2	°	-33.5	°	-32.8	°
On prism exit	-57.8	°	-56.3	°	-54.7	°
On plate	-1.55	°	0	°	1.51	°
Inside plate	-1.55	°	0	°	1.51	°

Figure 3.5: Grism compressor dispersion calculator.

Third-order dispersion compensation in fiber-based chirped-pulse amplifiers is not only possible using a grism compressor. Proper fiber design using triple-cladding fibers can also lead to a stretcher dispersion, that inversely matches that of a grating compressor. This scheme would be favorable over the usage of a grism arrangement, as the compressor does not need prisms for TOD compensation, which reduces the overall complexity.

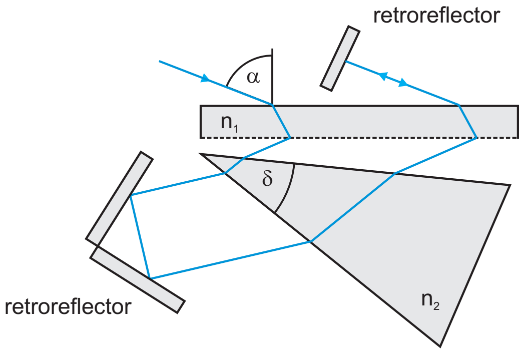

Figure 3.6: Simplified grism compressor setup.

Triple-cladding fibers are well known as dispersion compensating fibers from telecommunication applications at wavelengths of 1.5 µm. The typical index profile of such a fiber is shown in Figure 3.7 (a). A high-index core is surrounded by a low-index trench, which again is surrounded by a ring with higher refractive index [Grü00, Grü05].

A typical dispersion curve of such a fiber is depicted in Figure 3.7 (b). In the region of interest, the second-order dispersion is positive, while the dispersion slope, measured by the ratio β_3/β_2 is negative. Hence, this type of fiber can be used to compensate for the dispersion of a grating compressor at least up to the third order, as both have the same sign of the ratio β_3/β_2. This scheme is experimentally implemented in Chapter 8.

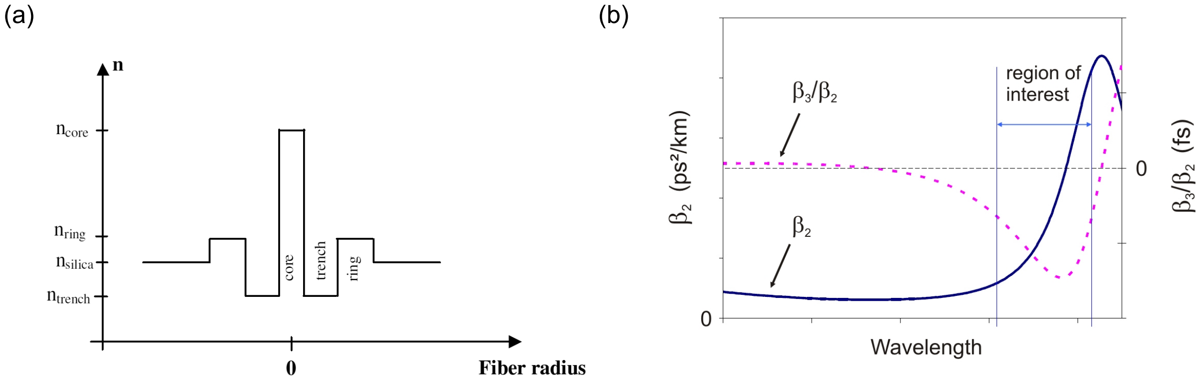

Figure 3.7: (a) Index profile and (b) dispersion curve of a typical triple-cladding fiber (from Reference [Grü10]).

4 Low-repetition rate stretched-pulse fiber laser

Ytterbium-based mode-locked fiber lasers have proven to be very competitive pulse sources generating pulse durations down to 28 fs and pulse energies above 20 nJ with the usage of single-mode fibers [Zho08, Cho07]. The typical repetition frequencies of these oscillators are in the range of 20 MHz to 100 MHz corresponding to intracavity fiber lengths of several meters [Cau97]. However, many applications like supercontinuum generation in fibers with small core sizes, micro- and nano-machining of delicate parts, cutting and imaging of biological tissue, e.g. in ophthalmology, require high pulse energies but to some extend very limited average powers. Therefore, femtosecond fiber lasers with low repetition frequencies could serve as a seed source for chirped-pulse amplifiers to generate high-energy pulses without the need for a complex and costly pulse picking unit. With increasing resonator length, the advantages of fiber lasers become significant as the light is guided inside the fiber core. In contrast, applying Herriott cells in bulk solid state lasers with low-repetition rates is more complex [Pap03, Pap09].

The development of mode-locked fiber oscillators with low repetition frequencies has not been in the focus of research and, therefore, only few such systems were demonstrated. Highly chirped pulses with durations of 150 ps could be generated in a largely normal dispersive oscillator at a repetition frequency of 3 MHz, which could be compressed to 670 fs after successive amplification [Ren08]. A further increase of the intracavity fiber length resulted in microjoule pulse energies but with nanosecond pulse durations [Kob08].

Recently, a fiber laser with a repetition frequency of 2 MHz was demonstrated, which emitted pulses with energies of 0.23 nJ and durations of 400 fs at a wavelength of 1030 nm [Zho06]. Mode-locking was achieved via nonlinear polarization evolution, while the laser with anomalous total dispersion was operated in the stretched-pulse regime without intracavity TOD compensation. Besides that, 200 fs long soliton pulses could be generated by using nonlinear polarization evolution in combination with a single-wall carbon nanotube saturable absorber at 1.5 µm wavelength [Fon07].

In this chapter, a hybridly mode-locked ytterbium-doped fiber laser with a repetition frequency of 1.8 MHz is studied. A grism compressor was applied for intracavity second-order as well as third-order dispersion compensation, which resulted in the generation of 3.8 ps long pulses, which could externally be compressed to durations of 93 fs with a grating arrangement. To the best of knowledge, these are the shortest pulses from a mode-locked fiber laser with a fundamental repetition frequency below 20 MHz. The corresponding pulse energy before compression was 1.0 nJ. Parts of this chapter have been published in Reference [Say09].

4.1 Experimental setup

Figure 4.1 shows the setup of the fiber ring oscillator. It consists of an about 115 m long fiber section, which is followed by a 2.8 m long free-space section, each containing several optical components. The used fibers had a mode field diameter of about 6 µm and support a single transversal mode. The outputs of the fiber-integrated components were connected by fusion splicing.

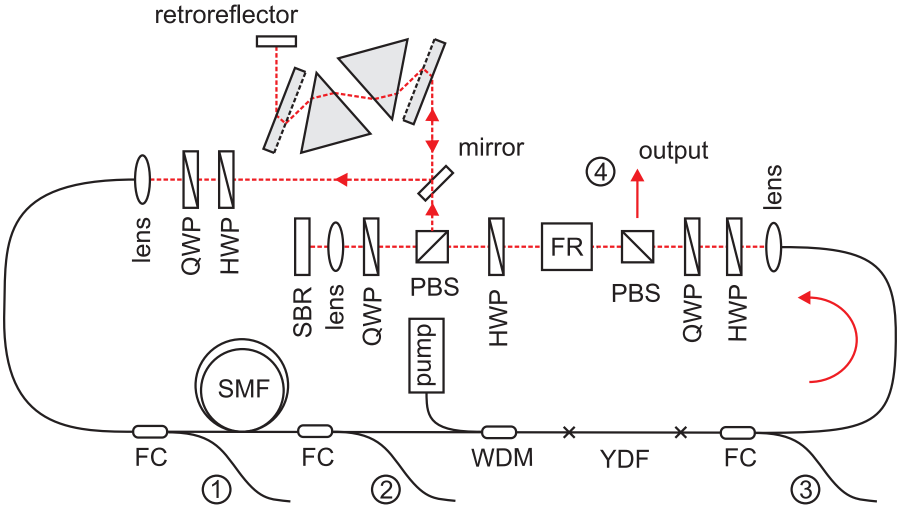

Figure 4.1: Experimental setup. HWP half-wave plate, QWP quarter-wave plate, SBR saturable Bragg reflector, PBS polarizing beam splitter, FR Faraday rotator, FC fiber output coupler, SMF single-mode fiber, WDM wavelength-division multiplexer, YDF ytterbium-doped fiber. The different output ports are labeled by numbers.

In the direction of pulse propagation, a 10 % fiber output coupler (FC) is followed by approximately 100 m of single-mode fiber, a second FC, a wavelength-division multiplexer, 38 cm of ytterbium-doped gain fiber INO Yb 125, and a third FC. Angle-polished connectors together with collimators were used at several outputs labeled port 1 to 3. The three output couplers were incorporated into the oscillator to measure the spectrum and pulse energy at different positions and, therefore, to gain knowledge about the pulse evolution. The main output port is labeled port 4. A single-mode fiber-coupled laser diode, emitting up to 600 mW at 976 nm wavelength, was used to optically pump the active fiber.

A Faraday rotator between two polarizing beam splitters acted as an optical isolator to assure unidirectional beam propagation. Passive mode-locking was achieved by the implementation of a semiconductor saturable absorber mirror (SESAM) from Batop GmbH together with nonlinear polarization evolution in the fiber section. The SESAM with a low-intensity absorption of 60 percent and a very fast relaxation time constant of 500 fs was applied in a reflective setup. A lens with a focus length of 8 mm was used to increase the peak power on the SESAM. Several quarter- and half-wave plates were incorporated into the resonator to properly adjust the polarization state for NPE mode-locking.

4.2 Characteristics of the grism compressor

A grism compressor was implemented to compensate for the group delay dispersion of the fiber section [Kan97, Zao07]. It incorporated a single highly efficient transmission grating with a groove density of 700/mm in combination with a single prism in an arrangement as depicted in Figure 3.6. This scheme is more compact and easier to align compared to the usage of two gratings and two prisms [Akt06, Cha10]. The back side of the grating was supplied with an anti-reflective coating for maximum efficiency.

The dispersion of the grism compressor was calculated for a center wavelength of 1030 nm as described in Section 3.2 using the following parameters (see Figure 3.4). The apex angle of the fused silica prism was 50°, while the prism grating angle Ω was set to 1.65°. The surfaces of the prism were also provided with an anti-reflective coating. The fused silica transmission grating was 6.35 mm thick. For the center wavelength, the distances p_1 and p_2 of the beam to the prism tip were 5 mm and 26 mm, respectively. The distance L_{45}, which corresponds to the distance prism-retroreflector-prism, was set to 51 cm. The grating incidence angle fulfilled the Littrow condition $\alpha_{in} = \arcsin(\lambda g/2) = 21.1°$ for maximum efficiency, where g stands for the grating line density.

The grism arrangement with the above mentioned parameters provided anomalous second-order as well as anomalous third-order dispersion. The needed second- and third-order dispersion to compensate for was assumed to be 2.8 ps^2 and 0.003 ps^3, respectively. Figure 4.2 shows the calculated dispersion of the grism compressor together with the needed dispersion curve, which corresponds to the intracavity fiber dispersion with the opposite sign. Due to the large total fiber length, the dispersion contributions of the optical components like the Faraday rotator TGG crystal were neglected. The dispersion curves fit very well concerning the absolute value and the dispersion slope with a third- to second-order dispersion ratio of 1.0 fs. Experimentally, the compressor's TOD to SOD ratio had been adjusted to match the one of the fiber section by varying the angle of incidence on the grating as well as the angle Ω between the prism and the grating. The total grism compressor efficiency was about 68 %.

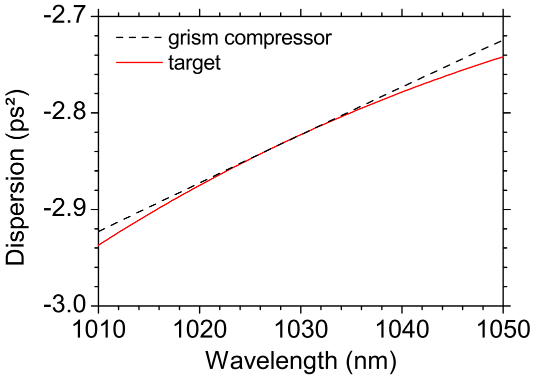

Figure 4.2: Calculated grism compressor dispersion and target dispersion.

4.3 Results at 1.8 MHz repetition frequency

After carefully adjusting the wave plates and the grism compressor, self-starting mode-locking was achieved at pump powers above 189 mW. Because multiple pulsing was usually observed at this pump power level, stable single-pulse operation was set up by decreasing the pump power to 160 mW. The pulses with the shortest compressed pulse durations were found at a net cavity dispersion of around -0.04 ps^2.

Figure 4.3 (a) shows the stable single pulse train measured with a fast photodiode. The temporal separation of the pulses was 554 ns corresponding to 1.8 MHz fundamental repetition frequency. True single-pulse operation was verified by the usage of a long-range autocorrelator with a 150 ps delay range. The oscillator emitted an average power of 1.8 mW corresponding to pulse energies of 1.0 nJ before compression. The spectrum measured at the main output port 4 is depicted in Figure 4.3 (b). It exhibits a central wavelength of 1035 nm and a RMS width of 22 nm. After compression with reflection gratings having a line density of 600/mm, pulse energies of 0.6 nJ were measured.

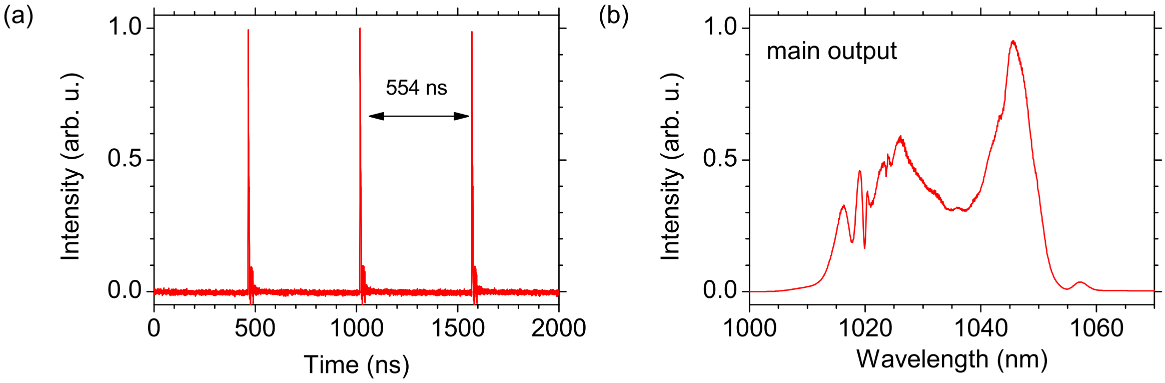

Figure 4.3: (a) Pulse train and (b) spectrum measured at port 4.

The intensity autocorrelations of the output pulses before and after compression are shown in Figure 4.4 (a) and (b). The FWHM of the autocorrelation functions are 5.3 ps and 128 fs, respectively, corresponding to pulse durations of 3.8 ps before and 93 fs after compression. The deconvolution factor of 1.38 was calculated by using the ratio of the FWHM of the bandwidth limited autocorrelation and the FWHM of the Fourier transform of the power spectrum assuming a constant phase. The calculated autocorrelation of the Fourier limited pulses is also shown in Figure 4.4 (b) and has a FWHM of 67 fs. Thus, the compressed pulse duration was about 37 % above the Fourier limit.

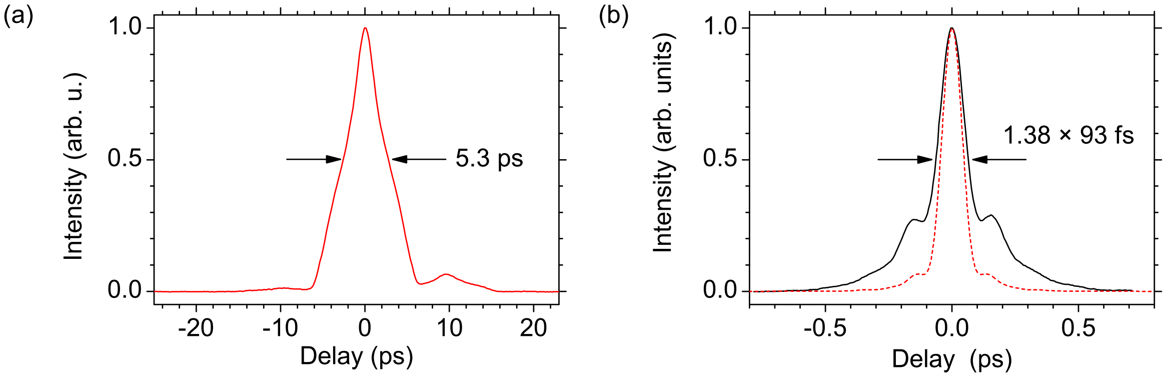

Figure 4.4: (a) Intensity autocorrelation measured at output port 4 with a FWHM of 5.3 ps. (b) Measured intensity autocorrelation of the compressed pulses (solid) and calculated transform limited autocorrelation (dashed).

The autocorrelation in Figure 4.4 (b) exhibits some side lobes, which may be due to self-phase modulation induced spectral broadening in the fiber section and the corresponding nonlinear pulse chirp. This chirp could not be compensated for by the grating compressor and resulted in the observed deviation of the pulse duration from the Fourier limit. The second-order and third-order dispersion values of the external pulse compressor were about -0.027 ps^2 and

3.8×10^{-5} ps^3, respectively. Two artifacts at delays of ±9.6 ps were always observed in the autocorrelation depicted in Figure 4.4 (a). They were visible independently of the pulse duration and were caused by the approximately 1 mm thick beam splitter in the autocorrelator.

To gain knowledge about the intracavity pulse evolution, the spectra at output ports 1 to 3 were measured as depicted in Figure 4.5 (a), (b), and (c). The central wavelength of both the spectra measured at ports 1 and 2 was 1027 nm, while the corresponding RMS widths were 11 nm and 9 nm, respectively. The spectrum measured at port 3 is strongly broadened and has a RMS width of 20 nm. Simultaneously, the center wavelength shifted to 1030 nm.

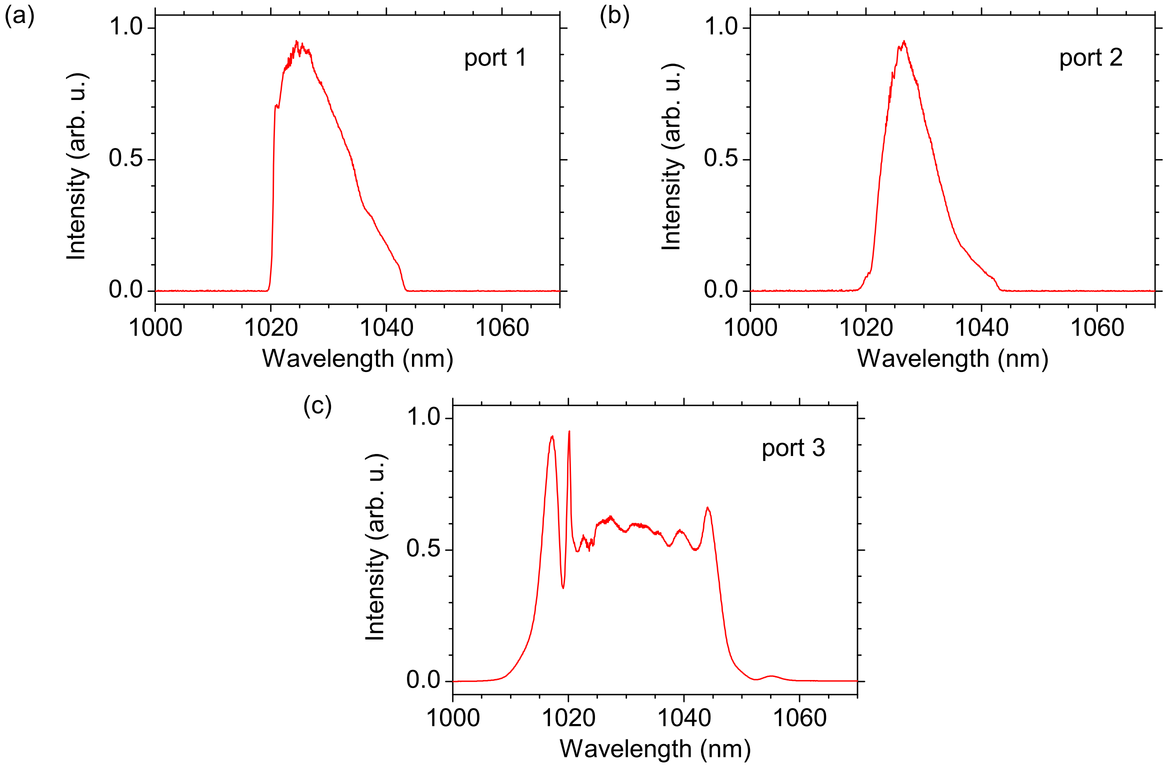

Figure 4.5: Spectral evolution inside the laser. The spectra are measured at the different output ports of the oscillator as depicted in Figure 4.1.

The observed spectral narrowing, occurring between port 1 and port 2, can be explained by the strong anomalous chirp of the pulses after propagating through the grism arrangement and experiencing SPM in the long fiber section. The strong spectral broadening occurring between port 2 and port 3 can be explained by self-phase modulation in the fiber. The spectral filtering observed between port 3 and port 1 is supposed to be caused by the combined action of nonlinear polarization evolution and SESAM mode-locking. Both mechanisms filter the chirped pulses nonlinearly in the time domain, which results in spectral narrowing in the spectral domain. It is also notable that the output pulses were dechirped with much less group delay dispersion than that of the intracavity grism compressor. Together with the net cavity dispersion close to zero, this implies that the laser is operating in the stretched-pulse regime.

4.4 Conclusion

A passively mode-locked ytterbium-doped fiber oscillator with a low repetition rate of 1.8 MHz was demonstrated. It incorporated an intracavity grism compressor for third-order dispersion compensation. With that, it was possible to generate 93 fs long pulses with energies of 0.6 nJ after compression with a conventional grating compressor. To the best of knowledge, these are the shortest pulses from a fiber oscillator with a repetition rate below 20 MHz.

Pulse energy scaling does not seem to be feasible with this scheme, as spectral broadening due to self-phase modulation already occurred and additionally gained nonlinear phase contributions will most likely lead to longer pulse durations. A further decrease of the repetition rate by increasing the intracavity fiber length could not be realized as the dimensions of the used grism arrangement were too small for larger dispersion values and the given spectral width. It also turned out that mode-locking was harder to achieve for longer cavity lengths and, simultaneously, the robustness against environmental disturbances like vibrations decreased. For applications, e.g. as a seed source for a fiber CPA system, the oscillator should be temperature-stabilized to minimize changes of the state of polarization due to the temperature-dependent fiber birefringence. Also, all fibers as well as the free-space parts should be fixed and mechanically maximally stable.

5 Low-repetition rate dissipative-soliton fiber laser

Femtosecond fiber oscillators with low repetition frequencies—as studied in the last chapter—cannot only be realized using the stretched-pulse regime with sections of normal and anomalous dispersion. Dissipative-soliton lasers, which use an all-normal dispersion cavity design in combination with spectral filtering, are also capable of being operated in the low repetition frequency range. This type of laser has been studied extensively in the last years with the aim of generating shorter pulses with increased energy. These efforts led to pulse energies above 20 nJ with pulse durations below 200 fs using core-pumped normal-dispersive fibers together with bulk optical components [Cho07]. However, dissipative-soliton lasers with low repetition frequencies have not yet been studied in detail concerning maximum pulse energy and minimum pulse duration. Only few such lasers have been reported. One system emitted 150 ps long pulses at 3 MHz repetition frequency with energies of 15 nJ, which could be compressed to 670 fs after subsequent amplification [Ren08].

Here, the dissipative-soliton regime is investigated concerning large cavity lengths. Pulse energies up to 50 nJ and, separately, pulse durations below 500 fs could be achieved at 2.1 MHz repetition frequency. It is experimentally shown, that the achievable compressed pulse duration increases with increasing cavity dispersion. In the studied oscillators, exclusively single-mode or effectively single-mode fibers with a V number below 2.44 were used to avoid higher-order mode issues. However, using large-mode area fibers, pulse energies of up to 0.5 µJ can be generated with this laser type [Chi11]. Parts of this chapter have been published in References [Hap10, Mor10].

5.1 Birefringent filter characteristics

Birefringent quartz plates in combination with polarizing beam splitters (PBS) were used for spectral filtering [Eva49a, Eva49b, Li90, Zhu90]. These filters do not need coatings, can withstand peak powers of several hundred MW/cm^2, and their single-pass loss is below 2-3 % [Kob92]. A schematic of the filter setup is depicted in Figure 5.1 (a). The transmission characteristic is a periodic function of wavelength and depends on the plate thickness. Thicker plates lead to smaller filter bandwidths and vice versa. The filter transmission bandwidth is shown in Figure 5.1 (b) for measured and calculated plate thicknesses from 2 mm to 20 mm corresponding to FWHM bandwidths of 32.9 nm to 3.0 nm. Especially for broad emission cross sections like that of ytterbium-doped glass and due to the periodic filter characteristic, it can be hard to lock the laser to a specific center wavelength. In this case, two or more plates can be combined to achieve a single wavelength transmission window with suppressed side maxima.

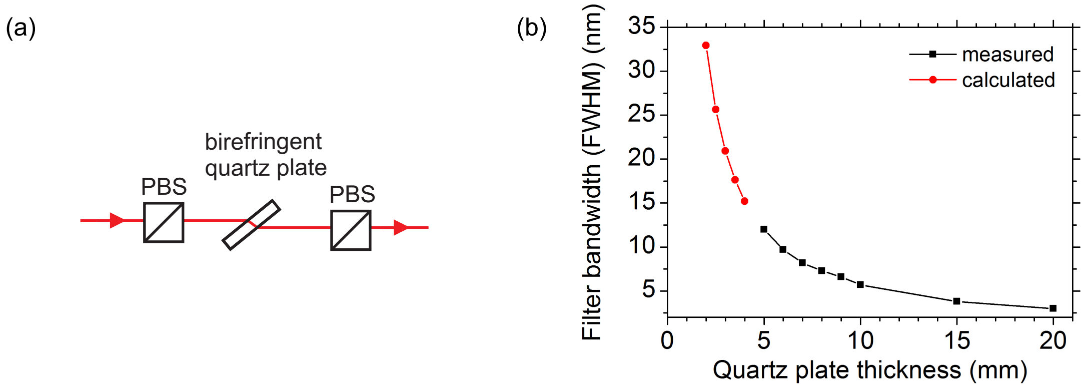

Figure 5.1: (a) Schematic of the birefringent quartz plate filter. PBS polarizing beam splitter. (b) Bandwidth of the filter as a function of plate thickness.

The refraction index of crystalline quartz at 1030 nm wavelength can be calculated using a Sellmeier equation to $n_o = 1.534572$ and $n_e = 1.543327$ for the ordinary and the extraordinary ray, respectively [Gho99]. The corresponding index difference is thus $\Delta n = 8.754 \times 10^{-3}$. With that, the filter properties can be calculated as follows.

According to Reference [Kob92], the intensity transmission for a p-polarized beam through a birefringent plate with thickness l and a subsequent polarizer behaves in accordance to

$$T = \left(\cos^2 \alpha + \sin \alpha \cdot e^{-2i\delta}\right)^2 , \tag{5.1}$$

where $\delta \approx \pi l \Delta n \sin^2 \gamma / (\lambda \sin \epsilon)$ for small values of $\Delta n \ll n_o$ and n_e, $\alpha = \arctan(\tan \theta / \sin \epsilon)$, and $\gamma = \arccos(\cos \theta \cos \epsilon)$. According to the experiments, it is assumed that the optical axis of the birefringent quartz plate lies in the plane parallel to the plate surface. The incidence angle ϵ of the beam to the plate surface normal is chosen to be the Brewster's angle for minimum loss, which for crystalline quartz is 57°. The filter transmission thus shows a sinusoidal dependence on the wavelength. Tuning the center wavelength of the filter is accomplished by variation of the angle θ, which means rotating the plate around the axis normal to the surface. Simultaneously, the modulation depth can be varied from zero to 100 percent by rotating the plate further. The rotation of the filter is, together with the intracavity wave plate settings, a crucial parameter when searching for mode-locking.

5.2 Experimental setup

The setup of the laser is depicted in Figure 5.2. The ring oscillator consists of a free-space and a fiber section and is mode-locked via nonlinear polarization evolution and successive out-coupling at the polarizing beam splitter. This nonlinear filtering together with a birefringent filter ensures spectral and temporal reproduction of the pulse after one roundtrip.

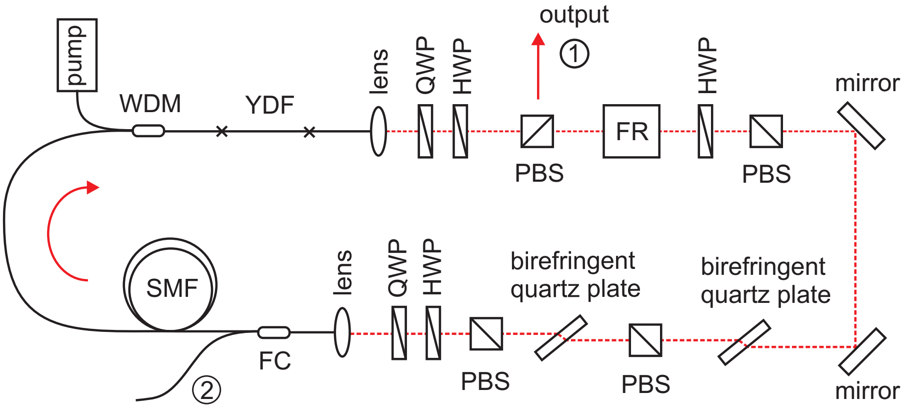

Figure 5.2: Experimental setup. HWP half-wave plate, QWP quarter-wave plate, PBS polarizing beam splitter, FR Faraday rotator, FC fiber output coupler, SMF single-mode fiber, WDM wavelength-division multiplexer, YDF ytterbium-doped fiber.

Light from a single-mode laser diode at the wavelength of 976 nm was coupled into the resonator by a 976 nm/1030 nm wavelength-division multiplexer. This was used to pump the 29 cm long single-mode ytterbium-doped fiber Nufern SM-YSF-HI with a core diameter of 7.5 µm. A 88 cm long piece of passive single-mode fiber was spliced to the end of the active fiber. The length of this fiber was crucial as most of the nonlinear polarization rotation took place in the active and the successive fiber. Packaged lenses with focus lengths of 8 mm were used for collimation of the beam.

A Faraday rotator between two polarizing beam splitters served as an optical isolator and ensured unidirectional laser operation. A combination of two quartz plates (5 mm and 10 mm thick) was used for spectral filtering corresponding to an effective filter bandwidth of 5.5 nm. Half- and quarter-wave plates in front of the collimators were used to adjust the polarization state and, therefore, to initiate mode-locking. A fiber coupler with an output coupling ratio of 3 % was implemented 1.5 m behind the collimator and used for monitoring the optical power in the cavity. To reduce the repetition frequency, a spool with about 96 m of single-mode fiber was spliced into the fiber section. The passive fibers Liekki Passive-10/125 and CorActive Si-08-10 for the coupler with a core diameter of 10 µm had a V number of 2.44 and effectively support one single transverse mode. A maximum mode field diameter for the active and passive fibers was chosen to minimize the peak power and, therefore, the nonlinear material response in the long fiber section. None of the fibers were polarization-maintaining. The pulses were compressed using in parallel arranged reflection gratings with a line density of 1200/mm. The total compressor efficiency was about 65 %.

5.3 Results at 2.1 MHz repetition frequency

After adjusting the wave plates, the oscillator emitted a stable pulse train with a temporal pulse separation of 478 ns corresponding to the fundamental repetition frequency of 2.1 MHz as shown in Figure 5.3 (a). At a pump power of 244 mW, the average power measured at the NPE rejection port 1 was 87 mW, which corresponds to a pulse energy of 41 nJ.

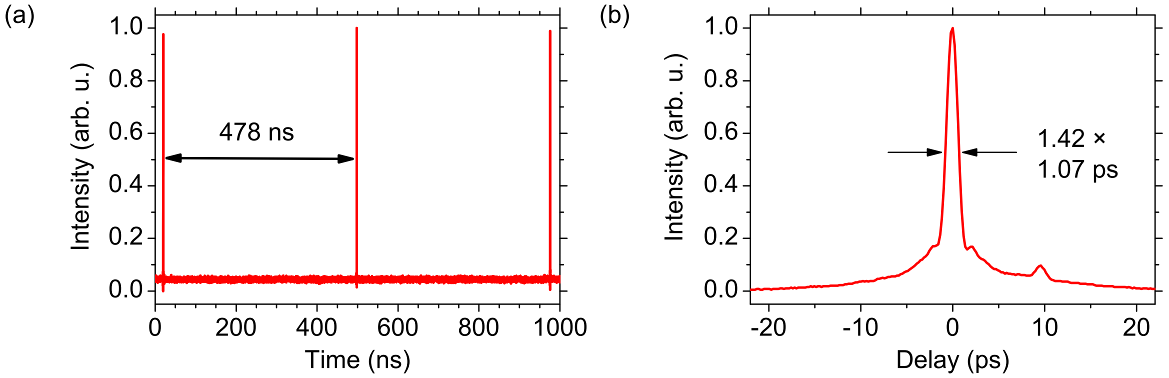

Figure 5.3: (a) Pulse train and (b) autocorrelation of the 41 nJ pulses at 2.1 MHz repetition frequency.

The autocorrelation of the pulses after compression is shown in Figure 5.3 (b). Its FWHM of 1.52 ps corresponds to a pulse duration of 1.07 ps assuming a deconvolution factor of 1.42, which was calculated from the ratio of the pulse duration and autocorrelation width of the Fourier limited pulse. The side peak at a delay of 9.6 ps is due to a reflection at the beam splitter inside the autocorrelator and existed independently of the pulse parameters.

The output spectrum with a center wavelength of 1031 nm is shown in Figure 5.4 (a) and (b) in linear and logarithmic scale. It exhibits a spectral FWHM of 4.7 nm and steep edges on both sides.

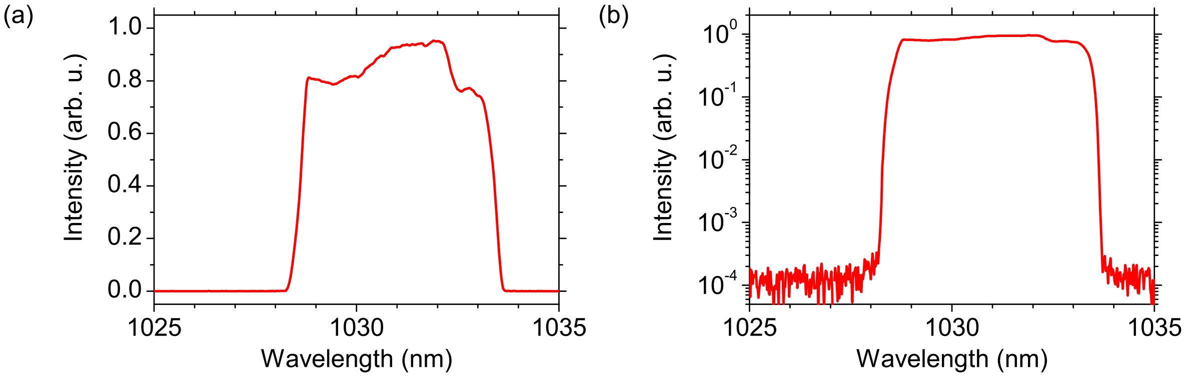

Figure 5.4: Spectrum of the 41 nJ pulses at 2.1 MHz in (a) linear and (b) logarithmic scale.

Measuring the duration of the chirped pulses directly from the oscillator was not possible as the pulses were too long to be measured with the available autocorrelator having a delay range of ±75 ps and too short for the available photodiodes. The pulse width was therefore estimated by the needed compressor dispersion of about $-11.6\ \mathrm{ps}^2$ to roughly 100 ps. When changing the filter bandwidth to 3.0 nm or 3.9 nm, the chirped pulse duration stayed approximately the same. To verify stable mode-locking without Q-switching, Q-switched mode-locking, or period doubling, the radio-frequency spectra of the output pulse train were measured. Figure 5.5 (a) shows a 500 Hz span measurement with a resolution bandwidth of 1 Hz. The linewidth is below 3.5 Hz at a signal to background ratio of 60 dB. Figure 5.5 (b) shows a measurement over a span of 100 MHz with a resolution bandwidth of 3 kHz, which also confirms stable mode-locking.

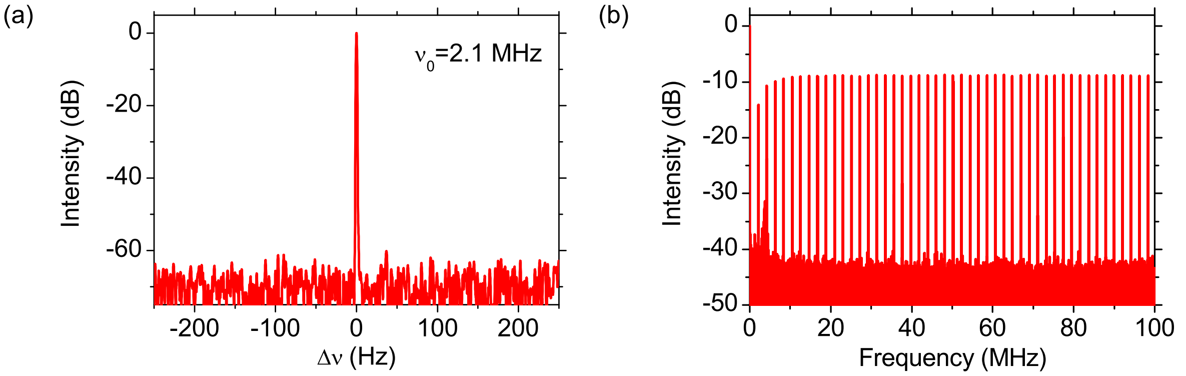

Figure 5.5: Radio frequency spectra of the 41 nJ pulses with a span of (a) 500 Hz and (b) 100 MHz.

At a pump power of 450 mW, a similar mode-locked state with a slightly higher pulse energy of 50 nJ and an average power of 105 mW could be set up with careful adjustment of the wave plates and the filter rotation. The autocorrelation of the compressed pulses with a FWHM of 1.4 ps is shown in Figure 5.6 (a). With the calculated deconvolution factor of 1.4, the pulse duration can be estimated to 1.0 ps. The corresponding spectrum is depicted in Figure 5.6 (b). At higher pump powers, the laser showed unstable multiple pulsing and single-pulse operation could not be achieved by adjusting the wave plates and the filter. This behavior can be explained by the overdriving of the NPE mode-locking mechanism [Ild04a].

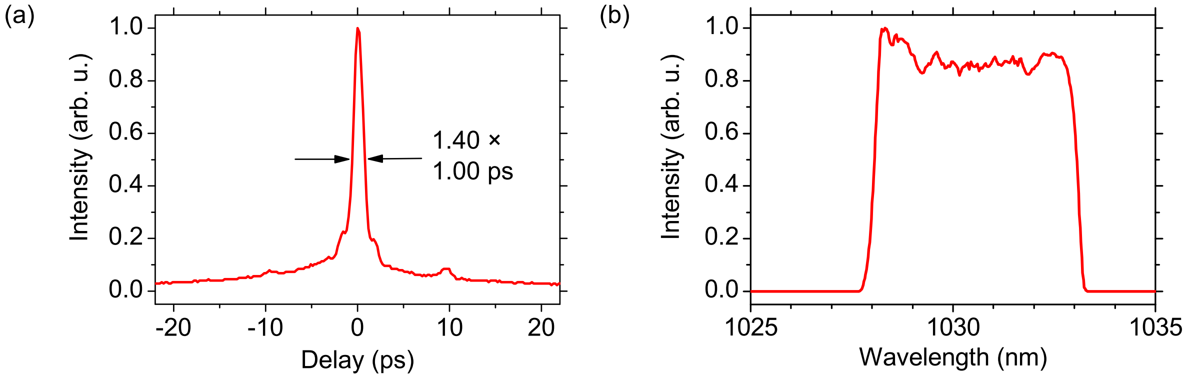

Figure 5.6: (a) Autocorrelation measurement of the 50 nJ pulses at 2.1 MHz repetition frequency and (b) corresponding spectrum with a filter bandwidth of 5.5 nm.

Due to the large fiber length and the NPE mode-locking, the laser is sensitive to fiber vibrations and temperature variations as these change the fiber birefringence and, therefore, the polarization state. For this reason, the fibers were fixed on the table. Although no temperature stabilization was applied, the oscillator was able to run for time durations larger than one hour. As the temperature in the laboratory varied over the day, a readjustment of the wave plates was necessary from time to time.

Variation of the filter bandwidth

In order to generate shorter pulse durations, the influence of the filter bandwidth on the pulse parameters was studied. Stable mode-locking at 2.1 MHz repetition frequency was also achieved with filter bandwidths of 3.0 nm and 3.9 nm. A combination of the 5 mm thick filter together with the 15 mm (20 mm) thick plate was used, which corresponds to a bandwidth of 3.9 nm (3.0 nm). For larger filter bandwidths than 5.5 nm, stable mode-locked operation could not be achieved.

Figure 5.7 (a) shows the intensity autocorrelation of the pulses for a filter bandwidth of 3.9 nm. Compared to the previous setup, the pulse energy at the pump power of 330 mW decreased to 27 nJ corresponding to 56 mW average power, but shorter pulse durations of 492 fs could be generated. The spectrum with a FWHM of 7.1 nm is depicted in Figure 5.7 (b) and allowed for pulses with a Fourier limit of 388 fs. The deviation of the pulse duration from the Fourier limit of 22 % is much smaller compared to the measurement with the 5.0 nm bandwidth filter.

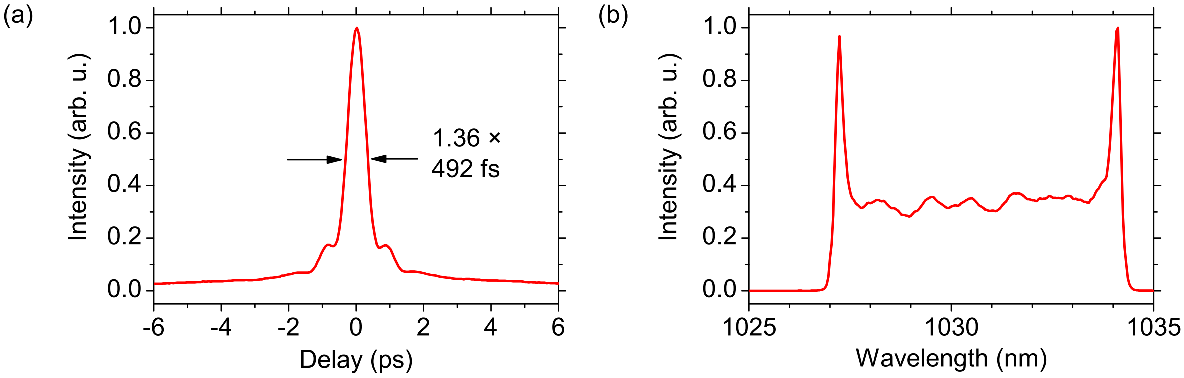

Figure 5.7: (a) Autocorrelation measurement of the 27 nJ pulses at 2.1 MHz repetition frequency and (b) corresponding spectrum using a filter bandwidth of 3.9 nm.

The filter bandwidth was further decreased to 3.0 nm. At the same pump power of 330 mW, the oscillator emitted pulses with energies of 21 nJ with an average output power of 44 mW. The pulse duration can be estimated to 503 fs as shown in the autocorrelation in Figure 5.8 (a) exhibiting a width of 690 fs. The deviation of the pulse duration from the Fourier limit of 18 % is smaller compared to using larger filter bandwidths. The spectrum with a FWHM of 6.5 nm is depicted in Figure 5.8 (b). The results are similar to the measurements with the 3.9 nm filter bandwidth.

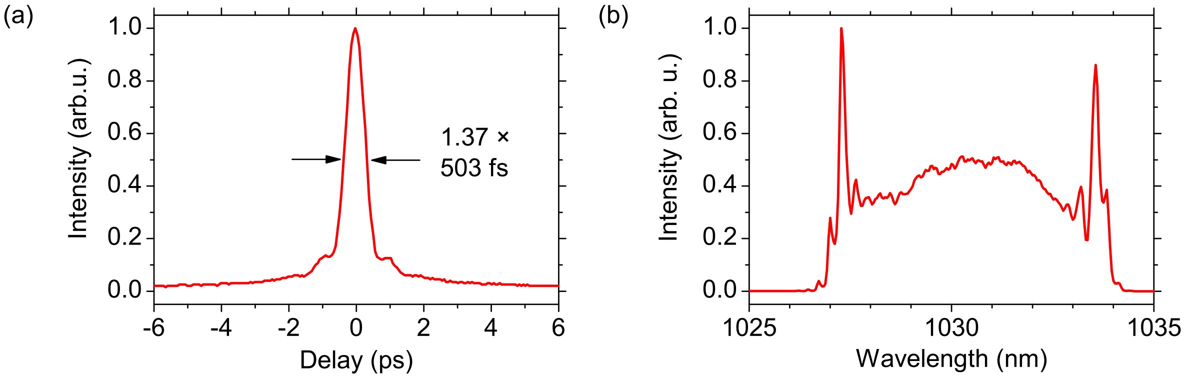

Figure 5.8: (a) Autocorrelation measurement of the 21 nJ pulses at 2.1 MHz repetition frequency and (b) corresponding spectrum using a filter bandwidth of 3.0 nm.

5.4 Results at 5.4 MHz repetition frequency

It can be shown that in order to achieve shorter pulse durations from an all-normal dispersion fiber laser with a low repetition rate, the overall dispersion of the above described oscillator should be reduced [Chi10, Cho08a, Cho08c]. Hence, the fiber was shortened and, consequently, the repetition rate increased.

At the repetition frequency of 5.4 MHz, the corresponding intracavity fiber length was approximately 37 m. The active fiber was 29 cm long, whereas the passive fiber behind the ytterbium-doped fiber had a length of 1.42 m. A combination of the 5 mm and the 15 mm thick quartz plates was used for spectral filtering of the pulses, which resulted in an effective filter bandwidth of 3.9 nm. All other optical components were unchanged as described in the last section.

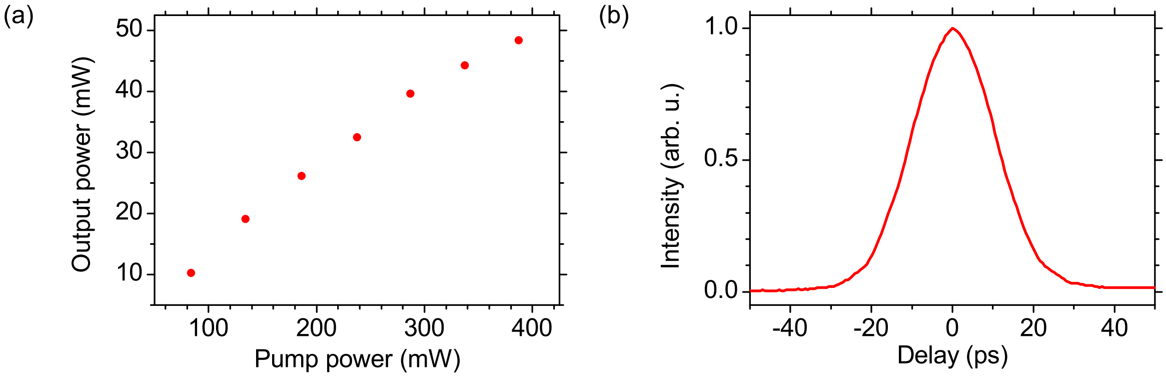

Figure 5.9: (a) Characteristic of the laser with 5.4 MHz repetition frequency and a filter bandwidth of 3.9 nm. (b) Autocorrelation measurement of the uncompressed pulses with energies of 9 nJ.

Figure 5.9 (a) shows the almost linear power characteristics of the laser. A maximum of 48 mW at a pump power of 387 mW could be achieved corresponding to a maximum pulse energy of about 9 nJ. With this setup, the pulses directly from the oscillator were also strongly chirped but were short enough to be measured with the available autocorrelator considering its limited delay range. Figure 5.9 (b) shows a typical autocorrelation of the chirped pulses with pulse energies of 9 nJ with a FWHM of approximately 25 ps. The pulses were compressed using a reflection grating pair with a line density of 1200/mm.

Figure 5.10 (a) shows the autocorrelation of the compressed pulses with energies of 9 nJ. With the deconvolution factor of 1.36, the pulse duration can be estimated to 302 fs. The corresponding spectrum is shown in Figure 5.10 (b). It shows the typical peaks at the edges, which are due to

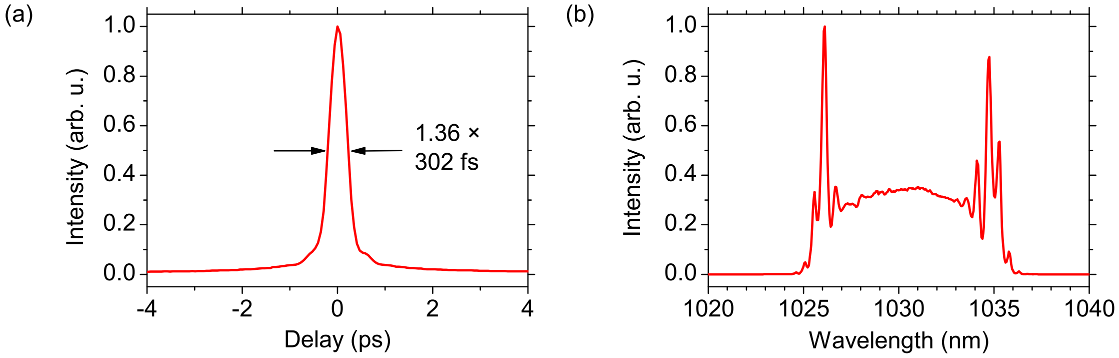

Figure 5.10: (a) Autocorrelation measurement of the 9 nJ pulses at 5.4 MHz repetition frequency and (b) corresponding spectrum with a filter bandwidth of 3.9 nm.

the combined action of normal group-velocity dispersion, self-phase modulation, and spectral filtering. The influence of the pulse energy due to pump power variation for this setup is discussed in the following.

Variation of the pulse energy

Figure 5.11 (a) shows the spectral width as a function of pulse energy. The FWHM continuously increases with pulse energy from 5.2 nm at 2 nJ to 9.5 nm at 9 nJ. The corresponding Fourier limited as well as the measured pulse duration is depicted as a function of pulse energy in Figure 5.11 (b). The Fourier limited pulse duration continuously decreases with increasing pulse energy from 495 fs at 2 nJ to 257 fs at 9 nJ. Experimentally, the shortest pulse duration with 302 fs could be achieved at pulse energies of 8 nJ. The pulses with larger energy may have accumulated a larger nonlinear phase, which could not be compensated to generate shorter pulses despite the larger spectral width.

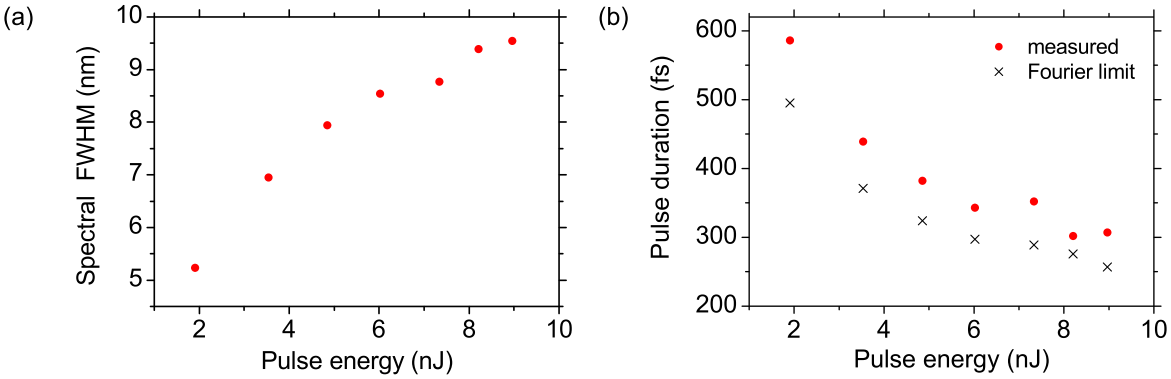

Figure 5.11: (a) Spectral width and (b) pulse duration as a function of pulse energy at 5.4 MHz repetition rate and 3.9 nm filter bandwidth.

Figure 5.12 (a) to (f) show the spectral evolution with increasing pulse energy. At a value of 1.9 nJ, the spectrum is smooth and has the characteristic side peaks. When the pulse energy increases, the spectral width becomes larger and the spectra become also more structured. This behavior was also observed in simulations and experiments described in Reference [Cho07] for smaller intracavity fiber lengths, and is thus also an intrinsic feature of dissipative-soliton fiber oscillators with low repetition frequencies.

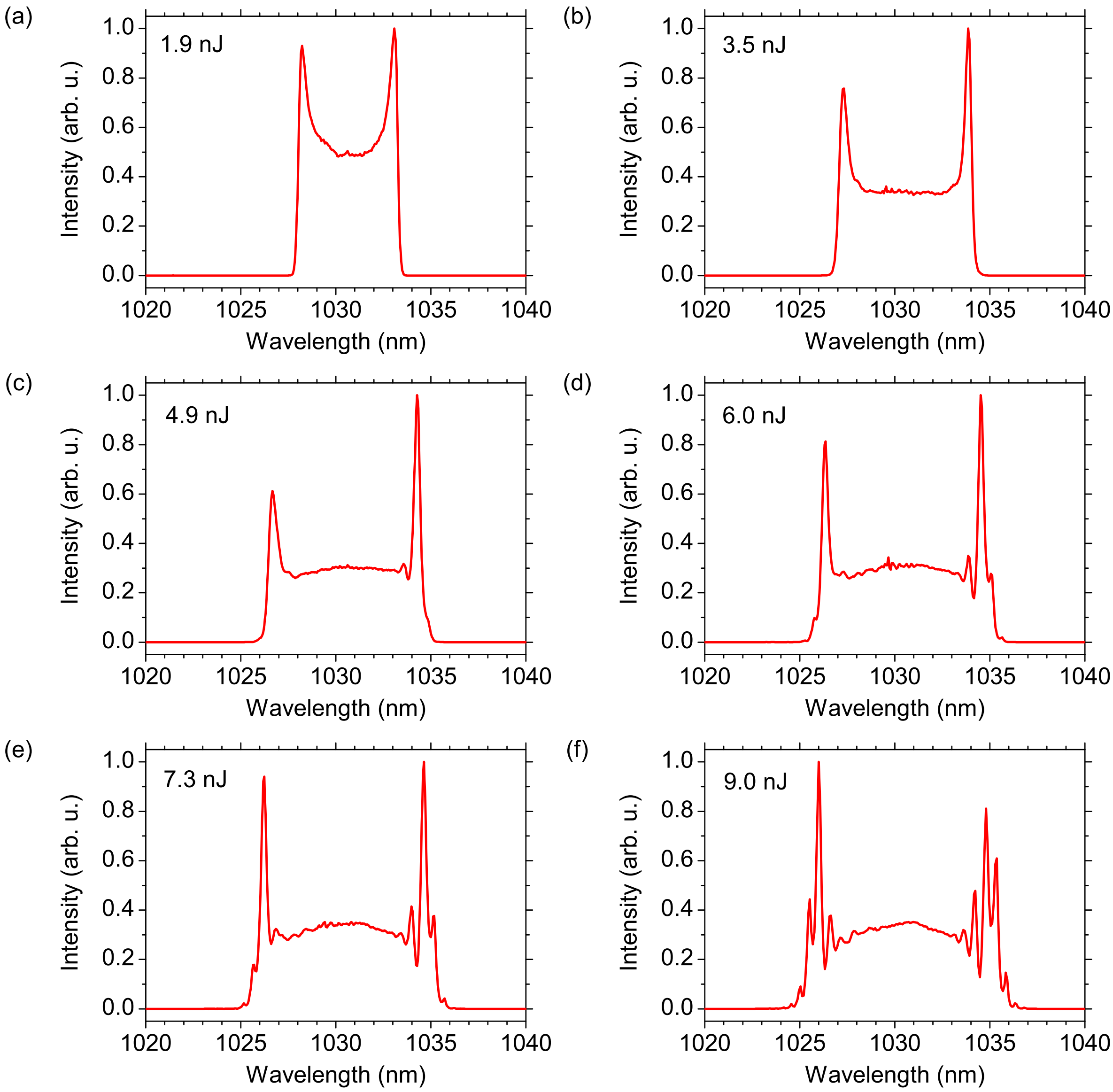

Figure 5.12: Output spectra of the oscillator with the repetition frequency of 5.4 MHz and 3.9 nm filter bandwidth at the indicated pulse energies.

5.5 Results at 29 MHz repetition frequency

A further reduction of the intracavity dispersion was realized by decreasing the total fiber length to about 6.4 m. The experimental setup is similar to that of the above described oscillators. The active fiber was 40 cm long and the passive fiber behind it 1 m. Together with about 1 m of free-space beam propagation, the corresponding pulse repetition frequency was measured to be 29 MHz. The total resonator dispersion was thus about 0.12 ps^2. Stable mode-locking could be achieved with filter bandwidths between 5.7 nm and 12.0 nm. Above a pump power of about 350 mW, mode-locking was initiated after proper adjustment of the wave plates. As expected, the laser was more robust against environmental disturbances like vibrations than the described oscillators with a smaller repetition frequency.

The autocorrelation of the compressed pulses and the corresponding spectrum for the setup with a 7.3 nm filter bandwidth are shown in Figure 5.13 (a) and (b). At an average power of 119 mW, corresponding to pulse energies of 4.1 nJ, the pulses could be dechirped to 199 fs. The results for different filter bandwidths are shown in Table 5.1. The shortest pulse durations could be achieved with bandwidths of 6.6 nm, 7.3 nm, and 8.2 nm. With smaller and larger filter bandwidths, the compressed pulse durations increased.

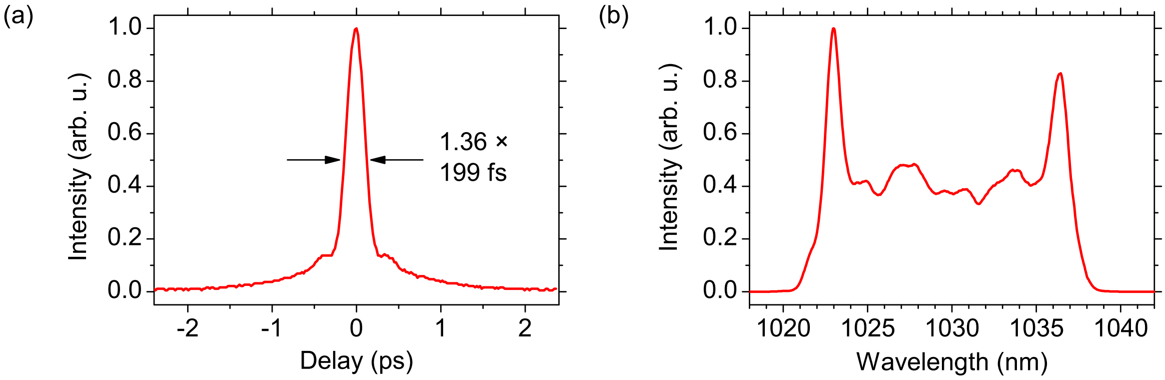

Figure 5.13: (a) Autocorrelation and (b) output spectrum of the oscillator with the repetition frequency of 29 MHz and 7.3 nm filter bandwidth.

Here, the pulse energy was not limited by the onset of multiple pulsing but by the limited available pump power. The attempt of integrating a second laser diode for counter-propagating pumping was not successful. Despite the implementation of two dichroic filters and increasing the active fiber length, one diode was destroyed. However, the pulses were compressed using fused silica transmission gratings with a line density of 1250/mm and a total compressor efficiency of about 80 %.

Filter bandwidth	Output power	Pulse energy	Pulse duration
5.7 nm	116 mW	4.0 nJ	222 fs
6.6 nm	90 mW	3.1 nJ	197 fs
7.3 nm	119 mW	4.1 nJ	199 fs
8.2 nm	105 mW	3.6 nJ	194 fs
9.7 nm	55 mW	1.9 nJ	293 fs
12.0 nm	61 mW	2.1 nJ	270 fs

Table 5.1: Pulse parameters of the oscillator with 29 MHz repetition frequency.

5.6 Conclusion

In this chapter, the pulse regime of dissipative solitons in all-normal dispersion fiber oscillators was studied regarding low repetition frequencies. By varying the intracavity fiber length, oscillators with repetition rates of 29 MHz, 5.4 MHz, and 2.1 MHz could successfully be mode-locked. It turned out that with increasing intracavity dispersion—equivalent to increasing the fiber length—the chirped output pulse duration increased. Simultaneously, the spectral widths decreased and, consequently, the dechirped pulse durations increased. For larger intracavity fiber lengths, birefringent filters with smaller spectral bandwidths had to be used. The shortest dechirped pulse durations achieved were 194 fs at 29 MHz repetition frequency, 302 fs at 5.4 MHz, and 1.0 ps at 2.1 MHz.

By increasing the intracavity fiber length compared to previously demonstrated dissipative-soliton lasers, larger pulse energies could be generated by using single-mode fibers. Maximum pulse energies of 4.1 nJ at 29 MHz, 9 nJ at 5.4 MHz, and 50 nJ at 2.1 MHz repetition frequency were achieved. Further scaling of the pulse energy does not seem feasible using single-mode fibers as initiating mode-locking becomes more difficult at larger intracavity fiber lengths. Due to the increased intracavity fiber dispersion, the needed compressor dispersion also increased. At the repetition frequency of 2.1 MHz, grating separations larger than 1.5 m, measured along the beam, were necessary for the compression of the pulses. This separation could be reduced by the usage of gratings with a larger line density but this would also induce larger amounts of third-order dispersion, which could lead to longer compressed pulses. However, the needed large external compressor dispersion sets a practical limitation concerning the overall size of the laser system.

6 High-average power dissipative-soliton laser

As the optical power delivered by single-mode fiber-coupled laser diodes is limited to approximately 1–2 W at 976 nm wavelength, a further pulse parameter scaling of dissipative-soliton lasers is challenging using the core pumping scheme as studied in the last chapter. With core pumping, an increase in pulse energy is thus only possible by reducing the repetition frequency at a constant achievable average power. But, as shown in the last chapter, inserting additional fiber into the cavity leads to an increased total dispersion and to larger compressed pulse durations. Leaving the cavity dispersion small by using a large intracavity free-space propagation otherwise opposes the advantages of the waveguide medium. A way around this issue is the implementation of the cladding pumping scheme, where the pump light is not coupled into the doped fiber core but into a waveguiding cladding, which surrounds the core [Sni88, Rip95, Dom99]. With this scheme, the large output powers from multi-mode fiber-coupled diode lasers can be successfully used to amplify single-mode radiation.

In this chapter, a dissipative-soliton laser based on double-cladding fibers is demonstrated. It was passively mode-locked by nonlinear polarization evolution (NPE) in combination with spectral filtering and generated pulse energies of 31 nJ and average powers of 1.5 W before compression. At the repetition frequency of 48 MHz, the pulses could be compressed to durations of 139 fs having pulse energies of 25 nJ. The average power behind the compressor was 1.2 W. The performance of this laser is similar to a recently demonstrated double-cladding dissipative-soliton laser [Kie09], which was capable of producing pulses with energies of 15 nJ and 80 fs after compression at the repetition frequency of 70 MHz.

6.1 Experimental setup

A sketch of the experimental setup is shown in Figure 6.1. It is similar to the oscillators described in the last chapter. The ring oscillator consists of an about 85 cm long free-space and an approximately 3.6 m long fiber section. In the direction of pulse propagation, the light is coupled into the passive fiber Liekki Passive-10/125 with a 10 µm core diameter, travels through the in-house made pump combiner with single-mode signal feedthrough, before it is subsequently amplified in an about 1.5 m long ytterbium-doped double-cladding fiber Liekki Yb1200-10/125DC. A multi-mode fiber-coupled laser diode, emitting up to 25 W at 976 nm, was used as a pump source. Its output fiber with a core diameter of 105 µm was fusion spliced to the pump combiner. The amplified beam was collimated by a lens with focus length of 8 mm and sent through a dichroic mirror, which filtered out the unabsorbed pump radiation.

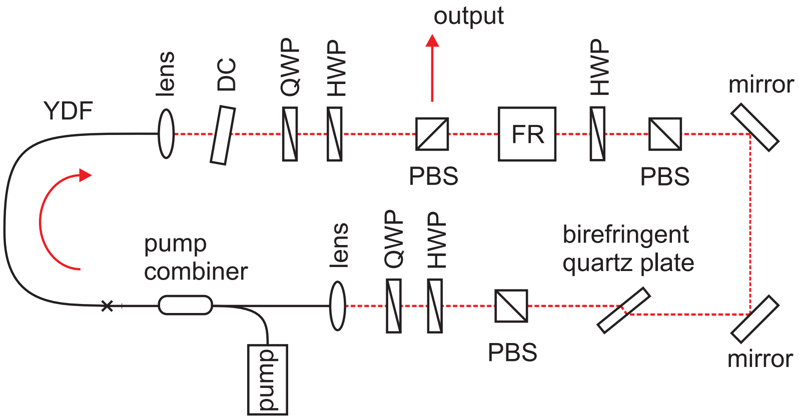

Figure 6.1: Experimental setup. HWP half-wave plate, QWP quarter-wave plate, DC dichroic mirror, PBS polarizing beam splitter, FR Faraday rotator, YDF ytterbium-doped fiber.

Two polarizing beam splitters (PBS) together with a TGG crystal based Faraday rotator were used as an optical isolator to ensure unidirectional pulse propagation. The first PBS was also used as the rejection port for nonlinear polarization evolution mode-locking and served as the main output port. To ensure a consistent pulse evolution over one round-trip, a 5 mm thick quartz plate was used for spectral filtering. It was placed in the beam under Brewster's angle of 57° between two polarizing beam splitters. The resulting filter bandwidth was 12 nm. Two half-wave and two quarter-wave plates were implemented to adjust the polarization state for the NPE mode-locking. The light was coupled into the fiber core with a lens having a focus length of 8 mm. A photograph of the oscillator is shown in Figure 6.2.

6.2 Results at 48 MHz repetition frequency

Figure 6.3 (a) shows the spectrum measured at the NPE rejection port, which is labeled as output in Figure 6.1. It exhibits a RMS width of 16.4 nm and a FWHM of 25 nm. The corresponding pulse energy was 31 nJ before and 25 nJ after compression with fused silica

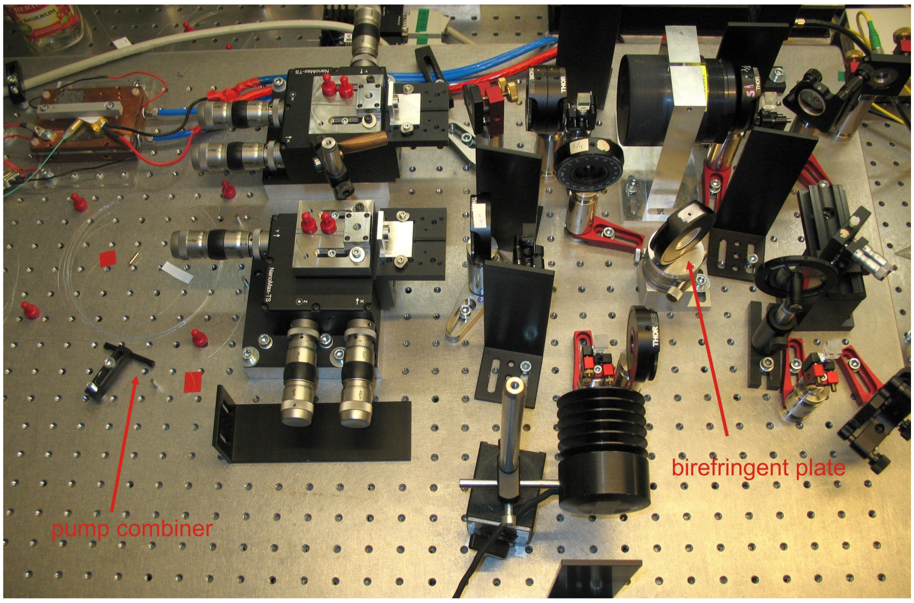

Figure 6.2: Photograph of the double-cladding dissipative-soliton laser.

transmission gratings having a total efficiency of about 80 %. The average output powers before and after compression were 1.5 W and 1.2 W, respectively. The pulse train measured with a fast photodiode is depicted in Figure 6.3 (b). The temporal pulse separation of 20.7 ns corresponds to the fundamental repetition frequency of 48.3 MHz.

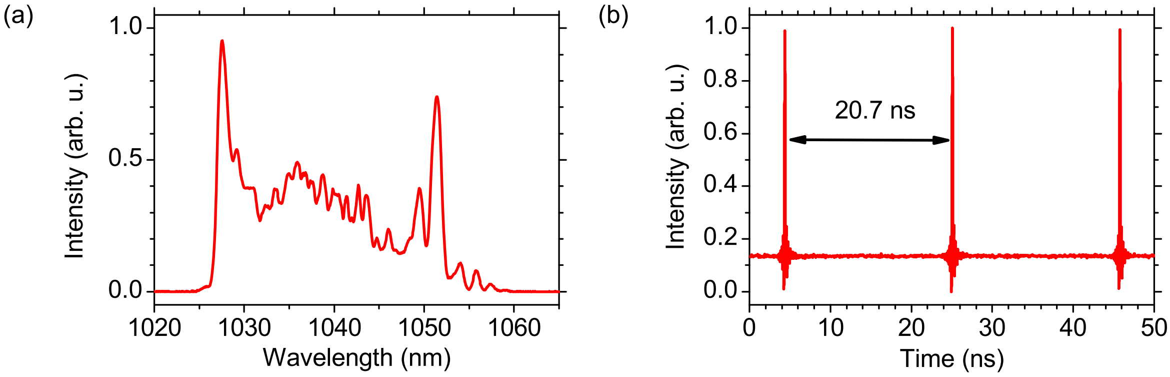

Figure 6.3: (a) Output spectrum of the oscillator and (b) corresponding pulse train.

The pulses directly from the oscillator were slightly chirped. Figure 6.4 (a) shows the corresponding autocorrelation with a FWHM of 4.6 ps. With the deconvolution factor of 1.37, the chirped pulse duration was about 3.4 ps. The pulses were externally compressed using in parallel arranged fused silica transmission gratings with a line density of 1250/mm and a perpendicular separation of about 5 mm. This corresponds to a compressor dispersion of about -0.07 ps^2. The autocorrelation of the dechirped pulses is shown in Figure 6.4 (b), having a FWHM of 191 fs. Using the deconvolution factor, the compressed pulse duration can be estimated to be 139 fs.

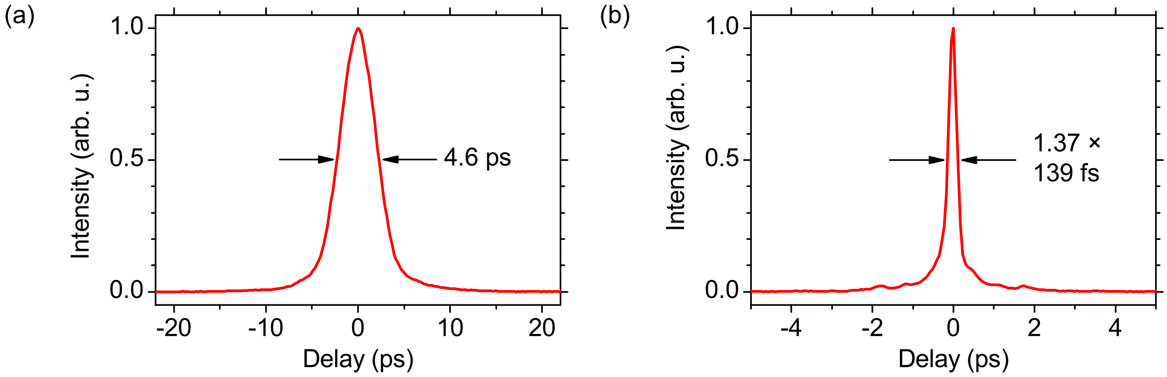

Figure 6.4: Autocorrelation of the (a) uncompressed and (b) compressed pulses.

To verify stable mode-locked operation, radio-frequency spectra were measured with a fast photodiode and an electrical spectrum analyzer. The measured spectra with a span of 2 GHz and a span of 10 kHz around the center repetition frequency are shown in Figure 6.5 (a) and (b), respectively. Both confirm single-pulse mode-locking without Q-switching, Q-switched mode-locking, or period doubling.

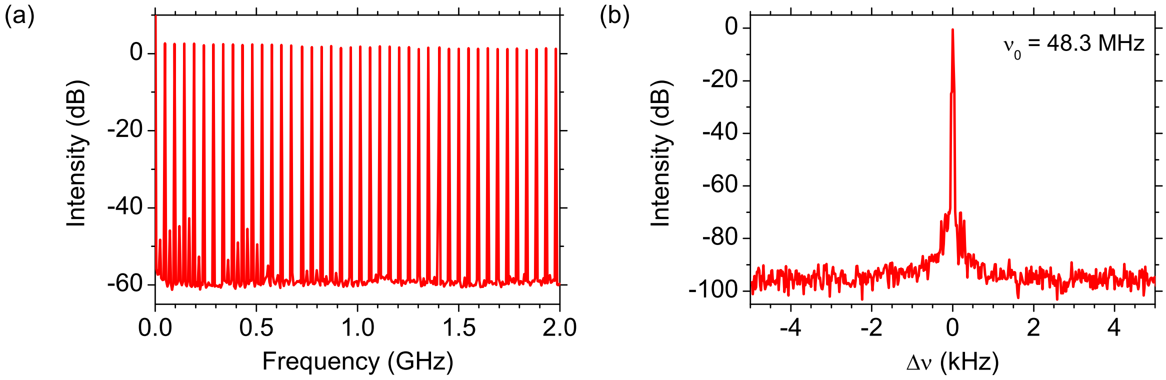

Figure 6.5: Radio frequency spectra of the pulse train with a span of (a) 2 GHz and (b) 10 kHz.

When first assembling the laser, it turned out that it tended to operate exclusively in the continuous-wave (CW) regime. The cause were small back reflections inter alia at the angle-cleaved fiber end facets. The following procedure helped suppressing CW operation and finally enabling mode-locking. First, the fiber ends were angle-cleaved and the beam collimated. The pump power was subsequently increased, while the laser beam was blocked in the free-space section of the resonator and the output spectrum was checked with an optical spectrum analyzer. This typically resulted in a broad amplified spontaneous emission (ASE) spectrum for small pump powers up to the pump power threshold, where the broad ASE spectrum changed to a single CW emission peak. As the beam was blocked, the CW operation was caused by back reflections inside the cavity and the mentioned pump power threshold was a measure for the fraction of back reflected power. The smaller the back reflected power fraction, the higher was the pump power threshold for CW operation. After maximizing this pump power threshold by repeated angle-cleaving of the fibers, the beam block was removed and it was successfully searched for mode-locking by adjusting the birefringent filter as well as the wave-plates inside the cavity.

6.3 Conclusion

A dissipative-soliton oscillator with an average output power of 1.2 W after compression was demonstrated. The corresponding pulse energy at the repetition rate of 48 MHz was 25 nJ. The large average power—compared to the core-pumped oscillators—was achieved by using the double-cladding pumping scheme in combination with a high-power multi-mode pump diode. The achieved compressed pulse duration was 139 fs.

Because the oscillator was not optimized concerning pulse energy and pulse duration, the output pulse parameters are expected to be further scalable. The experimental experience gained by studying this laser helped building double-cladding pumped large-mode area dissipative-soliton lasers with improved output pulse parameters [Chi11, Chi12]. Record pulse parameters using the dissipative-soliton regime in combination with double-cladding pumping were recently demonstrated using a rod-type fiber laser, which emitted 91 fs long pulses with energies of 0.8 µJ at average powers of 60 W [Bau12].

7 All-fiber dissipative-soliton laser

Despite the impressive pulse parameters achieved with dissipative-soliton oscillators, they almost exclusively contain free-space optics [Wis08]. A reason for this may be the lack in performance and availability of fiber-based components at 1 µm wavelength compared to bulk optics, which can handle much higher peak and average powers. However, all-fiber-integrated oscillators would fully profit from the advantages of the waveguide medium such as alignment-free operation and an improved decoupling from technical noise and would thus be very attractive as a seed source for all-fiber CPA systems [Mor12].

A few fully fiber-integrated ytterbium-based femtosecond lasers without dispersion compensation have been demonstrated. Pulses with durations of 5.6 ps and energies of 1.3 nJ could be generated in a linear resonator by nonlinear polarization rotation mode-locking in polarization-maintaining fibers [Nie07]. Another approach used a semiconductor saturable absorber mirror (SESAM) applied to a fiber connector in combination with nonlinear polarization evolution (NPE) mode-locking to achieve pulses with energies of 0.8 nJ, which could be dechirped to 627 fs [Pro07]. The same combination of SESAM and NPE was successfully applied to a fiber-integrated oscillator to generate pulses with 0.2 nJ energy, which were compressed to 195 fs duration [Fek09]. Using a saturable absorber based on carbon nanotubes resulted in pulse energies of 3 nJ and dechirped pulse durations of 235 fs [Kie08]. Similar results with 230 fs and 1.5 nJ were demonstrated using a fiber-based Lyot filter [Özg10]. The application of NPE and a fiber coupler based filter for stabilizing mode-locking resulted in 1.8 nJ pulses with compressed pulse durations of 179 fs [Sch08]. Shorter pulses with 131 fs duration could be demonstrated by using dispersion-managed soliton pulse shaping but exhibiting comparatively low pulse energies of about 55 pJ [Sho10].

In this chapter, a passively mode-locked fiber laser is studied, which, to the best of knowledge, emitted the largest pulse energies and shortest pulses from an all-fiber-integrated ytterbium-based laser. Mode-locking was achieved by NPE while utilization of a 90 % linear output coupler reduced the intracavity peak power to prevent damage of the fiber-coupled isolator. Linearly polarized pulses with energies of 3.6 nJ at a repetition frequency of 71.3 MHz and an average power of 259 mW were generated. After compression, pulses with durations of 76 fs and energies of 2.2 nJ were available. To achieve a minimum pulse duration with this setup, the total cavity dispersion was minimized by reducing the intracavity fiber length [Cho08b, Cho08a, Cho08c, Chi10] while the influence of NPE and spectral broadening had to be strong enough for mode-locking.

The studied oscillator was subsequently used as a seed source for the fiber amplifiers described in Chapter 8 and 9. Parts of this section have been published in Reference [Mor11].

7.1 Experimental setup

Figure 7.1 shows a sketch of the experimental setup. It incorporated a 21 cm long highly ytterbium-doped fiber with a 4.2 µm mode field diameter (MFD) and a 3.1 wt% doping concentration resulting in a 16 dB/cm peak absorption at 976 nm. The active fiber was core-pumped by a single-mode laser diode. A wavelength-division multiplexer (WDM) combined pump and signal light at 976 nm and 1030 nm, respectively. For pumping the active fiber, 731 mW at 976 nm wavelength were available behind the WDM. 58 cm of Corning HI 1060 Flex fiber with a MFD of 4.2 µm was spliced to the active fiber to increase the impact of the fiber nonlinearity. The length of this fiber was crucial for stable mode-locked operation. A too short fiber resulted in solely continuous-wave operation while a longer fiber lead to overdriving of the NPE mode-locking mechanism. All other passive fibers in the cavity had a MFD of about 6.3 µm.

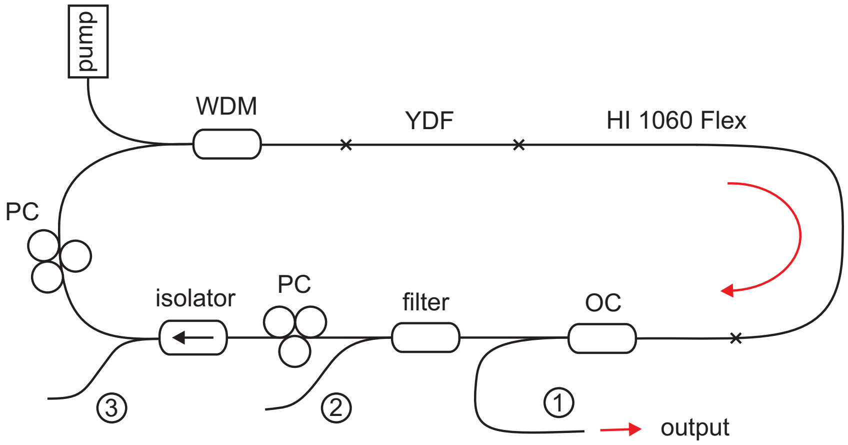

Figure 7.1: Schematic of the fiber ring cavity. WDM wavelength-division multiplexer, YDF ytterbium-doped fiber, OC output coupler, PC polarization controller.

For the main out-coupling, a fused fiber coupler with a 90 % output coupling ratio was used to reduce the pulse energy and to protect the fiber-based components from damage. A spectral filter was implemented as a second small-bandwidth WDM from AC Photonics, USA. Its spectral properties are shown in Figure 7.2 exhibiting an almost sinusoidal transmission spectrum with a FWHM of 10.6 nm around the center wavelength of 1033.8 nm. For measuring the spectral properties, a broadband amplified spontaneous emission light source was used.

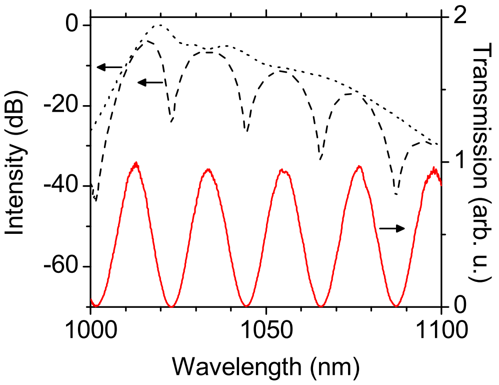

Figure 7.2: Measured relative transmission (solid curve) of the small bandwidth WDM and the corresponding spectra of the input (dotted) and output (dashed) light.

A fiber-based Faraday isolator ensured unidirectional pulse propagation and simultaneous outcoupling of light with one polarization for NPE mode-locking by the included polarizer. Two mechanical polarization controllers, based on squeezing and twisting of the fiber, were included to adjust the state of polarization before and behind the isolator. The total intracavity fiber length was about 2.9 m resulting in a total cavity dispersion of about 0.07 ps^2, while the output fiber pigtail had a length of approximately 1.0 m. The angle-polished connectors at the ports 1, 2, and 3 (see Figure 7.1) were supplied with anti-reflective coatings for minimal back reflections and reduced chance of fiber facet damage by the appearance of Q-switched pulses when searching for mode-locking.

As the NPE mode-locking mechanism is sensitive to changes of the polarization state in the resonator, the fibers were fixed with rubber mats and the housing was stabilized at a temperature of 27 °C with passive air-cooled heat-sinks under the enclosure. Otherwise, the induced birefringence would influence the mode-locking state or, at worst, inhibit mode-locking itself. A photograph of the laser with a footprint of 40 × 40 cm^2 is shown in Figure 7.3.

7.2 Results at 71 MHz repetition frequency

After the polarization controllers had been adjusted, self-starting mode-locking was achieved by increasing the pump power above the threshold of about 460 mW. Figure 7.4 (a) shows the stable

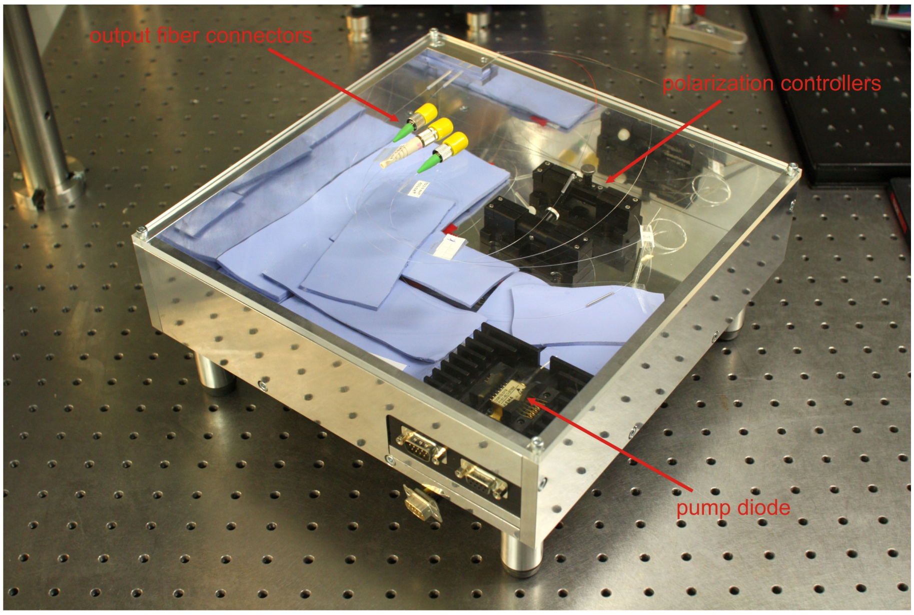

Figure 7.3: Photograph of the laser. The fiber components are fixed under rubber mats.

single-pulse train at the pump power of 731 mW measured with a photodiode having a 18.5 ps rise time and an oscilloscope with a bandwidth of 6 GHz. The pulses have a temporal separation of 14 ns corresponding to the repetition frequency of 71.3 MHz. Single-pulse operation was verified by checking with a fast photodiode and a sampling oscilloscope with a bandwidth of 70 GHz as well as with a long-range autocorrelator having a 150 ps scan range. Switching the pump diode off and on again led to the same mode-locked state.

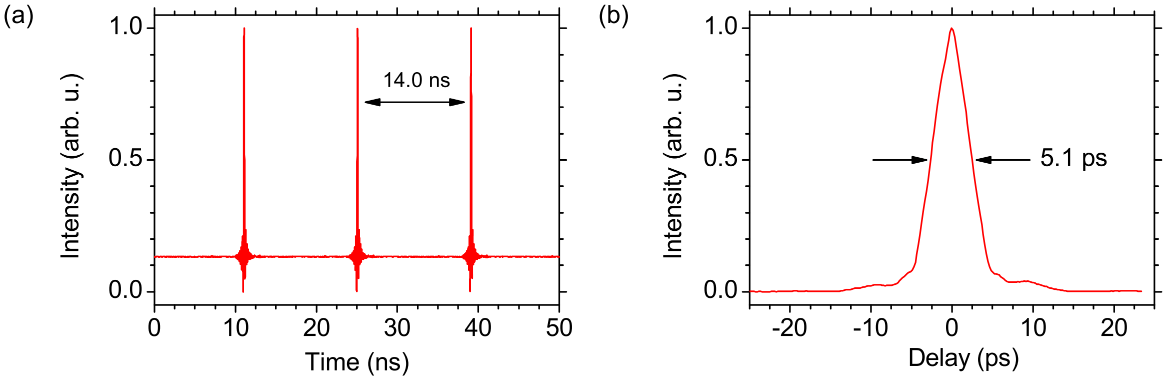

Figure 7.4: (a) Photodetector signal of the pulse train. (b) Autocorrelation of the uncompressed pulses.

Figure 7.4 (b) shows the autocorrelation of the uncompressed pulses with a FWHM of 5.1 ps. The small side peaks at ±9.6 ps delay were due to reflections at the approximately 1 mm thick beam splitter in the autocorrelator and appeared independently of the mode-locked state. For pulse compression, in parallel arranged reflection gratings with a line density of 300/mm were used.

This line density was appropriate for the relatively small amount of needed compressor dispersion and led to a manageable perpendicular grating separation of about 17 cm. Additionally, the gratings exhibit a third-order to second-order dispersion ratio of -1.7 fs, which is small compared to larger grating line densities and resulted in minimized TOD induced pulse distortion. With the total compressor efficiency of about 61 %, the pulse energy after dechirping was 2.2 nJ. The dispersion of the grating arrangement was calculated to approximately -0.06 ps^2. As the light from the main output was nonlinearly polarized from the action of NPE, a polarizing beam splitter was placed in the beam. A combination of a quarter- and a half-wave plate in front of the PBS was adjusted to achieve the smallest autocorrelation width. The corresponding transmitted average power of the linearly polarized light was 259 mW, while an average power of 44 mW was filtered out. Thus, pulse energies of 3.6 nJ were available in front of the compressor.

Figure 7.5 (a) shows the autocorrelation of the compressed pulses with a FWHM of 103 fs and the autocorrelation of the Fourier limited pulses having a FWHM of 86 fs. With the deconvolution factor of 1.351, calculated from the Fourier limited pulse and the autocorrelation widths, the durations of the chirped and dechirped pulses were 3.8 ps and 76 fs, respectively. The compressed pulse width is thus 19 % above the Fourier limit of 64 fs.

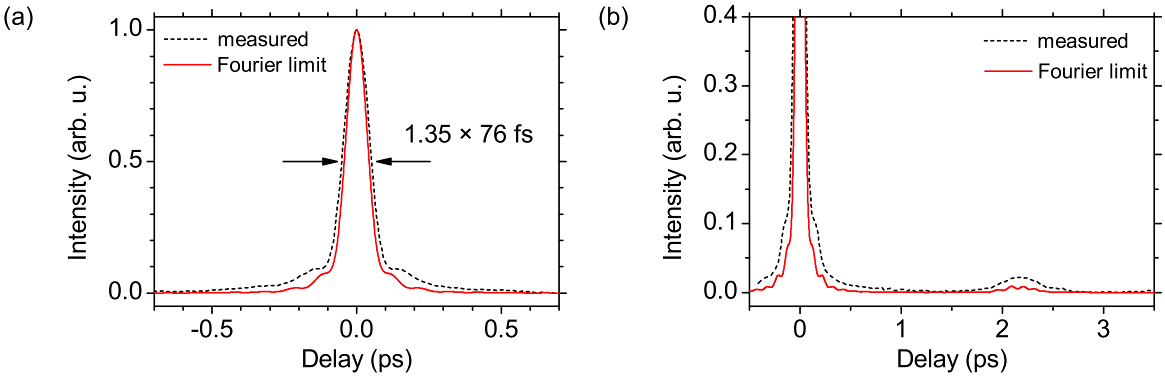

Figure 7.5: (a) Autocorrelation of the compressed pulses (solid curve) and of the Fourier limited pulses (dashed curve) and (b) detail of the side peak in the autocorrelation.

In the autocorrelation measurement, a satellite pulse was noticed at approximately 2.2 ps apart from the main pulse. It contained only a small fraction of the pulse energy as can be seen in the autocorrelation in Figure 7.5 (b). The origin of the pulse may be explained by the periodic transmission function of the small-bandwidth filter. As the filter had a FWHM of 10.6 nm and the output spectra were much broader, the filter transmitted light at wavelengths, that correspond to the side maxima of its transmission function. These pulses at different wavelengths were then temporally separated by the group delay dispersion of the fiber. No further side pulses were observed. From the theory of Fourier transformation, it follows that a temporal side pulse corresponds to a modulation of the spectrum. The output spectrum depicted in Figure 7.6 (a) was thus modulated having a FWHM of 39.7 nm and a center wavelength of 1032 nm. It exhibits the typical peaked edges of all-normal dispersion fiber lasers. The modulation periodicity of 1.6 nm corresponds to the satellite pulse separation of 2.2 ps. Figure 7.6 (b) shows the spectrum, which was filtered out by the PBS.

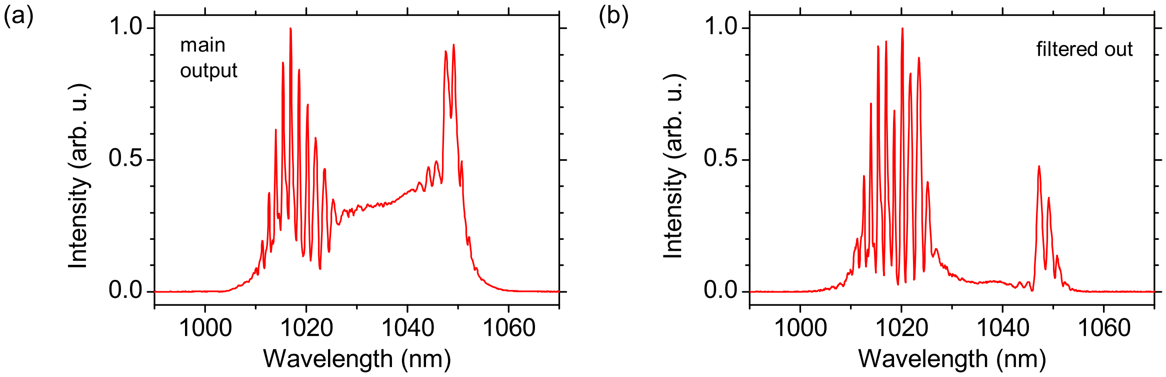

Figure 7.6: Measured spectra. (a) Transmitted and (b) rejected signal from the PBS behind the output coupler.

The stability of the generated pulse train was analyzed by measuring the radio-frequency spectra with an electrical spectrum analyzer and a fast photodetector. Figure 7.7 (a) and (b) show the results for a span of 1 GHz and 1 kHz, which indicate stable mode-locked operation without sidebands or harmonic frequencies at least 70 dB below the level at the fundamental repetition frequency. Additionally, the temperature-stabilized laser had been mode-locked for several days without any notable changes in spectrum, output power, or repetition frequency.

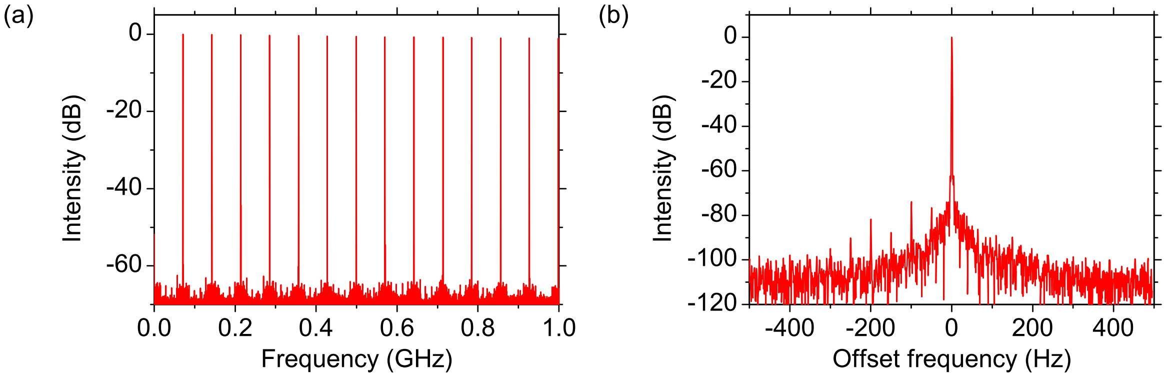

Figure 7.7: Radio-frequency spectra with a span of (a) 1 GHz and (b) 1 kHz centered at the fundamental repetition rate of 71 MHz.

7.3 Influence of pulse energy variation

To study the nonlinear dynamics of the laser, the pump power was varied, while the laser setup was unchanged and the case temperature held constant. The polarization controllers were adjusted to allow for a large pump power variation while the laser was mode-locked. The output characteristic is shown in Figure 7.8 (a) and exhibits an almost linear dependence of the average power on the pump power. For low pump powers above about 100 mW, the laser showed continuous-wave operation, while self-starting mode-locking was achieved above the threshold of about 460 mW.

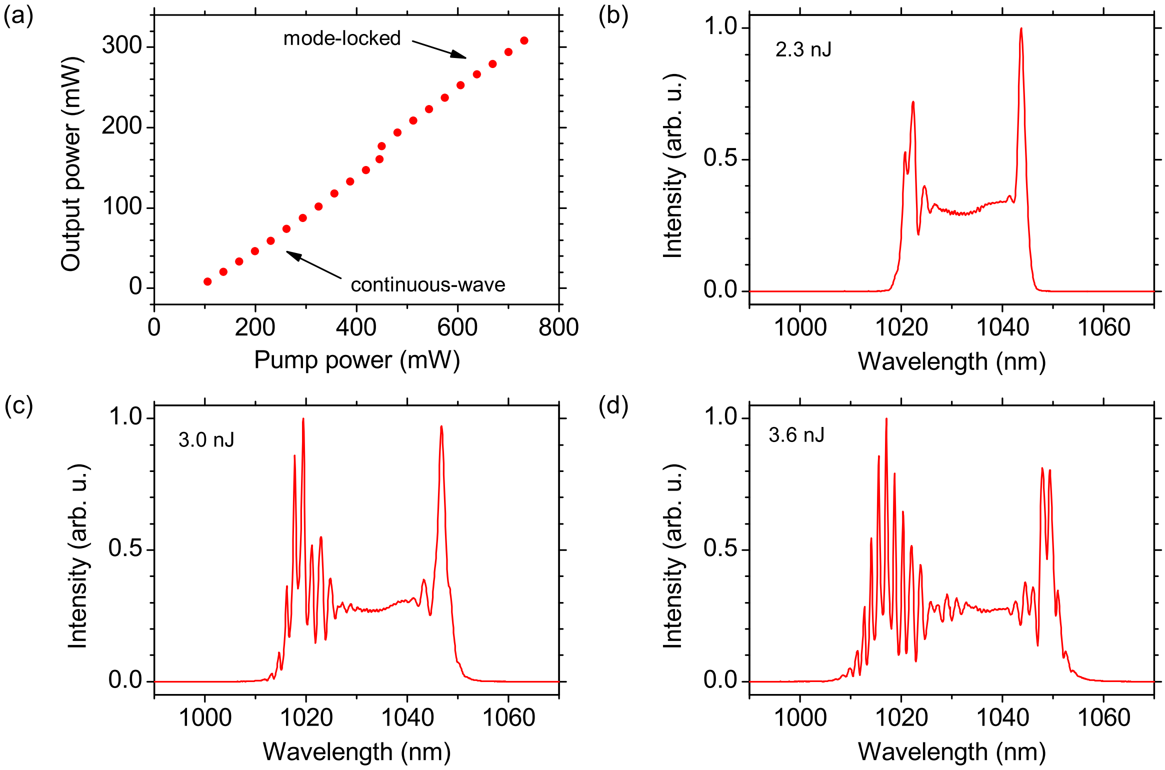

Figure 7.8: (a) Measured output power as a function of pump power. The diagrams (b), (c), and (d) show the output spectra for the indicated pulse energies.

With increased pump power, the output spectrum broadened and the dechirped pulse duration decreased as is typical for dissipative-soliton lasers. Figure 7.8 (b), (c), and (d) show the spectra of the linearly polarized light behind the PBS for pulse energies of 2.3 nJ, 3.0 nJ, and 3.6 nJ corresponding to average powers of 194 mW, 253 mW, and 308 mW. With larger pulse energies, the spectra become broader and allow for shorter pulse durations but are also more structured.

Below pump powers of about 543 mW, the mentioned satellite pulse was not observable in the autocorrelation anymore. This corroborates the fact that the side pulse was caused by the periodic transmission function of the used spectral filter. For small spectral widths, no side pulse was generated by light passing through a side maximum of the filter and subsequent dispersive delay in the fiber section. Filter stacking was not realized because an additional fiber-integrated filter would increase the total resonator dispersion and thus increase the minimum pulse duration.

Figure 7.9 (a) shows the dependence of the spectral width on the pulse energy. The FWHM increased almost linearly with increasing pulse energy from 26.0 nm at 2.3 nJ up to 39.4 nm for pulse energies of 3.6 nJ. Simultaneously, the measured and Fourier limited pulse widths decreased from 115 fs and 102 fs at 2.3 nJ pulse energy down to 82 fs and 66 fs for pulse energies of 3.6 nJ, respectively, as shown in Figure 7.9 (b). The pulse energies were as before measured in front of the compressor.

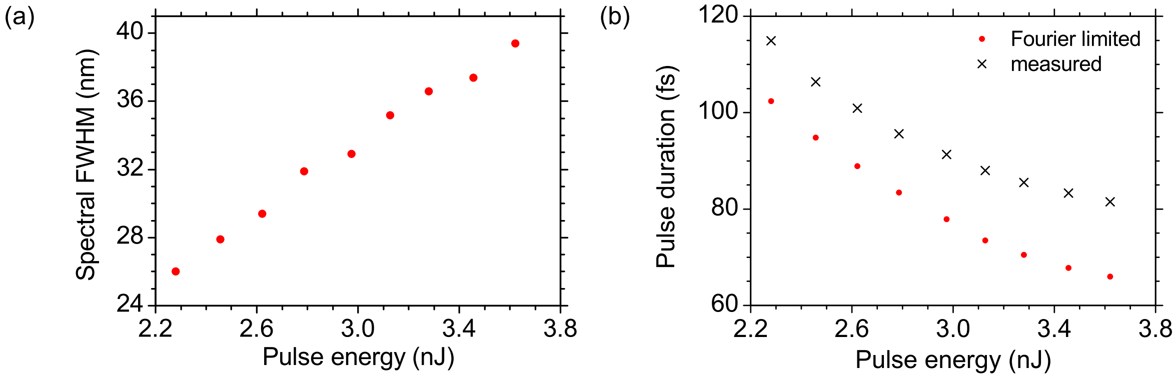

Figure 7.9: (a) Dependence of the spectral FWHM on the pulse energy. (b) Measured and Fourier limited pulse durations as a function of pulse energy.

Figure 7.10 (a) shows the deviation of the measured pulse duration from the Fourier limit. It can be deduced that the pulses with large energy could not be dechirped as close to the Fourier limit as the pulses with lower energies. The deviation of the measured pulse width from the Fourier limited width increased from 12.2 % at 2.3 nJ to 23.5 % for pulse energies of 3.6 nJ. This can be attributed to the accumulated nonlinear phase contributions, which cannot be compensated for by the grating arrangement.

It is also notable that the needed compressor dispersion to dechirp the pulses was strongly dependent on the pulse energy. Figure 7.10 (b) shows the needed compressor dispersion as a function of pulse energy. For large pulse energies, less grating dispersion is needed compared to pulses with lower energies. The compressor dispersion for the indicated pulse energies varied from about -0.078 ps^2 at 2.3 nJ to about -0.067 ps^2 at 3.6 nJ pulse energy.

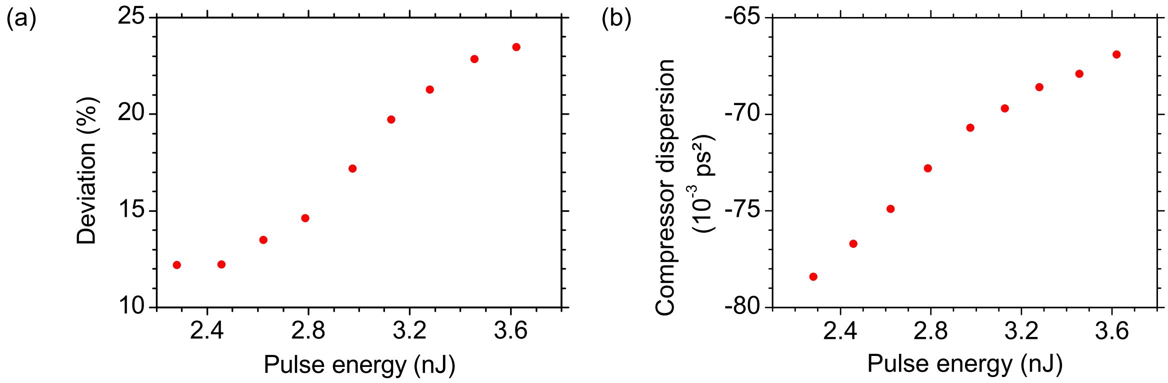

Figure 7.10: (a) Deviation of the measured pulse FWHM from the Fourier limited FWHM. (b) Compressor dispersion for minimum pulse width as a function of pulse energy.

7.4 Conclusion

In this chapter, a femtosecond dissipative-soliton oscillator was studied, which exclusively used all-fiber-integrated components. With that, linearly polarized pulses with pulse energies of 2.2 nJ and pulse durations of 76 fs at 71 MHz repetition frequency were generated. To the best of knowledge, these are the shortest pulses from an all-fiber-integrated Yb-based oscillator. Due to the all-fiber setup and the temperature-stabilization, the output pulse train was very stable over time. Operating the laser with constant output parameters was achieved over a period of several days without any readjustment.

As the generated output spectrum was much broader than the used intracavity spectral filter width, spectral components were transmitted through the side maxima of the filter and, as a consequence, a small side pulse evolved at the maximum pump power. This could be solved by limiting the output pulse energy, and thus the spectral width, as well as by using a filter with a larger transmission bandwidth. When applying the latter, the length of the passive fiber behind the active fiber, where a large part of the spectral broadening and NPE takes place, has to be adjusted for successful mode-locking. When using a larger filter bandwidth, it is possible that the pump power from one laser diode is not large enough for the needed spectral broadening. So the addition of a second single-mode pump diode via polarization-coupling could then be considered. Filter stacking to suppress the side maxima of the sinusoidal transmission function over wavelength was not possible due the additional fiber that would have to be integrated into the cavity. This would enlarge the total dispersion and increase the achievable pulse duration.

8 All-fiber amplifier with fiber-based third-order dispersion compensation

The all-fiber oscillator described in the last chapter generated pulses with durations below 100 fs, but the pulse energy was limited to a few nanojoule. To generate ultrashort pulses with larger energies in the microjoule range, the chirped-pulse amplification (CPA) scheme is usually applied [Str85]. Using grating arrangements for stretching and compression allows for very large pulse stretching ratios together with a good compressibility due to the matched dispersion of stretcher and compressor [Tre69, Mar87, Pes87]. However, using fibers for pulse stretching and thus building an all-fiber-based CPA system would greatly benefit from the waveguide feature of the fiber medium such as alignment-free operation, environmental robustness, and a much simpler setup.

At 1 µm wavelength, a combination of a standard step-index fiber stretcher and a grating arrangement for pulse compression can in principle be used, as their second-order dispersion coefficients exhibit an opposite sign. As described in Section 3.2, the third-order dispersion (TOD) contributions of the fiber stretcher and the grating compressor add up and corrupt the pulse shape for spectrally broad pulses and long stretcher fiber lengths. This limits the application of this scheme in ultrashort-pulse CPA systems. An alternative approach uses a fiber stretcher together with a hybrid compressor incorporating both gratings and prisms. These grism compressors are able to compensate for the TOD of a standard step-index fiber stretcher [Kan94, Kan95]. With such a fiber CPA system, pulse energies of about 5 µJ and pulse durations of 195 fs were demonstrated using large-mode area fibers [Fer09]. A similar amplifier system, that used effectively single-mode fibers with core diameters ≤ 10 µm, is described in detail in Chapter 9 of this thesis.

Besides these, an even simpler setup would incorporate a stretcher fiber, whose dispersion slope, i.e. the TOD, inversely matches that of a grating compressor. Pulses were successfully compressed using such a special fiber stretcher, having a β_3/β_2 ratio of -1.8 fs and a length of 0.5 m [Fer01]. Such a fiber stretcher was also used for pulse stretching in a linear large-mode area fiber CPA system, which generated 120 fs long pulses with energies of 520 nJ [Rue10]. To generate larger pulse energies, nonlinear chirped-pulse amplifiers are an option. They exploit the possibility of at least partial compensation of stretcher and compressor TOD by self-phase modulation [Kuz07]. Applying this scheme to a free-space pumped photonic crystal fiber amplifier resulted in pulse energies of up to 100 µJ with 270 fs duration [Zao08]. This energy level has not yet reached with all-fiber-integrated nonlinear amplifiers. Pulse energies of 123 nJ [Muk09] and 1 µJ [Kal10] were demonstrated using large-mode area fibers, exhibiting compressed pulse durations of 160 fs and 140 fs, respectively. However, the performance of nonlinear CPA systems sensitively depends on parameters such as the spectral shape, the pulse duration, and the pulse energy and these parameters cannot be varied independently.

In this chapter, a linear all-fiber-integrated CPA system is studied, whose specially designed fiber stretcher allowed for matching the grating compressor dispersion up to the third order [Grü10]. Contrary to previously demonstrated amplifiers, the presented system generated microjoule pulse energies in effectively single-mode fibers with a high-quality beam profile. These fibers offer advantages compared to large-mode area fibers, which exhibit higher-order mode issues, and compared to photonic crystal fibers, which have not yet been successfully integrated in an all-fiber setup due to their special transversal fiber profile. In contrast to the amplifiers reported in References [Muk09, Kal10], the demonstrated amplifier was operated in the linear regime, i.e. the pulse quality and duration did not depend on the pulse energy. The seed oscillator and the amplifier were both completely fiber-integrated and thus alignment-free except for the compressor. By using a single amplification stage, pulse durations of 189 fs and energies of 2.2 µJ after compression were achieved. The corresponding average power was 9.8 W at the repetition frequency of 4.5 MHz. To the best of knowledge, this is the first demonstration of femtosecond pulses with microjoule energies from an effectively single-mode fused silica solid-core fiber amplifier with core diameters of $\leq$ 10 µm, which is operated in the linear regime. Parts of this chapter have been published in Reference [Mor12].

8.1 Experimental setup

The experimental setup is shown in Figure 8.1. The all-fiber-integrated ytterbium-based dissipative-soliton oscillator described in Chapter 7 served as the seed source. The laser emitted an average power of about 290 mW at the repetition rate of 71 MHz. The approximately 4 ps long pulses propagated through a polarization-maintaining isolator for feedback protection. A fiber-coupled acousto-optic modulator (AOM) MT250-IR6-FIO-PM-0.5 from AA Sa, France, based on TeO_2 reduced the repetition rate to 4.5 MHz. The insertion loss of the AOM was below 4 dB. Subsequently, a combination of Nufern 1060-XP step-index fiber and a triple-cladding fiber (TCF) provided by OFS, Denmark, were used to stretch the pulses before amplification [Grü10]. The TCF exhibited negative third-order dispersion at 1030 nm wavelength and was incorporated to compensate for the cumulative TOD of the standard step-index fiber and the grating compressor.

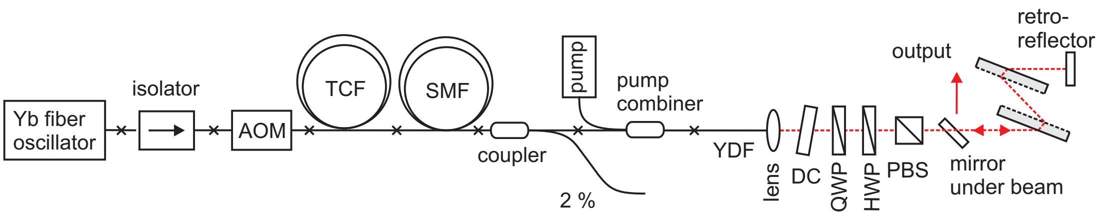

Figure 8.1: Experimental setup. AOM acousto-optic modulator, TCF triple-cladding fiber, SMF single-mode fiber, YDF ytterbium-doped fiber, DC dichroic mirror, HWP half-wave plate, QWP quarter-wave plate, PBS polarizing beam splitter.

A summary of its basic characteristics is listed in Table 8.1. The dispersion of the fiber stretcher module is described in detail in the next section. Due to the TCF's small mode field diameter of 2.8 µm compared to about 6.3 µm of the standard fiber, a splice loss of 1.1 dB occurred. Splicing of the TCF was carried out by OFS as manual splice optimization using an own Vytran FFS-2000 fusion splicer resulted in losses exceeding 2.6 dB per splice. It is notable that both stretcher fibers were not polarization-maintaining. Changing the polarization state of the output pulses by fiber movement was prevented by fixing all fibers on the optical table.

Variable	Unit	Value
β_2 at 1030 nm	$\mathrm{ps}^2/\mathrm{km}$	114
β_3 at 1030 nm	$\mathrm{ps}^3/\mathrm{km}$	-0.90
Attenuation at 1030 nm	dB/km	2.45
Effective area at 1030 nm	$\mu\mathrm{m}^2$	6.2
Mode field diameter at 1030 nm	µm	2.8
Cut-off wavelength	nm	945
Fiber diameter	µm	125

Table 8.1: Properties of the triple-cladding stretcher fiber.

To monitor the seed pulse characteristics, a fiber coupler was incorporated in front of the amplifier. Two percent of the average power was coupled out, which allowed for the measurement of the pulse energy and power spectrum. The amplifier was pumped by a multi-mode fiber-coupled laser diode with a maximum average power of about 25 W at 976 nm from a fiber with a core diameter of 105 µm. The pump diode was connected to the amplifier by splicing its output fiber to the pump input port of an in-house made pump combiner. The latter had a signal feedthrough with a 10 µm fiber core diameter. The output fiber of the pump combiner was a passive double-cladding fiber with a 10 µm core and 125 µm cladding diameter. It was spliced to a 2.5 m long ytterbium-doped fiber Liekki Yb1200-10/125DC. Both fibers with a 10 µm core diameter had a V number of 2.44. This was slightly above the single-mode threshold V_c=2.405 and corresponded to a cutoff wavelength of 1045 nm. By bending the fiber, significant losses for the higher-order modes can be induced. Thus, the effectively single-mode fibers were coiled to ensure single-mode operation.

The repetition rate was reduced to 4.5 MHz, which allowed seeding the amplifier with a just sufficiently large average power of about 4 mW. With this repetition frequency, microjoule pulse energies were achievable concerning the limited available pump power. After amplification, the beam was collimated and two dichroic mirrors separated the residual pump light from the signal. The polarization of the output pulses were adjusted with a quarter- and a half-wave plate to pass a polarizing beam splitter. The pulses then propagate through a polarization sensitive grating compressor. It consisted of two in parallel arranged transmission gratings manufactured by Fraunhofer IOF, Germany, with a line density of 1500/mm. The rear sides were provided with a broadband anti-reflective coating around the wavelength of 1030 nm. To achieve the maximum efficiency, the Littrow angle of 50.6° between the beam and the grating normal was chosen as incidence angle.

8.2 Stretcher and compressor dispersion

As the dispersion matching was important, the needed fiber stretcher and grating compressor characteristics were determined before the experimental realization. The dispersion curve of the used triple-cladding fiber from OFS is depicted in Figure 8.2 together with the modeled dispersion of Nufern 1060-XP for comparison. The values of the TCF were provided by OFS. It is obvious that its second-order dispersion is about five times larger than that of the standard fiber at 1030 nm wavelength. More important is the fact that both curves have a slope with the opposite sign. This had been exploited in the experiments described in this chapter to compensate for the TOD of the grating compressor.

Figure 8.3 (a) shows a comparison of the dispersion curves of Nufern 1060-XP, the TCF, and the grating arrangement with a line density of 1500/mm. An analytic formula for the calculation of the grating dispersion can be found in Reference [Die06]. An absolute dispersion of 10.8 ps^2 at 1030 nm wavelength was assumed corresponding to a grating separation of 50 cm along the ray with center wavelength. This was close to the maximum achievable dispersion considering the limited grating dimensions. At 1030 nm wavelength, the compressor had a β_3/β_2 ratio of -6.5 fs when used under Littrow condition. This ratio could neither be matched by that of the standard Nufern 1060-XP fiber ($\beta_3/\beta_2 = 1.0$ fs, modeled) nor by that of the triple-cladding fiber ($\beta_3/\beta_2 = -7.9$ fs) alone. However, the ratio of -6.5 fs could be matched by a combination of both fibers with appropriate lengths as described as follows.

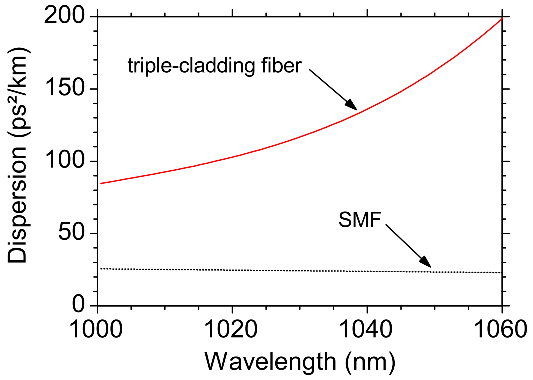

Figure 8.2: Dispersion curve of the triple-cladding fiber and Nufern 1060-XP fiber.

Figure 8.3 (b) depicts the dispersion of the combined stretcher module, which consisted of 80 m TCF and about 70 m Nufern 1060-XP fiber including the oscillator and the amplifier fibers. At the wavelength of 1030 nm, the absolute second-order dispersion value and the dispersion slope matched the target dispersion corresponding to a grating arrangement with a line density of 1500/mm. Because the overall stretcher module dispersion of about 10.8 ps^2 was large compared to that of the optical elements inside the acousto-optic modulator and the isolator, the latter were neglected in the dispersion calculation. Also, the active fiber was treated as standard fused silica step-index fiber with the above mentioned dispersion. This assumption is justified by the

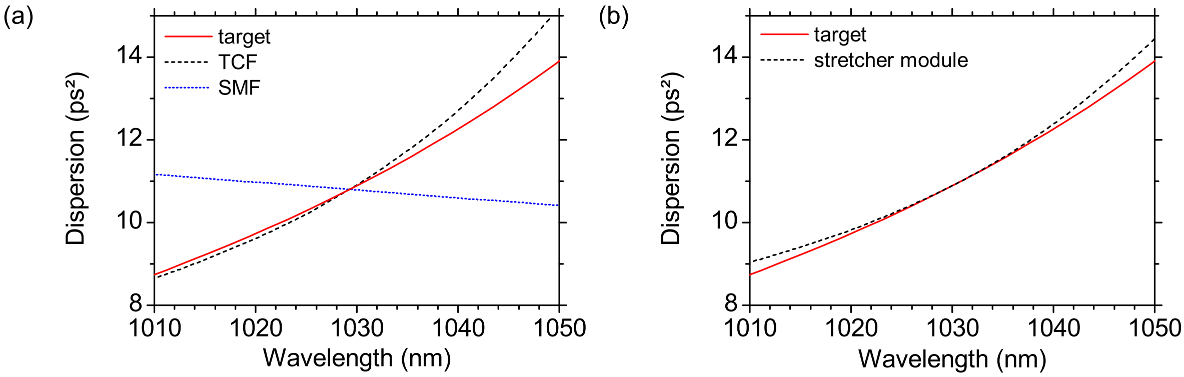

Figure 8.3: (a) Dispersion curves of the target (gratings, 1500/mm), Nufern 1060-XP (SMF, modeled), and the triple-cladding fiber (TCF). (b) Dispersion of the target (gratings, 1500/mm) and of the combined stretcher module.

small group delay dispersion of the ytterbium-doped fiber compared to that of the stretcher module. The used grating line density of 1500/mm is a compromise between diffraction efficiency, alignment tolerance, grating size, and overall compressor dimensions. Large line densities reduce the required grating separation whereas small line densities lead to an easier alignment and a reduction of the needed grating size due to the smaller Littrow diffraction angle. The line density also had to be below the maximum value of about 1570/mm, which corresponds to the ratio $\beta_3/\beta_2 = -7.9$ fs of the used triple-cladding stretcher fiber.

As the dispersion values of the fibers were not exactly known, the calculated stretcher fiber lengths had to be optimized in the experiment. Because the triple-cladding fiber was hard to splice, the length of the standard fiber was varied instead. In the following, it is estimated how a non optimum ratio β_3/β_2 of the stretcher module can be compensated for by fine-tuning of the grating compressor. Assuming a 10 m length difference of the standard fiber from the calculated optimum, the resulting β_3/β_2 ratio of the stretcher module, consisting of 80 m TCF and either 60 m or 80 m Nufern 1060XP fiber, would be 6.67 fs or 6.34 fs, respectively. Fine-tuning of the dispersion slope can then be realized by varying the incidence angle of the compressor gratings as follows. It can be shown that the ratio β_3/β_2 of a grating compressor is a function of wavelength, incidence angle, and line density

$$\beta_3/\beta_2 = -\frac{3\lambda}{2\pi c r}\left(r + \frac{\lambda}{d}\left(\frac{\lambda}{d} - \sin\alpha\right)\right), \tag{8.1}$$

where $r = 1 - (\lambda/d - \sin\alpha)$, α represents the angle between the incidence beam and the grating normal, λ the wavelength, and $g = 1/d$ the grating line density [Die06]. Inserting the above calculated β_3/β_2 ratios into Formula (8.1) thus resulted in corresponding incidence angles of 50.0° for 60 m SMF and 51.2° for 80 m SMF, respectively. Experimentally, the stretcher fiber length was thus varied in steps of about 10 m, while dispersion fine-tuning was realized by detuning the incidence angle about ±1° away from the Littrow angle of 50.6°. The optimum adjustment was indicated by the autocorrelation of the compressed pulses having the smallest width.

8.3 Temporal pulse stretching

To study the influence of the stretcher fiber length on the pulse duration, the pulses were stretched using different fiber lengths of Nufern 1060-XP and the triple-cladding fiber. A combination of several spools containing fibers with different lengths were used to achieve a variation of small and large stretched pulse durations. The lengths of the fibers on the spools were measured by Nufern, USA, and OFS, Denmark, respectively, and taken as is due to the large values. The temporal pulse profiles were subsequently measured with a fast photodiode and a sampling oscilloscope having a 70 GHz bandwidth. Figure 8.4 shows the stretched pulse duration as a function of fiber length. When stretching with the TCF, the pulse durations vary between values of 408 ps for 40 m length and 1246 ps for 140 m. Using Nufern 1060-XP, the values range from 181 ps for 50 m to 1834 ps for 1200 m fiber length.

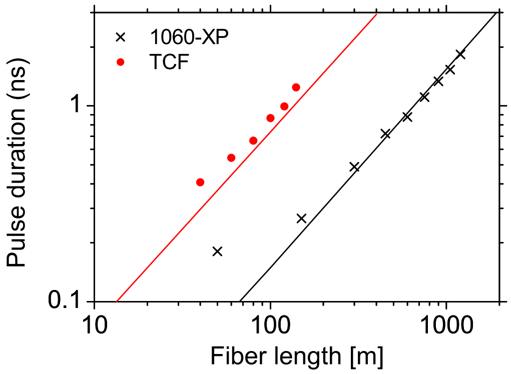

Figure 8.4: Stretched pulse duration for different fiber lengths. The lines represent the simulated pulse stretching.

For comparison, the pulse stretching of the seed pulses was simulated using the pulse propagation software Fiberdesk. With the seed spectrum of the oscillator, the fiber dispersion values of the Nufern 1060-XP fiber and the OFS triple-cladding fiber as described in Table 2.1 and Table 8.1, and assuming Fourier limited input pulses, the resulting pulse durations are depicted in Figure 8.4 as solid lines for the 1060-XP (black) and the TCF (red). The simulated and measured pulse lengths fit reasonable well concerning the dispersion values and lengths of the fibers were not exactly known. The deviation at small fiber lengths can be explained by the prechirp of the pulses in the experiment before entering the fiber stretchers.

For large fiber lengths and neglecting third-order dispersion in pulse stretching, Formula (3.1) describing the temporal pulse broadening can be reduced to $\sigma(\beta_2, L) = 2\beta_2 L/(2\sigma_0)$. This is equivalent to the condition $L \gg 2\sigma_0^2/\beta_2 = 1$ m for an assumed fiber dispersion of $\beta_2 = 20$ ps^2/km and a RMS width of $\sigma_0 = 100$ fs corresponding to the FWHM of 235 fs of a Gaussian pulse. In the experiments, the values of the used stretcher fibers were larger and the initial pulse durations smaller than assumed here. Therefore, the slopes of the curves, measured by fitting a linear function through the origin, are a measure for the fiber dispersion although all dispersion orders contribute to the dispersive pulse stretching. The identified values are 1.5 ps/m for Nufern 1060-XP and 8.7 ps/m for the triple-cladding fiber, respectively. The temporal pulse broadening in the triple-cladding fiber is thus about 5.8 times larger than in the Nufern 1060-XP fiber.

8.4 Results at 4.5 MHz repetition frequency

The profile of the stretched pulses using the setup described above is depicted in Figure 8.5 (a) having a full width at half maximum of approximately 940 ps. The pulse train with a repetition frequency of 4.5 MHz is shown in Figure 8.5 (b) exhibiting a temporal pulse separation of 224 ns. The average output power of the amplifier as a function of pump power is shown in Figure 8.6 (a). It was measured behind the two dichroic mirrors and had a maximum value of 13.0 W at the pump power of 21.0 W. The nonlinear behavior of the curve can be explained by the wavelength shift of the pump light with increasing pump power. This was noticed although the heatsink temperature was held constant. The wavelength shift of the pump laser with increasing average power may be reduced by placing the temperature sensor directly onto the diode housing.

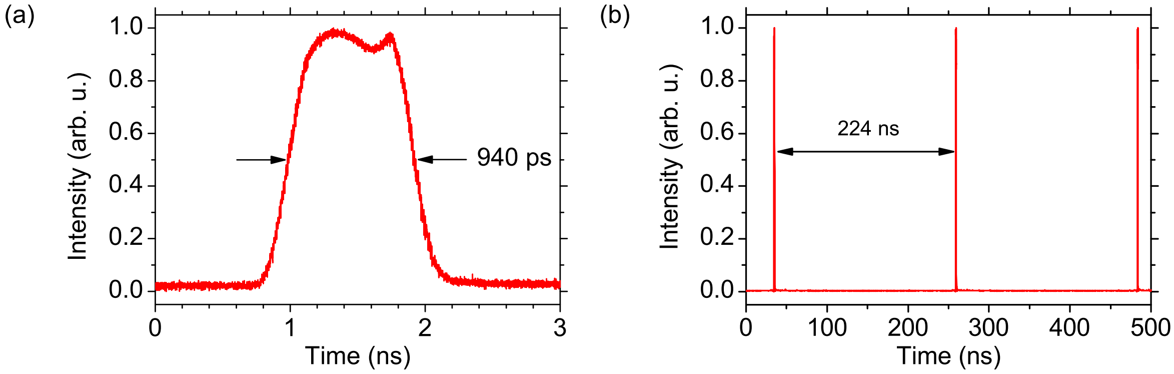

Figure 8.5: (a) Temporal profile of the stretched pulse. (b) Pulse train of the seed pulses.

Because the fibers following the acousto-optic modulator were not polarization-maintaining, the degree of polarization at the amplifier output was analyzed. Therefore, a calcite Wollaston prism with a 100,000:1 polarization extinction ratio was placed in the beam. The transmission through the polarizer was maximized by adjusting a quarter- and a half-wave plate. The maximum achieved linearly polarized output power was 12.5 W corresponding to pulse energies of 2.8 µJ at the repetition frequency of 4.5 MHz.

The resulting degree of polarization depicted in Figure 8.6 (b), which is defined as the ratio of the transmitted power to the power rejected by the polarizer, decreased for increasing pulse energies. This can be explained by the increase of amplified spontaneous emission and nonlinear polarization evolution with increasing pump power. However, the degree of polarization was larger than 95 percent for all pulse energies. The pulse train was also analyzed with a second

AOM to measure the optical power between two subsequent pulses, which resulted in an amplified spontaneous emission level of below one percent. After compression with the grating arrangement, a maximum pulse energy of 2.2 µJ was achieved.

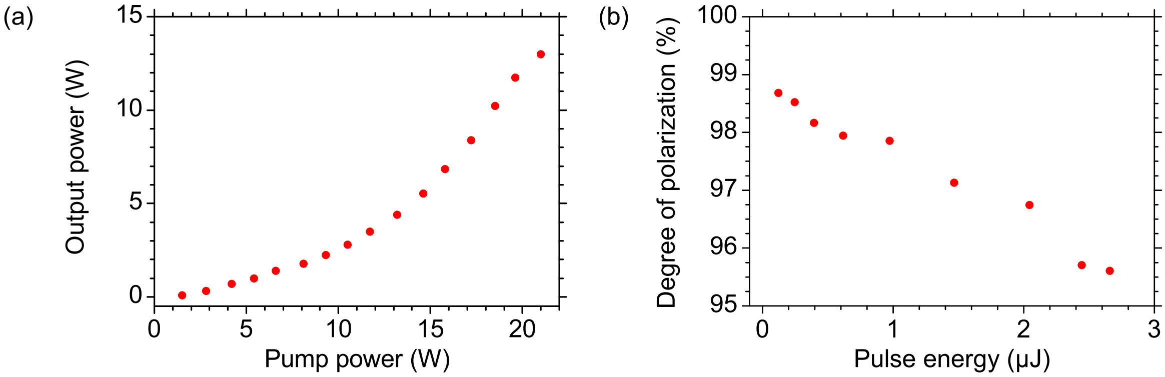

Figure 8.6: (a) Amplifier characteristic. (b) Degree of polarization as a function of pulse energy.

Figure 8.7 (a) shows the spectrum of the amplified pulses with energies of 2.2 µJ after compression. Due to spectral gain narrowing in the active fiber, the spectral width decreased from 36.6 nm before to 12.6 nm after amplification. Because the spectrum of a strongly chirped pulse is mapped to the time domain, the temporal pulse duration behind the amplifier also decreased to about 398 ps. Raman scattering was not observed at this power level.

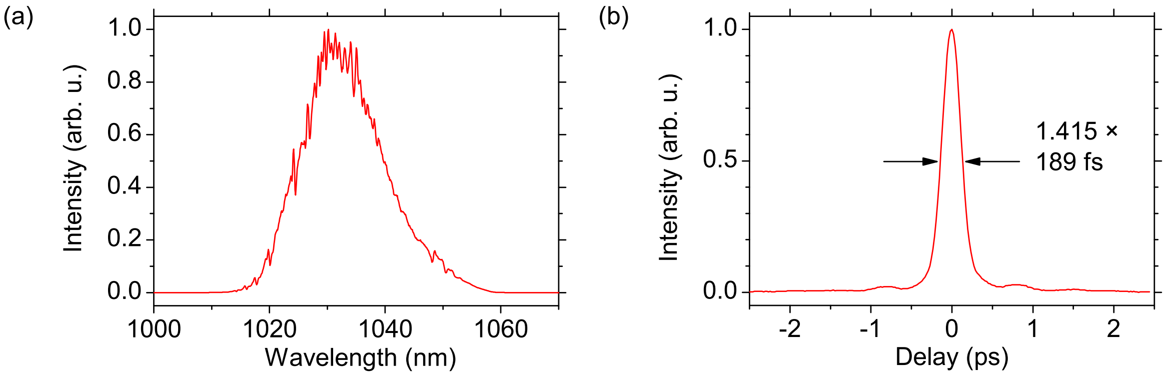

Figure 8.7: (a) Spectrum and (b) autocorrelation of the compressed pulses with pulse energies of 2.2 µJ.

The autocorrelation of the compressed pulses is depicted in Figure 8.7 (b) exhibiting a FWHM of 267 fs. This indicates pulse durations of 189 fs using the deconvolution factor of 1.415, which was calculated from the ratio of the Fourier limited autocorrelation and pulse widths. The compression factor was thus about 2,100 related to the stretched pulse duration directly after amplification. The lengths of the two different stretcher fibers as well as the incidence angle of the grating compressor were adjusted experimentally as described above to achieve the smallest compressed pulse duration. This was achieved with 80 m of the TCF and about 118 m of standard step-index fiber length including oscillator and amplifier components. The discrepancy between the calculated fiber lengths and the experimentally identified may originate from experimental and numerical dispersion uncertainties. Further optimization of the system concerning the total dispersion may be possible as the spectrum of the output pulses allows for a Fourier limited pulse duration of 115 fs at 2.2 µJ pulse energy. The grating separation of 533 mm, measured along the ray with center wavelength, corresponds to the compressor dispersion of about -11.5 ps^2. Readjustment of the grating separation and, therefore, the group delay dispersion of the compressor, was not necessary when varying the output pulse energy.

To demonstrate the importance of the triple-cladding fiber regarding third-order dispersion compensation, the TOD induced pulse distortion was analyzed in a stretcher compressor system, where the triple-cladding fiber had been replaced by a standard step-index fiber. The stretcher fiber was assumed to be Nufern 1060-XP while the same grating arrangement with a line density of 1500/mm was used for pulse compression. Assuming the total fiber dispersion of 11.5 ps^2, the estimated TOD of the fiber was 0.011 ps^3, while that of the grating compressor was 0.075 ps^3. As both contributions are cumulative, the sum of about 0.086 ps^3 was then added to the spectral phase of a Fourier limited pulse having the spectrum of the seed pulses.

The resulting temporal pulse profile is depicted in Figure 8.8 (a). It exhibits a multitude of oscillations in the pulse tail, which are typical for the influence of third-order dispersion. Simultaneously, the energy was spread over a span of several tens of picoseconds. Due to the oscillations in the pulse profile, a large pedestal had formed in the corresponding simulated autocorrelation shown in Figure 8.8 (b). These simulations show that it is not possible to achieve pulse durations of 100 fs after compression in a linear CPA system, when using large dispersive stretching with > 10 ps^2 and a combination of standard step-index fiber stretcher and a grating compressor. In the modeling, fiber nonlinearity and higher-order dispersion contributions were neglected.

8.5 Limitations

By further increasing the pump power, maximum pulse energies of 2.6 µJ after compression could be achieved. Although larger pulse energies are favored for many applications, a drawback of this finding is that for energies larger than 2.2 µJ the nonlinearity of the fiber amplifier starts influencing the pulse quality. This was noticed by the need for a readjustment of the grating separation and, therefore, the compressor dispersion. Also, the spectral width changed with

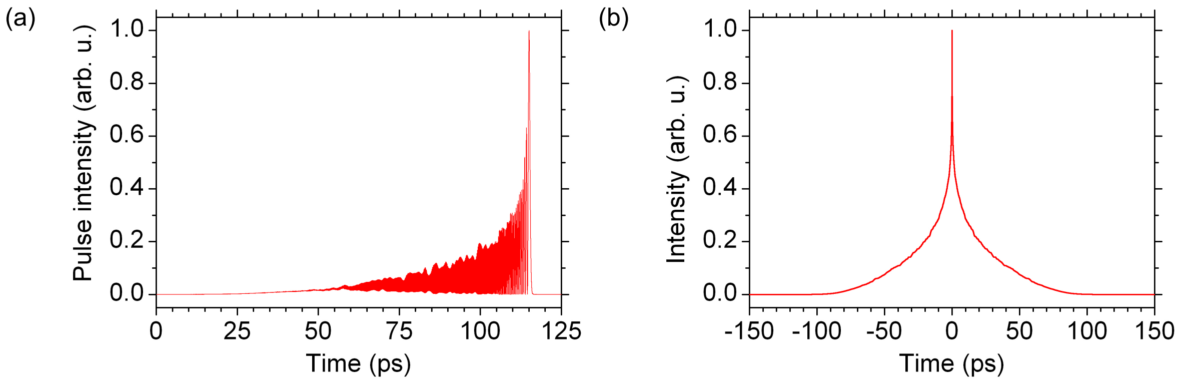

Figure 8.8: (a) Simulated temporal shape and (b) autocorrelation of the pulses without third-order dispersion compensation.

increasing pulse energy and, with it, the Fourier limited pulse duration. The dependence of the Fourier limited pulse duration on the pulse energy is shown in Figure 8.9 (a). For small pulse energies, the curve shows an almost linear increase of the Fourier limited pulse duration, which can be attributed to spectral gain-narrowing. For pulse energies larger than about 2.2 µJ, the Fourier limit decreased to 109 fs for pulse energies of 2.6 µJ. This may be caused by spectral broadening due to self-phase modulation, which additionally resulted in a nonlinear pulse chirp. This also may be the reason, why the increased spectral width could not be used to achieve smaller pulse durations by simple readjustment of the grating compressor.

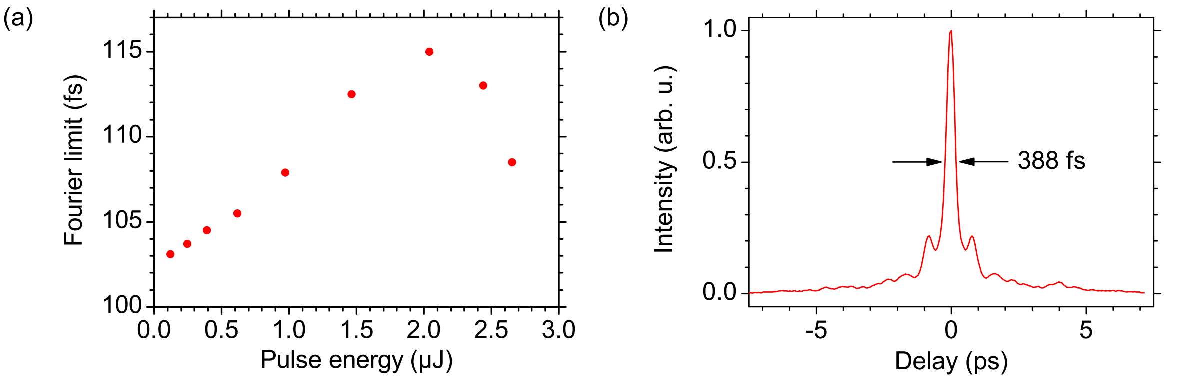

Figure 8.9: (a) Dependence of the Fourier limit of the amplified pulses on the pulse energy. (b) Autocorrelation of the pulses with the maximum achieved pulse energy.

With increasing pulse energy, a pedestal in the autocorrelation measurement evolved due to the accumulated nonlinear chirp. The corresponding autocorrelation for the maximum pulse energy of 2.6 µJ is shown in Figure 8.9 (b). The FWHM increased to 388 fs compared to 267 fs of the autocorrelation in Figure 8.7 (b). A further temporal pulse stretching by increasing the stretcher fiber lengths would most likely result in larger pulse energies achievable in the linear amplifier regime. Experimentally, this could not be realized as this would have required a larger compressor dispersion and, therefore, a larger grating separation. This was constrained by the limited grating dimensions.

To analyze the influence of the pulse energy on the spectrum, the output spectra were measured at different pulse energies. Figure 8.10 shows the resulting spectral evolution as a function of pulse energy. For a better visibility, a vertical offset of 10 dB was manually applied to each curve. The spectra exhibit steep edges with a ratio of maximum value to background of about 40 dB. Although the spectral profiles are very similar for the indicated energy levels, spectral components at wavelengths around 1080 nm had built up at the highest pulse energy of 2.6 µJ. This may caused by an increased level of amplified spontaneous emission due to larger applied pump powers as well as inelastic Raman scattering of the photons by optical phonons in the glass matrix.

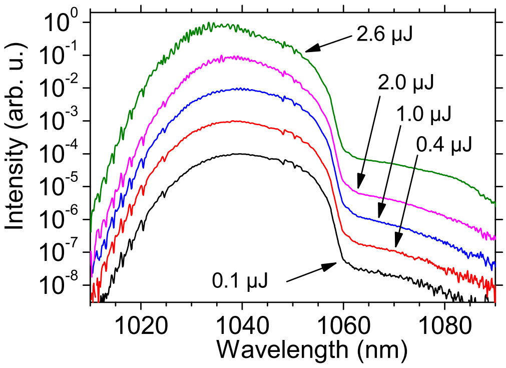

Figure 8.10: Spectral evolution with increasing pulse energy. The spectra were vertically offset by 10 dB.

8.6 Conclusion

In summary, a single-stage all-fiber chirped-pulse amplifier system was studied. It was seeded by a dissipative-soliton laser and was completely fiber-integrated except for the pulse compressor. A specially designed fiber stretcher was incorporated, whose dispersion inversely matched that of the grating compressor up to the third order. Pulse energies of 2.2 µJ with pulse durations of 189 fs were achieved after compression. The corresponding average power was 9.8 W.

For larger generated pulse energies, the fiber nonlinearity influenced the quality of the output pulses. The accumulated nonlinear chirp could not be compensated for by the grating compressor, which resulted in larger pulse durations. To overcome this limitation, further pulse stretching by increasing the stretcher fiber length could be applied but would simultaneously require a larger grating size and grating separations larger than 53 cm, which is contrary to a favored compact setup. Another possibility would be to use large-mode area fibers to reduce the peak power. Because of the large core size, these fibers exhibit a larger saturation average power compared to single-mode fibers. This would imply the usage of a second amplification stage. Additionally, higher-order mode issues have to be considered.

However, the demonstrated system is a compact and easy-to-integrate fiber-based alternative to bulk solid-state lasers. Further system optimization would involve the usage of polarization-maintaining fibers. Unfortunately, the triple-cladding stretcher fiber is not yet available in a polarization-preserving version.

9 All-fiber amplifier with grism-based third-order dispersion compensation

In the last chapter, a fiber-based chirped-pulse amplifier with a fiber-based third-order dispersion compensation was studied. It allowed for the usage of a specially designed fiber stretcher in combination with a standard grating arrangement for pulse compression. However, it is also possible to compensate for the third-order dispersion of a standard step-index fiber stretcher by using a specially designed grism compressor, which incorporates both prisms and gratings.

In this chapter, an all-fiber-integrated CPA system is studied, which used a standard fiber for pulse stretching. Compression was achieved with a suitable grism compressor. Pulse energies of 0.6 µJ with durations of 152 fs could be generated. The average power after compression was 3.6 W at the repetition frequency of 5.9 MHz. The usage of effectively single-mode step-index fibers allowed for an easy integration by fusion splicing and an avoidance of higher-order mode issues of large-mode area fibers.

9.1 Experimental setup

A sketch of the experimental setup is shown in Figure 9.1. It is similar to the setup described in Chapter 8. The amplifier system was seeded by the all-fiber dissipative-soliton oscillator described in Chapter 7 with very similar output parameters. The pulses passed an optical fiber-coupled isolator, which transmitted only a single polarization and protected the laser from back reflections. A fiber-coupled TeO_2-based acousto-optic modulator MT250-IR6-FIO-PM-0.5 from AA Sa, France, with a 6 ns rise time was used to reduce the 71 MHz repetition rate of the oscillator down to 5.9 MHz. The repetition frequency was chosen to seed the amplifier with a sufficiently large average power of about 6 mW. By this, a single amplification stage could be used to generate high-energy pulses.

The pulses were subsequently stretched in a 300 m long Nufern 1060-XP fiber before they entered the amplification stage. The fiber length and, therefore, the stretcher dispersion corresponded to the available dispersion of the grism compressor as described in Section 9.2. A fiber coupler, which extracted two percent of the optical power, was incorporated to monitor the spectrum and the average power of the seed pulses.

An in-house made multi-mode pump combiner with a 105 µm pump core diameter input and a 10 µm core diameter feedthrough was used to couple the light from a high-power laser diode into the double-cladding output fiber. The 2.5 m long ytterbium-doped fiber Liekki Yb1200-10/125DC was spliced to the output of the pump combiner. Behind the active fiber, the beam was collimated with a lens, and the residual pump light was separated with two dichroic mirrors. A combination of a quarter-wave and a half-wave plate was used to adjust the polarization to let a maximum intensity pass a polarizing beam splitter. The linearly polarized light then propagated through the polarization sensitive grism compressor setup. Subsequently, the pulse characteristics such as energy, spectrum, and pulse duration were analyzed.

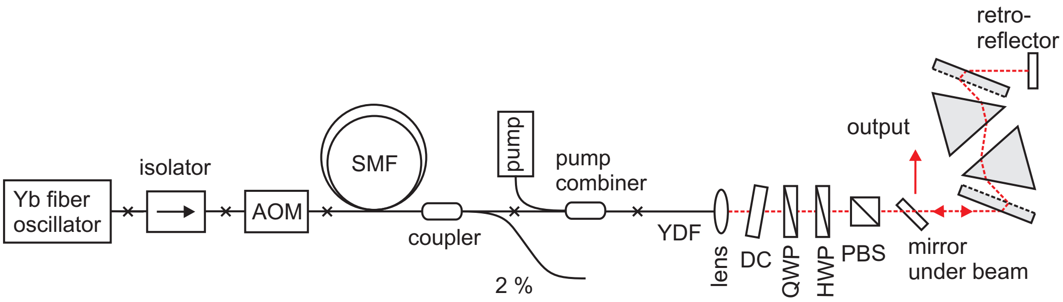

Figure 9.1: Sketch of the experimental setup. AOM acousto-optic modulator, SMF single-mode fiber, YDF ytterbium-doped fiber, DC dichroic mirror, HWP half-wave plate, QWP quarter-wave plate, PBS polarizing beam splitter.

9.2 Characteristics of the grism compressor

In this section, the geometrical and dispersive properties of the applied grism compressor are described. First, it was numerically searched for a suitable grism design to compensate for the normal fiber dispersion of 24.1 $\mathrm{ps}^2/\mathrm{km}$ with a ratio of third- to second-order dispersion of 1.0 fs at 1040 nm wavelength, which was then experimentally realized. Therefore, the developed dispersion calculation program described in Section 3.2 was used to analyze a variety of possible setups. After extensive variation of parameters such as the grating line density, prism material, prism apex angle, prism-grating angle Ω, and prism separation L_{45} (see Figure 3.4), an appropriate grism compressor design had been identified. In the procedure, the prism material and the grating line density were held constant when varying the angles and distances. Two parameters that were identified as important to achieve a negative β_3 value were the prism-grating angle and the prism apex angle. The resulting setup exhibited a total anomalous second-order dispersion of about $-6.6\ \text{ps}^2$ and the required ratio $\beta_3/\beta_2 = 1.0$ fs. It is described in detail in the following.

A design including a single prism and a single grating, similar to the one described in Chapter 4, was chosen for easy alignment and a compact footprint [Akt06, Cha10]. A fused silica transmission grating, manufactured by Fraunhofer IOF, Germany, with a thickness of 6.35 mm and a line density of 1500/mm was used. The line density is a trade-off between the larger diffraction efficiency of gratings with lower line density and the achievable dispersion given a limited compressor footprint. The maximum fabricable grating size of $130 \times 20\ \text{mm}^2$ was chosen to allow for the largest possible grating separation and, therefore, the largest pulse stretching factor. The compressor included a prism with an apex angle of 66.5° made of Pilkington BSC517642C glass, whose dispersion well matches that of common Schott N-BK7 glass. As the transmission gratings can only be designed to support s-polarization for grating line densities larger than about 1000/mm at 1 µm wavelength [Cla09], the Brewster's angle could not be used for the refraction at the optical surfaces of prism and grating. Therefore, the prism facets as well as the rear side of the grating were supplied with anti-reflective coatings by the Coatings Group of the Laser Zentrum Hannover. They were optimized for broadband light around 1040 nm wavelength and for a variety of incidence angles.

Table 9.1 shows the geometrical parameters of the grism compressor. A maximum prism separation along the center wavelength was assumed to be $L_{45} = 500$ mm, which in principle determined the total grism compressor dimensions. As the compressor used a folded design, the resulting footprint reduced to approximately half the size of a setup using two gratings and two prisms. The grating incidence angle of $\alpha_{in} = 51.3°$ corresponded to the Littrow condition for maximum diffraction efficiency. The prism was placed into the beam with an angle of $\Omega = -15.8°$ with respect to the grating surface. The involved prism sides were 120 mm and 130 mm long, while the prism had a height of 20 mm. The dimensions of the optical components were large enough to support a spectrum reaching from 1020 nm to 1070 nm wavelength.

Line density	Wavelength	Incidence angle	Apex angle	Prism grating angle
1500/mm	1040 nm	51.3°	66.5°	−15.8°

D_2	D_2	P_1	P_2	L_{45}
32.2 mm	32.2 mm	10.0 mm	44.7 mm	500 mm

Table 9.1: Parameters of the grism pulse compressor (see also Figure 3.4).

The calculated second-order and third-order dispersion at 1040 nm wavelength were $-6.64\ \text{ps}^2$

and -0.0067 ps^3, respectively. The corresponding ratio $\beta_3/\beta_2 = 1.0$ fs thus matched that of the fiber stretcher at 1040 nm wavelength. Figure 9.2 (a) shows the matched dispersion curves of the grism compressor and the target, which corresponds to the calculated dispersion of 277 m standard fiber with the opposite sign (see Section 2.1).

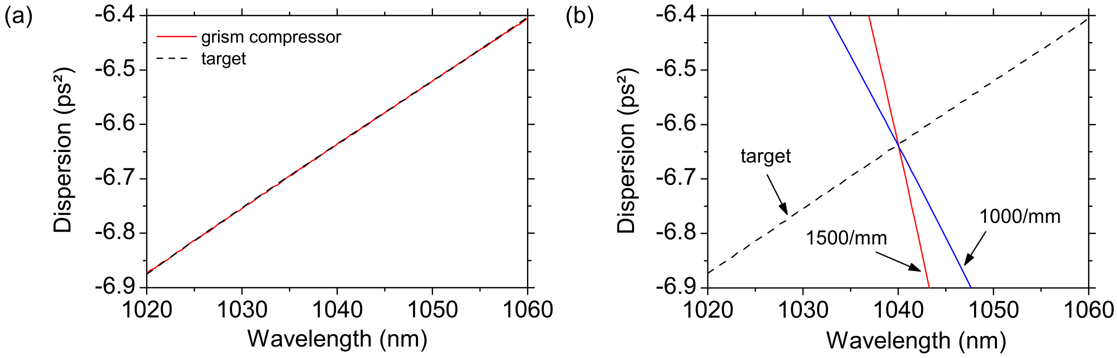

Figure 9.2: (a) Dispersion of the grism compressor and the target. (b) Comparison with the dispersion of grating compressors with different line densities.

For a comparison, the target dispersion curve and the dispersion of two grating compressors with different line densities are depicted in Figure 9.2 (b). It is known that the slope of the curves, corresponding to the third-order dispersion, can be varied by changing the grating line density from 1500/mm to 1000/mm. However, the TOD coefficient of the grating compressor has always the opposite sign compared to the target curve's β_3 value independently of the line density. Thus, it is not possible to match the target dispersion curve even closely using a grating compressor.

A photograph of the experimentally realized grism compressor is shown in Figure 9.3.

9.3 Results at 5.9 MHz repetition frequency

Figure 9.4 (a) shows the temporal profile of the stretched seed pulses measured with a fast photodiode and a 70 GHz sampling oscilloscope exhibiting a FWHM of 477 ps. The pulse train behind the acousto-optic pulse picker is shown in Figure 9.4 (b). The temporal pulse separation of 168 ns corresponds to the pulse repetition frequency of 5.9 MHz.

The average power as a function of pump power was measured directly behind the two dichroic mirrors, which separated the residual pump light from the signal. Figure 9.5 (a) shows the resulting power characteristics of the amplifier. At the pump power of 12.5 W, the output power of the amplifier was 5.8 W. At this power level, the corresponding pulse energy before compression was 1.0 µJ.

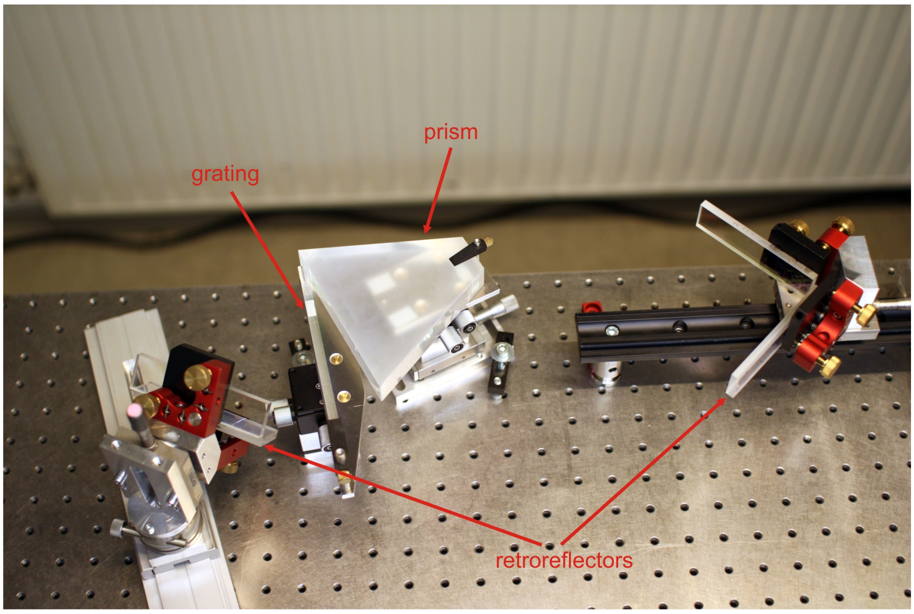

Figure 9.3: Photograph of the grism compressor.

As also observed in the last chapter, the nonlinear behavior of the curve is due to a wavelength shift of the pump diode with increasing output power. However, after compression with the above described grism arrangement, pulse energies of 0.6 µJ could be achieved taking the compressor efficiency of about 62 % into account. The average power after compression was thus 3.6 W.

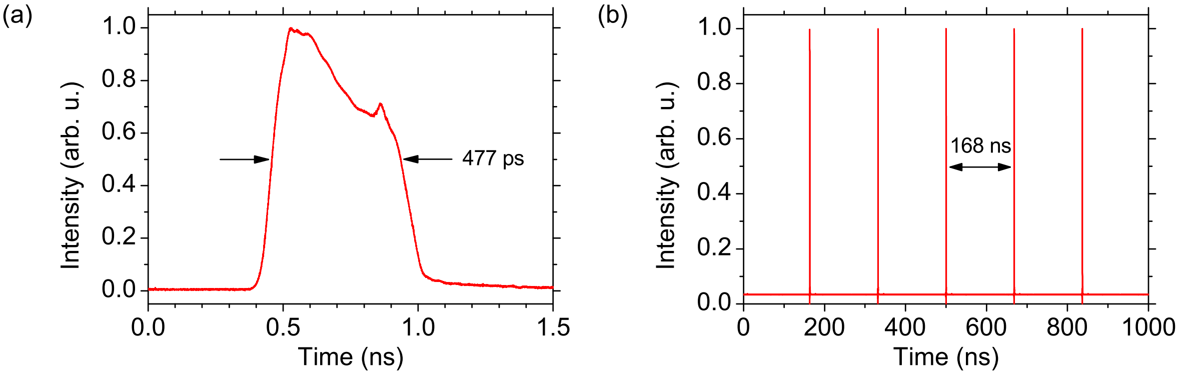

Figure 9.4: (a) Pulse profile after stretching. (b) Measured pulse train.

Like in the experiments described in the last chapter, the degree of polarization was measured using a calcite Wollaston prism with a 100,000:1 polarization extinction ratio. The transmission of linearly polarized light was optimized by adjusting a quarter- and a half-wave plate in front of the polarizer. Figure 9.5 (b) depicts the degree of polarization as a function of pulse energy after compression. It shows that the polarization degree was above 93 % for the reported pulse energies. Thus, the pulses could efficiently pass the polarization sensitive grism compressor. These results are similar to the measurements described in Section 8.4.

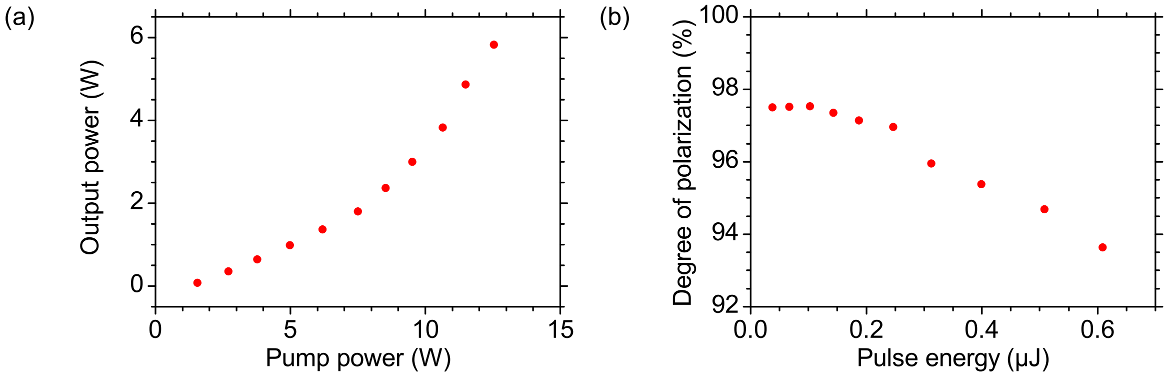

Figure 9.5: (a) Characteristic of the amplifier and (b) degree of polarization.

Similar to the characteristics of the amplifier described in Chapter 8, the spectral width decreases with increasing pulse energy due to spectral gain-narrowing. As a consequence, the Fourier limited pulse duration, calculated with the power spectrum assuming a constant spectral phase, also increased. The dependence of the Fourier limited pulse duration on the pulse energy is depicted in Figure 9.6. It shows the increase of the Fourier limit from about 107 fs at pulse energies of 0.1 µJ to about 115 fs for energies of 0.6 µJ after compression.

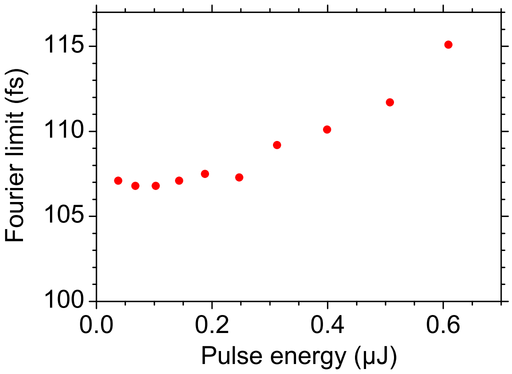

Figure 9.6: Fourier limited pulse duration as a function of pulse energy.

The autocorrelation of the compressed pulses is shown in Figure 9.7 (a). It exhibits a full width at half maximum of 214 fs. With the deconvolution factor of 1.407, which was calculated by using the ratio of the FWHM of the bandwidth limited autocorrelation and the FWHM of the Fourier transform of the power spectrum assuming a constant phase, the pulse duration can be estimated to 152 fs. The corresponding output spectrum is depicted in Figure 9.7 (b). The spectral full width at half maximum decreased from 36.4 nm before to 14.8 nm after amplification. Up to this pulse energy, the amplifier operated in the linear regime, i.e. the autocorrelation width stayed constant without readjustment of the compressor when increasing the pulse energy.

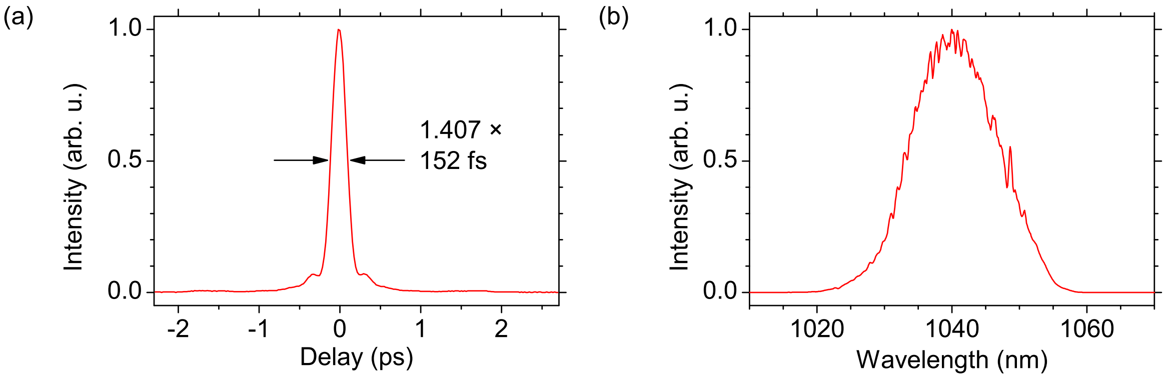

Figure 9.7: (a) Autocorrelation and (b) spectrum of the pulses with energies of 609 nJ.

Above the indicated pulse energies, the influence of the fiber nonlinearity on the pulse quality became noticeable. The nonlinear chirp, which was accumulated due to self-phase modulation in the fiber section, led to a pedestal in the autocorrelation similar to the one depicted in Figure 8.9 (b) in Chapter 8. The width of the autocorrelation function simultaneously increased, which indicated pulse durations larger than the duration of 152 fs, which was measured in the linear amplification regime. The influence of the nonlinearity on the pulse quality onset for pulse energies larger than about 0.6 µJ while in the amplifier described in the last chapter this threshold was reached at larger energies of about 2.2 µJ. This was expected as the 300 m of standard stretcher fiber resulted in stretched pulse durations of 477 ps while the specially designed fiber stretcher used in the experiments described in Chapter 8 led to stretched pulse durations of 940 ps. Thus, the pulse peak power was larger in the amplifier studied in this chapter. However, it can be expected that for larger pulse stretching ratios the system can be operated in the linear amplification regime with larger output pulse energies.

9.4 Conclusion

In summary, an all-fiber-based single-stage chirped-pulse amplification system was studied. It was seeded by an all-fiber-integrated dissipative-soliton laser. The dispersion of the applied standard step-index fiber stretcher including third-order dispersion was compensated for by a suitably designed grism compressor. Pulse energies of 0.6 µJ with pulse durations of 152 fs after compression were achieved. The corresponding average power was 3.6 W at the repetition frequency of 5.9 MHz. Larger pulse energies could be obtained but the fiber nonlinearity negatively influenced the pulse quality, which resulted in larger compressed pulse durations due to the accumulated nonlinear chirp.

Compared to pulse energies of 2.2 µJ and pulse durations of 189 fs achieved with the fiber CPA system described in Chapter 8, the amplifier system studied in this chapter generated smaller pulse energies of 0.6 µJ but also shorter pulses with 152 fs duration. The larger pulse energies achieved in the linear amplification regime can be explained by the larger pulse stretching ratio to pulse durations of 940 ps compared to 477 ps in the experiments described in this chapter. Thus, further pulse stretching is expected to also lead to pulses with larger energies and femtosecond durations. For that, the parameters of the used grism compressor have to be adapted, which would lead to larger overall compressor dimensions. However, the demonstrated chirped-pulse amplifier represents a compact and environmentally robust fiber-based alternative to bulk solid-state laser sources. Further optimization includes the usage of polarization-maintaining fibers for an increased robustness.

Compared to the amplifier studied in this chapter, the CPA system described in the last chapter has two advantages. First, it uses a standard grating compressor, which is easier to align, less complex, and thus lower in price compared to a grism compressor, which incorporates at least one prism. Second, the pulse stretching ratio can be much larger given an overall compressor footprint, which allows for larger output pulse energies. A minor disadvantage for applications is the fact that the triple-cladding fiber from OFS is not yet commercially available.

10 Conclusion

In this work, femtosecond fiber laser systems were studied with respect to all-fiber-integrability, low pulse repetition frequencies, and pulse energy scaling. The robustness of fiber laser systems against environmental disturbances would be largely increased by using exclusively fiber-based components and by stably connecting these by fusion splicing. For these reasons, all fibers used in this work had a solid fused silica core with core diameters ≤ 10 µm to avoid higher-order mode issues of large-mode area fibers and challenges of splicing photonic crystal fibers. In addition, ultrashort pulse fiber oscillators with low repetition frequencies would render costly and complex pulse picking units unnecessary in subsequent amplification stages for pulse energy scaling.

First, a fiber oscillator was studied with respect to a low repetition frequency. Operating in the stretched-pulse regime, the laser could successfully be mode-locked by using nonlinear polarization evolution in combination with a saturable absorber at a pulse repetition frequency of 1.8 MHz. 93 fs long pulses with energies of 0.6 nJ were generated after compression with a grating arrangement. The short pulse duration was achieved by implementing an appropriately designed grism compressor, which was optimized for intracavity dispersion compensation up to the third-order dispersion term. To the best of knowledge, these are the shortest pulses from a fiber oscillator with a repetition rate below 20 MHz. Further pulse energy scaling does not seem to be feasible with the applied stretched-pulse regime, as the pulses already accumulated nonlinear phase contribution due to self-phase modulation at the reported pulse energies. Thus, a further increase in pulse energy will most likely lead to larger output pulse durations. A further decrease of the pulse repetition frequency by increasing the intracavity fiber length was constrained by the grism compressor dimensions but may, in principle, be possible. In that case, the laser should be maximally mechanically stable and temperature stabilized to minimize changes of the polarization state due to fiber movement or temperature variations.

To generate larger pulse energies than described above, the dissipative-soliton regime was studied in regard to low pulse repetition frequencies. Contrary to the stretched-pulse regime, the pulse evolution is governed by pulse stretching at normal dispersion, spectral broadening due to self-phase modulation, and spectral filtering of chirped pulses. Using this scheme, mode-locking was successful at repetition frequencies of 29 MHz, 5.4 MHz, and 2.1 MHz. At these frequencies, maximum pulse energies of 4.1 nJ, 9 nJ, and 50 nJ, respectively, were achieved before compression. An increase of the intracavity dispersion—equivalent to increasing the fiber length—resulted in longer chirped as well as dechirped output pulses. The smallest compressed pulse durations at the above mentioned repetition rates were 194 fs, 302 fs, and 1.00 ps, respectively. Also, the spectral widths decreased with increasing intracavity fiber length and, consequently, the Fourier limited pulse durations increased. At the same time, smaller filter bandwidths had to be used at larger pulse repetition frequencies. Although the oscillator could not be mode-locked at a repetition rate of 0.5 MHz, pulse energy scaling may be possible by increasing the fiber length. Practical limitations are given by the fact that with decreasing repetition frequency the needed extracavity compressor dispersion also increases. Grating separations of > 1.5 m were necessary at 2.1 MHz repetition rate, which sets a practical limitation concerning the overall size of the laser system.

As inter alia the above described experiments showed, the intracavity dispersion should be minimized in order to achieve the shortest possible pulses in the dissipative-soliton pulse regime. This leads to large repetition frequencies and in core-pumped fiber oscillators, the achievable pulse energy is then constrained by the pump power of single-mode laser diodes, which is limited to about 1 to 2 W. To overcome this limitation, the double-cladding pumping scheme was applied to a dissipative-soliton laser. It used a high-power multi-mode laser diode for pumping and emitted an average output power of 1.2 W after compression. The 139 fs long pulses had energies of 25 nJ. As the experimental setup was not optimized regarding pulse energy and pulse duration, these parameters could later further scaled using fused silica solid-core fibers as described in References [Chi11, Chi12].

To fully profit from the advantages of the fiber as a waveguide medium such as alignment-free operation and environmental robustness, the gained knowledge of the dissipative-soliton regime was used to build an all-fiber-integrated oscillator with minimum compressed output pulse duration. For that, a wavelength-division multiplexer was used for spectral filtering and a fiber-pigtailed isolator substituted the free-space Faraday isolator previously used. After optimization of the laser parameters such as fiber length, filter bandwidth, and out-coupling ratio, linearly polarized pulses with energies of 2.2 nJ at 71 MHz repetition frequency could be generated. After compression with transmission gratings, pulse durations of 76 fs were measured. These are, to the best of knowledge, the shortest pulses demonstrated with an all-fiber-integrated design. The demonstrated laser was alignment-free and temperature-stabilized, which resulted in very stable output pulse parameters over time periods of several days without any readjustment.

Because the output spectrum was broader than the used intracavity spectral filter width, spectral components were transmitted through the side maxima of the filter, which had a periodic sinusoidal transmission characteristic. Consequently, a small side pulse evolved at the maximum pump power corresponding to the broadest spectrum. A solution to this would be the limitation to pulse energies with corresponding narrower spectra or using a spectral filter with a broader transmission characteristic. In the latter case, inter alia the filter bandwidth, the out-coupling ratio, and the length of the passive fiber behind the ytterbium-doped fiber, where spectral broadening and nonlinear polarization evolution takes place, have to be optimized.

As the pulse energy of the all-fiber laser was limited to about 3 nJ, the pulses were amplified using two different concepts. Both were designed to be fully fiber-integrated except for the pulse compressor. First, a specially designed fiber stretcher was used, whose dispersion inversely matched that of the grating compressor up to the third order. With that, pulse energies of 2.2 µJ and pulse durations of 189 fs could be generated after compression. The corresponding average power was 9.8 W at the repetition frequency of 4.5 MHz. Up to this power level, the amplifier operated in the linear regime, i.e. the output pulse duration was independent of the pulse energy.

At larger output pulse energies, the fiber nonlinearity negatively influenced the pulse quality, which resulted in larger pulse durations due to the accumulated nonlinear phase, which could not be compensated for by the compressor. Further pulse stretching would overcome this limitation, but at the same time would require a larger compressor dispersion and thus grating separations larger than 53 cm as used in the described experiments. This would oppose the aim of a compact amplifier footprint, so another way to decrease the peak power and thus the influence of the fiber nonlinearity would be the usage of large-mode area fibers. Due to their larger saturation average power compared to single-mode fibers, a preamplifier would be needed to generate a sufficiently large seed average power. Also, issues with higher-order modes have then to be considered. The demonstrated system, however, represents a compact and easy-to-integrate fiber-based alternative to bulk solid-state lasers. The system could be further optimized by using polarization-maintaining fibers as soon as the used specially designed fiber stretcher described in Reference [Grü10] is available in a polarization-preserving version.

The second amplifier used a standard fiber stretcher in combination with a specially designed grism compressor with a matched third- to second-order dispersion ratio. With that, an all-fiber-based single-stage chirped-pulse amplifier system was developed resulting in output pulse energies of 0.6 µJ and pulse durations of 152 fs after compression. The average power was 3.6 W at the repetition frequency of 5.9 MHz. Up to this pulse energy, the amplifier operated in the linear regime.

Similarly to the setup with the specially designed fiber stretcher, larger pulse energies could be obtained, but the fiber nonlinearity negatively influenced the pulse quality, which, due to the accumulated nonlinear chirp, resulted in longer compressed pulse durations. The generated pulse energy of 0.6 µJ was smaller compared to the 2.2 µJ achieved with the specially designed fiber stretcher. This can be explained by the smaller pulse stretching to 477 ps compared to 940 ps in the experiment described above. Thus, generating larger pulse energies in the linear amplifier regime is expected to be possible by further pulse stretching. In this case, the grism compressor dimensions have to be adapted according to the increased required dispersion and the given spectral bandwidth leading to a larger overall footprint. Besides energy considerations, smaller pulse durations of 152 fs compared to 189 fs achieved with the special fiber stretcher were measured. This may be due to differently strong influences of spectral gain-narrowing in the two amplifiers due to different output pulse energies. However, the all-fiber CPA system incorporating a standard fiber for pulse stretching and a grism arrangement for compression can be regarded as a compact and environmentally robust fiber-based alternative to bulk solid-state laser sources. Also in this case, further optimization would include the usage of polarization-maintaining fibers for increased stability and robustness.

Appendices

A References used for pulse parameter comparison in Figure 1.1

A. Albert, V. Couderc, L. Lefort, and A. Barthélémy. *High-energy femtosecond pulses from an ytterbium-doped fiber laser with a new cavity design.* IEEE Photon. Technol. Lett. **16**, pp. 416–418 (2004).

J. An, D. Kim, J. W. Dawson, M. J. Messerly, and C. P. J. Barty. *Grating-less, fiber-based oscillator that generates 25 nJ pulses at 80 MHz, compressible to 150 fs.* Opt. Lett. **32**, pp. 2010–2012 (2007).

J. R. Buckley, S. W. Clark, and F. W. Wise. *Generation of ten-cycle pulses from an ytterbium fiber laser with cubic phase compensation.* Opt. Lett. **31**, pp. 1340–1342 (2006).

J. Boullet, Y. Zaouter, E. Cormier, and J. Limpert. *31μJ, 220fs, 1MHz fiber chirped pulse amplification system.* Conference on Lasers and Electro-Optics/Quantum Electronics and Laser Science Conference and Photonic Applications Systems Technologies, OSA Technical Digest (CD) (Optical Society of America, 2008) , paper CThB1 (2008).

J. R. Buckley, F. W. Wise, F. Ö. Ilday, and T. Sosnowski. *Femtosecond fiber lasers with pulse energies above 10 nJ*. Opt. Lett. **30**, pp. 1888–1890 (2005).

J. Buckley, A. Chong, S. Zhou, W. Renninger, and F. W. Wise. *Stabilization of high-energy femtosecond ytterbium fiber lasers by use of a frequency filter*. J. Opt. Soc. Am. B **24**, pp. 1803–1806 (2007).

A. Chong, J. Buckley, W. Renninger, and F. Wise. *All-normal-dispersion femtosecond fiber laser*. Opt. Express **14**, pp. 10095–10100 (2006).

A. Chong, W. H. Renninger, and F. W. Wise. *All-normal-dispersion femtosecond fiber laser with pulse energy above 20 nJ*. Opt. Lett. **32**, pp. 2408–2410 (2007).

A. Chong, W. H. Renninger, and F. W. Wise. *Route to the minimum pulse duration in normal-dispersion fiber lasers.* Opt. Lett. **33**, pp. 2638–2640 (2008).

A. Chong, W. H. Renninger, and F. W. Wise. *Environmentally stable all-normal-dispersion femtosecond fiber laser*. Opt. Lett. **33**, pp. 1071–1073 (2008).

Y. Deng, C.-Y. Chien, B. G. Fidric, and J. D. Kafka. *Generation of sub-50 fs pulses from a high-power Yb-doped fiber amplifier*. Opt. Lett. **34**, pp. 3469–3471 (2009).

T. Eidam, S. Hädrich, F. Röser, E. Seise, T. Gottschall, J. Rothhardt, T. Schreiber, J. Limpert, and A. Tünnermann. *A 325-W-average-power fiber CPA system delivering sub-400 fs pulses*. IEEE Journ. of Sel. Topics in Quantum Electron. **15**, pp. 187–190 (2009).

T. Eidam, S. Hanf, E. Seise, T. V. Andersen, T. Gabler, C. Wirth, T. Schreiber, J. Limpert, and A. Tünnermann. *Femtosecond fiber CPA system emitting 830 W average output power*. Opt. Lett. **35**, pp. 94–96 (2010).

X.-H. Fang, M.-L. Hu, W. Liu, L. Chai, C.-Y. Wang, and A. M. Zheltikov. *Generation of 150 MW, 110 fs pulses by phase-locked amplification in multicore photonic crystal fiber*. Opt. Lett. **35**, pp. 2326–2328 (2010).

J. Fekete, A. Cserteg, and R. Szipocs. *All-fiber, all-normal dispersion ytterbium ring oscillator*. Laser Phys. Lett. **6**, pp. 49–53 (2009).

A. Fernández, L. Zhu, A. J. Verhoef, D. Sidorov-Biryukov, A. Pugžlys, A. Baltuška, K.-H. Liao, C.-H. Liu, A. Galvanauskas, S. Kane, R. Holzwarth, and F. Ö. Ilday. *Broadly tunable carrier envelope phase stable optical parametric amplifier pumped by a monolithic ytterbium fiber amplifier*. Opt. Lett. **34**, pp. 2799–2801 (2009).

A. Galvanauskas, G. C. Cho, A. Hariharan, M. E. Fermann, and D. Harter. *Generation of high-energy femtosecond pulses in multimode-core Yb-fiber chirped-pulse amplification systems*. Opt. Lett. **26**, pp. 935–937 (2001).

M. Hanna, D. Papadopoulos, F. Druon, and P. Georges. *Distributed nonlinear fiber chirped-pulse amplifier system*. Opt. Express **17**, pp. 10835–10840 (2009).

F. He, H. S. S. Hung, J. H. V. Price, N. K. Daga, N. Naz, J. Prawiharjo, D. C. Hanna, D. P. Shepherd, D. J. Richardson, J. W. Dawson, C. W. Siders, and C. P. Barty. *High energy femtosecond fiber chirped pulse amplification system with adaptive phase control*. Opt. Express **16**, pp. 5813–5821 (2008).

F. Ilday, J. Buckley, L. Kuznetsova, and F. Wise. *Generation of 36-femtosecond pulses from a ytterbium fiber laser*. Opt. Express **11**, pp. 3550–3554 (2003).

F. Ö. Ilday, H. Lim, J. R. Buckley, and F. W. Wise. *Practical all-fiber source of high-power, 120-fs pulses at 1 μm*. Opt. Lett. **28**, pp. 1362–1364 (2003).

H. Kalaycioglu, B. Oktem, Ç. Şenel, P. P. Paltani, and F. Ilday. *Microjoule-energy, 1 MHz repetition rate pulses from all-fiber-integrated nonlinear chirped-pulse amplifier*. Opt. Lett. **35**, pp. 959–961 (2010).

L. Kuznetsova, A. Chong, and F. W. Wise. *Interplay of nonlinearity and gain shaping in femtosecond fiber amplifiers*. Opt. Lett. **31**, pp. 2640–2642 (2006).

K. Kieu, W. H. Renninger, A. Chong, and F. W. Wise. *Sub-100 fs pulses at watt-level powers from a dissipative-soliton fiber laser*. Opt. Lett. **34**, pp. 593–595 (2009).

L. Kuznetsova, F. Wise, S. Kane, and J. Squier. *Chirped-pulse amplification near the gain-narrowing limit of Yb-doped fiber using a reflection grism compressor*. Appl. Phys. B: Lasers and Optics **88**, pp. 515–518 (2007).

L. Kuznetsova and F. W. Wise. *Scaling of femtosecond Yb-doped fiber amplifiers to tens of microjoule pulse energy via nonlinear chirped pulse amplification*. Opt. Lett. **32**, pp. 2671–2673 (2007).

K. Kieu and F. W. Wise. *All-fiber normal-dispersion femtosecond laser*. Opt. Express **16**, pp. 11453–11458 (2008).

C. Lecaplain, C. Chédot, A. Hideur, B. Ortaç, and J. Limpert. *High-power all-normal-dispersion femtosecond pulse generation from a Yb-doped large-mode-area microstructure fiber laser*. Opt. Lett. **32**, pp. 2738–2740 (2007).

J. Limpert, T. Schreiber, T. Clausnitzer, K. Zöllner, H.-J. Fuchs, E.-B. Kley, H. Zellmer, and A. Tünnermann. *High-power femtosecond Yb-doped fiber amplifier*. Opt. Express **10**, pp. 628–638 (2002).

H. Lim, F. Ö. Ilday, and F. W. Wise. *Generation of 2-nJ pulses from a femtosecond ytterbium fiber laser*. Opt. Lett. **28**, pp. 660–662 (2003).

X. Liu, J. Lægsgaard, and D. Turchinovich. *Highly-stable monolithic femtosecond Yb-fiber laser system based on photonic crystal fibers*. Opt. Express **18**, pp. 15475–15483 (2010).

C. Lecaplain, B. Ortaç, and A. Hideur. *High-energy femtosecond pulses from a dissipative soliton fiber laser*. Opt. Lett. **34**, pp. 3731–3733 (2009).

A. Malinowski, A. Piper, J. H. V. Price, K. Furusawa, Y. Jeong, J. Nilsson, and D. J. Richardson. *Ultrashort-pulse* Yb^{3+}*-fiber-based laser and amplifier system producing >25-W average power*. Opt. Lett. **29**, pp. 2073–2075 (2004).

I. Martial, D. Papadopoulos, M. Hanna, F. Druon, and P. Georges. *Nonlinear compression in a rod-type fiber for high energy ultrashort pulse generation*. Opt. Express **17**, pp. 11155–11160 (2009).

P. K. Mukhopadhyay, K. Özgören, I. L. Budunoglu, and F. Ö. Ilday. *All-fiber low-noise high-power femtosecond Yb-fiber amplifier system seeded by an all-normal dispersion fiber oscillator*. IEEE J. Sel. Top. Quantum Electron. **15**, pp. 145–152 (2009).

C. K. Nielsen and S. R. Keiding. *All-fiber mode-locked fiber laser*. Opt. Lett. **32**, pp. 1474–1476 (2007).

J. W. Nicholson, S. Ramachandran, and S. Ghalmi. *A passively-modelocked, Yb-doped, figure-eight, fiber laser utilizing anomalous-dispersion higher-order-mode fiber*. Opt. Express **15**, pp. 6623–6628 (2007).

B. Ortaç, J. Limpert, and A. Tünnermann. *High-energy femtosecond Yb-doped fiber laser operating in the anomalous dispersion regime*. Opt. Lett. **32**, pp. 2149–2151 (2007).

B. Ortaç, A. Hideur, T. Chartier, M. Brunel, C. Özkuln, and F. Sanchez. *90-fs stretched-pulse ytterbium-doped double-clad fiber laser*. Opt. Lett. **28**, pp. 1305–1307 (2003).

B. Ortaç, O. Schmidt, T. Schreiber, J. Limpert, A. Tünnermann, and A. Hideur. *High-energy femtosecond Yb-doped dispersion compensation free fiber laser*. Opt. Express **15**, pp. 10725–10732 (2007).

B. Ortac, C. Lecaplain, A. Hideur, T. Schreiber, J. Limpert, and A. Tünnermann. *Passively mode-locked single-polarization microstructure fiber laser*. Opt. Express **16**, pp. 2122–2128 (2008).

D. N. Papadopoulos, Y. Zaouter, M. Hanna, F. Druon, E. Mottay, E. Cormier, and P. Georges. *Generation of 63 fs 4.1 MW peak power pulses from a parabolic fiber amplifier operated beyond the gain bandwidth limit*. Opt. Lett. **32**, pp. 2520–2522 (2007).

D. N. Papadopoulos, I. Martial, M. Hanna, F. Druon, and P. Georges. *Active spectral phase control by use of an acousto-optic programmable filter in high-repetition-rate sub-80 fs nonlinear fiber amplifiers*. Opt. Lett. **33**, pp. 1431–1433 (2008).

D. N. Papadopoulos, M. Hanna, F. Druon, and P. Georges. *Compensation of gain narrowing by self-phase modulation in high-energy ultrafast fiber chirped-pulse amplifiers*. IEEE J. Sel. Top. Quantum Electron. **15**, pp. 182–186 (2009).

J. Prawiharjo, N. K. Daga, R. Geng, J. H. V. Price, D. C. Hanna, D. J. Richardson, and D. P. Shepherd. *High fidelity femtosecond pulses from an ultrafast fiber laser system via adaptive amplitude and phase pre-shaping*. Opt. Express **16**, pp. 15074–15089 (2008).

W. H. Renninger, A. Chong, and F. W. Wise. *Giant-chirp oscillators for short-pulse fiber amplifiers*. Opt. Lett. **33**, pp. 3025–3027 (2008).

F. Röser, J. Rothhard, B. Ortac, A. Liem, O. Schmidt, T. Schreiber, J. Limpert, and A. Tünnermann. *131 W 220 fs fiber laser system*. Opt. Lett. **30**, pp. 2754–2756 (2005).

F. Röser, T. Eidam, J. Rothhardt, O. Schmidt, D. N. Schimpf, J. Limpert, and A. Tünnermann. *Millijoule pulse energy high repetition rate femtosecond fiber chirped-pulse amplification system*. Opt. Lett. **32**, pp. 3495–3497 (2007).

F. Röser, D. Schimpf, O. Schmidt, B. Ortac, K. Rademaker, J. Limpert, and A. Tünnermann. *90 W average power 100 μJ energy femtosecond fiber chirped-pulse amplification system*. Opt. Lett. **32**, pp. 2230–2232 (2007).

A. Ruehl, A. Marcinkevicius, M. E. Fermann, and I. Hartl. *80 W, 120 fs Yb-fiber frequency comb*. Opt. Lett. **35**, pp. 3015–3017 (2010).

T. Schreiber, C. K. Nielsen, B. Ortac, J. Limpert, and A. Tünnermann. *Microjoule-level all-polarization-maintaining femtosecond fiber source*. Opt. Lett. **31**, pp. 574–576 (2006).

T. R. Schibli, I. Hartl, D. C. Yost, M. J. Martin, A. Marcinkevičius, M. E. Fermann, and J. Ye. *Optical frequency comb with submillihertz linewidth and more than 10 W average power*. Nat. Phot. **2**, pp. 355–359 (2008).

M. Schultz, H. Karow, O. Prochnow, D. Wandt, U. Morgner, and D. Kracht. *All-fiber ytterbium femtosecond laser without dispersion compensation*. Opt. Express **16**, pp. 19562–19567 (2008).

M. Schultz, H. Karow, D. Wandt, U. Morgner, and D. Kracht. *Ytterbium femtosecond fiber laser without dispersion compensation tunable from 1015 nm to 1050 nm*. Opt. Comm. **282**, pp. 2567–2570 (2009).

L. Shah, Z. Liu, I. Hartl, G. Imeshev, G. Cho, and M. Fermann. *High energy femtosecond Yb cubicon fiber amplifier*. Opt. Express **13**, pp. 4717–4722 (2005).

L. Shah, M. E. Fermann, J. W. Dawson, and C. P. J. Barty. *Micromachining with a 50 W, 50 μJ, sub-picosecond fiber laser system*. Opt. Express **14**, pp. 12546–12551 (2006).

L. Shah, Z. Liu, I. Hartl, G. C. Cho, and M. E. Fermann. *High-power ultra-fast fiber amplifiers*. Conference on Lasers and Electro-Optics/Quantum Electronics and Laser Science Conference and Photonic Applications Systems Technologies, Technical Digest (CD) (Optical Society of America, 2006) , paper CFN1 (2006).

D. Turchinovich, X. Liu, and J. Lægsgaard. *Monolithic all-PM femtosecond Yb-fiber laser stabilized with a narrow-band fiber Bragg grating and pulse-compressed in a hollow-core photonic crystal fiber*. Opt. Express **16**, pp. 14004–14014 (2008).

Y. Zaouter, D. N. Papadopoulos, M. Hanna, F. Druon, E. Cormier, and P. Georges. *Third-order spectral phase compensation in parabolic pulse compression*. Opt. Express **15**, pp. 9372–9377 (2007).

Y. Zaouter, J. Boullet, E. Mottay, and E. Cormier. *Transform-limited 100 µJ, 340 MW pulses from a nonlinear-fiber chirped-pulse amplifier using a mismatched grating stretcher-compressor*. Opt. Lett. **33**, pp. 1527–1529 (2008).

Y. Zaouter, D. N. Papadopoulos, M. Hanna, J. Boullet, L. Huang, C. Aguergaray, F. Druon, E. Mottay, P. Georges, and E. Cormier. *Stretcher-free high energy nonlinear amplification of femtosecond pulses in rod-type fibers*. Opt. Lett. **33**, pp. 107–109 (2008).

X. Zhou, D. Yoshitomi, Y. Kobayashi, and K. Torizuka. *Generation of 28-fs pulses from a mode-locked ytterbium fiber oscillator*. Opt. Express **16**, pp. 7055–7059 (2008).

C. Zhou, W. Yang, G. Zhang, Y. Cai, J. Li, P. Li, and Z. Zhang. *Novel ring cavity for ytterbium-doped mode-locked fiber laser incorporated with both SESAM and grating pair*. IEEE Photon. Technol. Lett. **21**, pp. 3–5 (2009).

S. Zhou, T. Takamido, S. Imai, and F. Wise. *Exploitation of stimulated Raman scattering in short-pulse fiber amplifiers*. Opt. Lett. **35**, pp. 2397–2399 (2010).

B Easy-to-implement grism compressor

Here, a simple and easy-to-implement grism compressor setup for the compensation of third-order dispersion at 1 µm wavelength is presented. The design uses off-the-shelf components like an equilateral prism and a transmission grating. One advantage of the proposed setup is that the prism can be placed in the beam close to the Brewster's angle, which in the case of the used prism material N-F2 is 58.0° at 1030 nm wavelength. Thus, the prism does not necessarily need an antireflective coating and is low-cost due to the equiangularity. Another advantage is the simple alignment due to the usage of a single prism and single grating as depicted in Figure 3.6 [Akt06, Cha10].

In the proposed setup, a grating line density of 1000/mm with a line separation of about the center wavelength is assumed for a maximum transmission efficiency a 1 µm wavelength. The geometrical parameters of the compressor setup are depicted in Table 10.1. Figure B.1 shows the resulting dispersion curve of the grism compressor together with the target dispersion curve, which corresponds to the standard fiber stretcher dispersion as described in Section 2.1. As both curves fit very well concerning the dispersion slope, the proposed grism setup can be used

Line density	Wavelength	Incidence angle	Apex angle	Prism grating angle
1000/mm	1030 nm	31.0°	60.0°	-22.0°

D_2	D_2	P_1	P_2	L_{45}
50 mm	50 mm	5 mm	40 mm	600 mm

Table 10.1: Parameters of the grism compressor with N-F2 prism (see also Figure 3.4).

for dispersion compensation of standard fiber at 1030 nm wavelength. The absolute dispersion value of about -4.0 ps^2 corresponds to a fiber length of about 167 m of standard fiber and thus opens up possibilities for applications outside as well as inside the laser cavity.

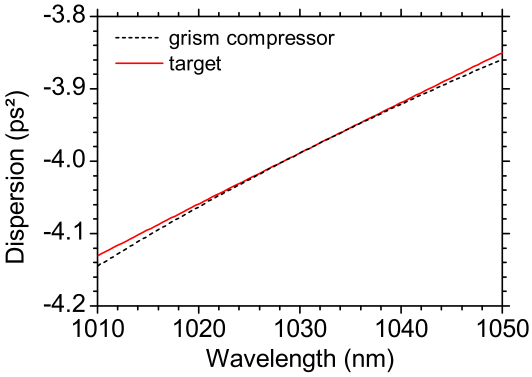

Figure B.1: Dispersion of the grism compressor with N-F2 prism and the target dispersion curve.

C Intracompressor parallel plate for dispersion tuning

A drawback of grating and grism compressors with large groove densities is the small angular alignment tolerance due to the highly diffractive nature of the gratings. Here, it is analyzed how an intracompressor parallel glass plate can be used to influence the dispersive properties of the compressor. This is similar to the concept of inserting a plane parallel plate between the gratings of a compressor for tunable third-order phase compensation as described in Reference [Bra98].

A sketch of the design is depicted in Figure C.1. It is similar to the grism compressor described in Section 3.2 except for the intracompressor parallel glass plate. The dispersive properties are calculated using the program described in Section 3.2, which allows simulating the insertion of plane plates made of various materials. If the prism material is set to "no material" and the corresponding prism angles and distances are set to zero, the program can also be used to calculate the dispersion of grating compressors with or without intragrating-pair parallel plates. In the following, the influence of a parallel fused silica plate inside a grism and a grating compressor is analyzed.

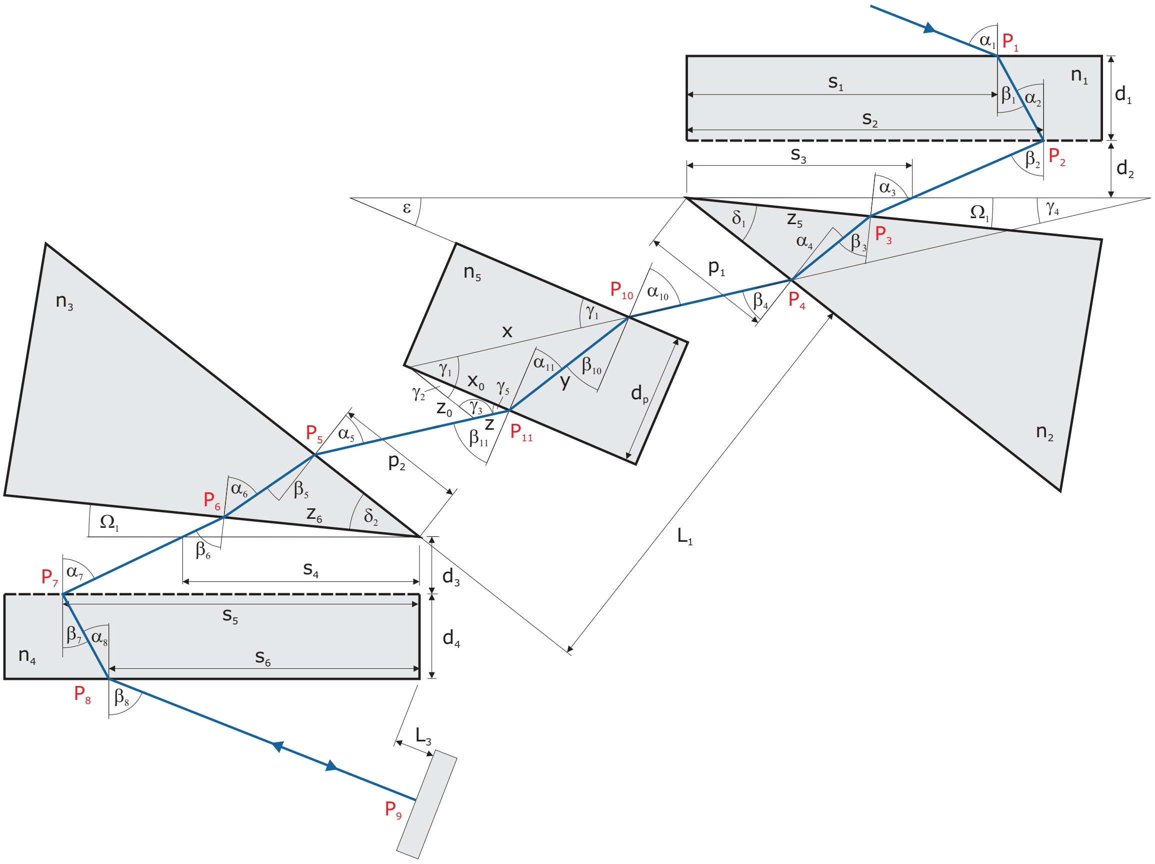
α_1
P_1
n_1
s_1
β_1
α_2
d_1
s_2
β_2
P_2
d_2
s_3
α_3
ε
δ_1
z_5
Ω_1
γ_4
α_4
β_3
P_3
p_1
n_5
P_{10}
α_{10}
β_4
P_4
n_3
γ_1
x
α_{11}
β_{10}
γ_1
x_0
γ_5
y
d_p
γ_2
z_0
γ_3
z
β_{11}
P_{11}
P_5
α_5
p_2
n_2
α_6
β_5
P_6
z_6
δ_2
L_1
Ω_1
β_6
P_7
α_7
s_4
d_3
s_5
d_4
β_7
α_8
n_4
s_6
P_8
β_8
L_3
P_9

Figure C.1: Sketch of the compressor with an intragrism-pair parallel plate.

Intragrism-pair parallel plate

To demonstrate the principle, a 20 mm thick fused silica glass plate is placed in the beam of the grism compressor described in Section 9.2. Figure C.2 shows the resulting dispersion together with the dispersion curves of the same setup with the fused silica glass plate placed into the beam under 45° and −45°. If the plate is placed under 45°, the dispersion curve is shifted to smaller absolute values, while placing it under −45° resulted in a shift towards larger absolute values. The gradient of the absolute dispersion when tilting the plate by one degree is approximated to 9.5×10^{-4} ps^2/°.

This value is now compared to that of the compressor without the plate. Thus, the change of dispersion with varying incidence angle is analyzed. The resulting gradient is 3.1×10^{-3} ps^2/°, which is about 3 times larger than the value corresponding to tilting the plate. This scheme can thus be considered when issues with dispersion fine tuning occur in femtosecond lasers and

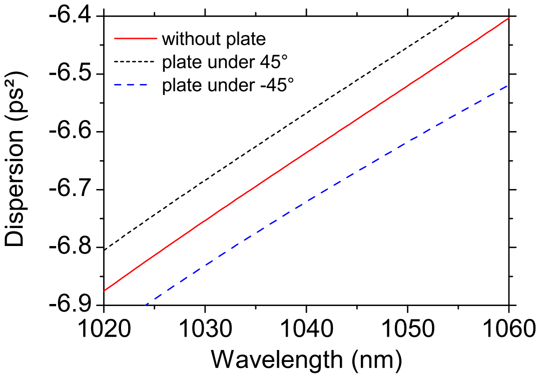

Figure C.2: Dispersion of the grism compressor with and without the glass plate.

amplifiers. Concerning the third-order dispersion, the β_3/β_2 ratio only changes slightly from 0.91 fs to 1.00 fs when tilting the plate from $-45°$ to $45°$.

Intragrating-pair parallel plate

To analyze the influence of the plate inside a grating compressor, the dispersion of the grating compressor described in Section 8.2 is used as a reference. As described above, a 20 mm thick fused silica plate is also used here, which is placed under $45°$ and $-45°$ into the beam. Figure C.3 shows the calculated dispersion curves of the grating compressor with and without the plate.

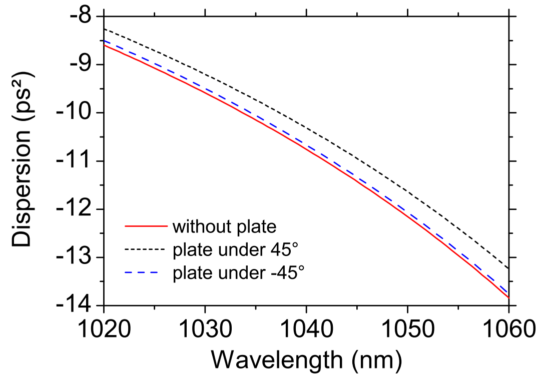

Figure C.3: Dispersion of the grating compressor with and without the glass plate.

Compared to the results with the grism compressor, the plate inside the grating compressor influences the dispersion curve differently. Here, tilting the plate away from $0°$ always results in a reduction of the absolute dispersion value, while the reduction is larger at $45°$ compared to the value at $-45°$. The corresponding dispersion gradient when tilting the plate is approximately 5.0×10^{-3} ps^2/° for increasing the plate angle and 1.0×10^{-3} ps^2/° for decreasing the plate angle. As in the case of the grism compressor, the calculated gradient of the compressor dispersion without the plate when varying the incidence angle of 0.46 $\mathrm{ps}^2/^\circ$ is larger than the gradient for the plate tilting. Thus, fine tuning of the dispersion can also be considered in the case of grating compressors. In this case, the default plate angle should be a nonzero value.

List of acronyms and abbreviations

AC	autocorrelation
arb. u.	arbitrary units
ASE	amplified spontaneous emission
CPA	chirped-pulse amplification
CW	continuous wave
DCF	double-cladding fiber
FOD	fourth-order dispersion
FC	fiber coupler
FR	Faraday rotator
FT	Fourier transform
FWHM	full width at half maximum
GDD	group delay dispersion
HWP	half-wave plate
LMA	large mode area
MFD	mode field diameter
NA	numerical aperture
NPE	nonlinear polarization evolution
PBS	polarizing beam splitter
QWP	quarter-wave plate
RF	radio frequency
RMS	root mean square
SAM	saturable absorber mirror
SESAM	semiconductor saturable absorber mirror
SMF	single-mode fiber
SOD	second-order dispersion
SPM	self-phase modulation

TCF	triple-cladding fiber
TOD	third-order dispersion
WDM	wavelength-division multiplexer
YDF	ytterbium-doped fiber

List of figures

1.1 Pulse parameters of state-of-the-art ytterbium-doped fiber oscillators (open circles) and amplifiers (full circles). The parameters achieved in this thesis are depicted in red. The references are listed in Appendix A. 2

2.1 Cross section and corresponding refractive index profile of a step-index fiber. . . 6
2.2 (a) Material and fiber dispersion. (b) Detail of graph (a). 8
2.3 (a) Typical emission and absorption cross sections of ytterbium-doped glass and (b) energy level diagram of ytterbium [Pas95]. 9
2.4 Schematic of the mode-locking mechanism using nonlinear polarization evolution (from Reference [Hau95]). 10
2.5 Dispersion, pulse duration, and chirp along the stretched-pulse resonator (from Reference [Wis08]). 11
2.6 (a) Dispersion, pulse duration, and chirp along the dissipative-soliton resonator (from Reference [Wis08]). (b) Spectral filtering of chirped pulses leads to a temporal shortening. 12

3.1 Schematic of a chirped-pulse amplification system. 13
3.2 (a) Stretched pulse duration due to second- and third-order dispersion. (b) Residual TOD leads to increased RMS widths after compression. 16
3.3 Typical dispersion curves of grating and grism compressors with the indicated grating line densities. 17
3.4 Sketch of the grism compressor. A ray through the device is depicted in blue. . . 18
3.5 Grism compressor dispersion calculator. 20
3.6 Simplified grism compressor setup. 20
3.7 (a) Index profile and (b) dispersion curve of a typical triple-cladding fiber (from Reference [Grü10]). 21

4.1 Experimental setup. HWP half-wave plate, QWP quarter-wave plate, SBR saturable Bragg reflector, PBS polarizing beam splitter, FR Faraday rotator, FC fiber output coupler, SMF single-mode fiber, WDM wavelength-division multiplexer, YDF ytterbium-doped fiber. The different output ports are labeled by numbers. 24

4.2 Calculated grism compressor dispersion and target dispersion. 26

4.3 (a) Pulse train and (b) spectrum measured at port 4. 27

4.4 (a) Intensity autocorrelation measured at output port 4 with a FWHM of 5.3 ps. (b) Measured intensity autocorrelation of the compressed pulses (solid) and calculated transform limited autocorrelation (dashed). 27

4.5 Spectral evolution inside the laser. The spectra are measured at the different output ports of the oscillator as depicted in Figure 4.1. 28

5.1 (a) Schematic of the birefringent quartz plate filter. PBS polarizing beam splitter. (b) Bandwidth of the filter as a function of plate thickness. 32

5.2 Experimental setup. HWP half-wave plate, QWP quarter-wave plate, PBS polarizing beam splitter, FR Faraday rotator, FC fiber output coupler, SMF single-mode fiber, WDM wavelength-division multiplexer, YDF ytterbium-doped fiber. 33

5.3 (a) Pulse train and (b) autocorrelation of the 41 nJ pulses at 2.1 MHz repetition frequency. 34

5.4 Spectrum of the 41 nJ pulses at 2.1 MHz in (a) linear and (b) logarithmic scale. 35

5.5 Radio frequency spectra of the 41 nJ pulses with a span of (a) 500 Hz and (b) 100 MHz. 35

5.6 (a) Autocorrelation measurement of the 50 nJ pulses at 2.1 MHz repetition frequency and (b) corresponding spectrum with a filter bandwidth of 5.5 nm. . . 36

5.7 (a) Autocorrelation measurement of the 27 nJ pulses at 2.1 MHz repetition frequency and (b) corresponding spectrum using a filter bandwidth of 3.9 nm. . . 37

5.8 (a) Autocorrelation measurement of the 21 nJ pulses at 2.1 MHz repetition frequency and (b) corresponding spectrum using a filter bandwidth of 3.0 nm. . . 37

5.9 (a) Characteristic of the laser with 5.4 MHz repetition frequency and a filter bandwidth of 3.9 nm. (b) Autocorrelation measurement of the uncompressed pulses with energies of 9 nJ. 38

5.10 (a) Autocorrelation measurement of the 9 nJ pulses at 5.4 MHz repetition frequency and (b) corresponding spectrum with a filter bandwidth of 3.9 nm. 39

5.11 (a) Spectral width and (b) pulse duration as a function of pulse energy at 5.4 MHz repetition rate and 3.9 nm filter bandwidth. 39

5.12 Output spectra of the oscillator with the repetition frequency of 5.4 MHz and 3.9 nm filter bandwidth at the indicated pulse energies. 40

5.13 (a) Autocorrelation and (b) output spectrum of the oscillator with the repetition frequency of 29 MHz and 7.3 nm filter bandwidth. 41

6.1 Experimental setup. HWP half-wave plate, QWP quarter-wave plate, DC dichroic mirror, PBS polarizing beam splitter, FR Faraday rotator, YDF ytterbium-doped fiber. 44

6.2 Photograph of the double-cladding dissipative-soliton laser. 45
6.3 (a) Output spectrum of the oscillator and (b) corresponding pulse train. 45
6.4 Autocorrelation of the (a) uncompressed and (b) compressed pulses. 46
6.5 Radio frequency spectra of the pulse train with a span of (a) 2 GHz and (b) 10 kHz. 46

7.1 Schematic of the fiber ring cavity. WDM wavelength-division multiplexer, YDF ytterbium-doped fiber, OC output coupler, PC polarization controller. 50
7.2 Measured relative transmission (solid curve) of the small bandwidth WDM and the corresponding spectra of the input (dotted) and output (dashed) light. 51
7.3 Photograph of the laser. The fiber components are fixed under rubber mats. . . . 52
7.4 (a) Photodetector signal of the pulse train. (b) Autocorrelation of the uncompressed pulses. 52
7.5 (a) Autocorrelation of the compressed pulses (solid curve) and of the Fourier limited pulses (dashed curve) and (b) detail of the side peak in the autocorrelation. 53
7.6 Measured spectra. (a) Transmitted and (b) rejected signal from the PBS behind the output coupler. 54
7.7 Radio-frequency spectra with a span of (a) 1 GHz and (b) 1 kHz centered at the fundamental repetition rate of 71 MHz. 54
7.8 (a) Measured output power as a function of pump power. The diagrams (b), (c), and (d) show the output spectra for the indicated pulse energies. 55
7.9 (a) Dependence of the spectral FWHM on the pulse energy. (b) Measured and Fourier limited pulse durations as a function of pulse energy. 56
7.10 (a) Deviation of the measured pulse FWHM from the Fourier limited FWHM. (b) Compressor dispersion for minimum pulse width as a function of pulse energy. 57

8.1 Experimental setup. AOM acousto-optic modulator, TCF triple-cladding fiber, SMF single-mode fiber, YDF ytterbium-doped fiber, DC dichroic mirror, HWP half-wave plate, QWP quarter-wave plate, PBS polarizing beam splitter. 61
8.2 Dispersion curve of the triple-cladding fiber and Nufern 1060-XP fiber. 63
8.3 (a) Dispersion curves of the target (gratings, 1500/mm), Nufern 1060-XP (SMF, modeled), and the triple-cladding fiber (TCF). (b) Dispersion of the target (gratings, 1500/mm) and of the combined stretcher module. 63
8.4 Stretched pulse duration for different fiber lengths. The lines represent the simulated pulse stretching. 65
8.5 (a) Temporal profile of the stretched pulse. (b) Pulse train of the seed pulses. . . 66
8.6 (a) Amplifier characteristic. (b) Degree of polarization as a function of pulse energy. 67
8.7 (a) Spectrum and (b) autocorrelation of the compressed pulses with pulse energies of 2.2 µJ. 67
8.8 (a) Simulated temporal shape and (b) autocorrelation of the pulses without third-order dispersion compensation. 69

8.9 (a) Dependence of the Fourier limit of the amplified pulses on the pulse energy. (b) Autocorrelation of the pulses with the maximum achieved pulse energy. . . . 69
8.10 Spectral evolution with increasing pulse energy. The spectra were vertically offset by 10 dB. 70

9.1 Sketch of the experimental setup. AOM acousto-optic modulator, SMF single-mode fiber, YDF ytterbium-doped fiber, DC dichroic mirror, HWP half-wave plate, QWP quarter-wave plate, PBS polarizing beam splitter. 74
9.2 (a) Dispersion of the grism compressor and the target. (b) Comparison with the dispersion of grating compressors with different line densities. 76
9.3 Photograph of the grism compressor. 77
9.4 (a) Pulse profile after stretching. (b) Measured pulse train. 77
9.5 (a) Characteristic of the amplifier and (b) degree of polarization. 78
9.6 Fourier limited pulse duration as a function of pulse energy. 78
9.7 (a) Autocorrelation and (b) spectrum of the pulses with energies of 609 nJ. . . . 79

B.1 Dispersion of the grism compressor with N-F2 prism and the target dispersion curve. 91
C.1 Sketch of the compressor with an intragrism-pair parallel plate. 92
C.2 Dispersion of the grism compressor with and without the glass plate. 93
C.3 Dispersion of the grating compressor with and without the glass plate. 93

List of tables

2.1 Group delay dispersion of fused silica and Nufern 1060-XP fiber at 1030 nm wavelength. 7

3.1 Dispersion lengths for Gaussian pulses with different pulse durations. 17

5.1 Pulse parameters of the oscillator with 29 MHz repetition frequency. 42

8.1 Properties of the triple-cladding stretcher fiber. 61

9.1 Parameters of the grism pulse compressor (see also Figure 3.4). 75

10.1 Parameters of the grism compressor with N-F2 prism (see also Figure 3.4). . . . 91

References

[Agr07] G. P. Agrawal. *Nonlinear fiber optics*. 4th ed. Academic Press (2007). (Cit. on pp. 5, 6, 15, 16)

[Akh05] N. Akhmediev and A. Ankiewicz. *Dissipative solitons*. Springer (2005). (Cit. on p. 12)

[Akt06] S. Akturk, X. Gu, M. Kimmel, and R. Trebino. *Extremely simple single-prism ultrashort-pulse compressor*. Opt. Express **14**, pp. 10101–10108 (2006). (Cit. on pp. 25, 75, 90)

[And92] D. Anderson, M. Desaix, M. Lisak, and M. L. Quiroga-Teixero. *Wave breaking in nonlinear-optical fibers*. J. Opt. Soc. Am. B **9**, pp. 1358–1361 (1992). (Cit. on p. 11)

[Ban00] P. S. Banks, M. D. Perry, V. Yanovsky, S. N. Fochs, B. C. Stuart, and J. Zweiback. *Novel all-reflective stretcher for chirped-pulse amplification of ultrashort pulses*. IEEE Journ. of Quantum Electron. **36**, pp. 268–274 (2000). (Cit. on p. 14)

[Bau12] M. Baumgartl, C. Lecaplain, A. Hideur, J. Limpert, and A. Tünnermann. *Fiber oscillator producing 91 fs pulses with 0.8 μJ at 60 W of average power*. Conference on Lasers and Electro-Optics, Optical Society of America, AT1A.2 (2012). (Cit. on p. 47)

[Boy03] R. W. Boyd. *Nonlinear Optics*. 2nd ed. Academic Press (2003). (Cit. on pp. 1, 9)

[Bra98] A. Braun, T. Sosnowski, S. Kane, P. Van Romday, T. Norris, and G. A. Mourou. *Tunable third-order phase compensation by refraction from an intragrating-pair parallel plate*. IEEE Journ. of Sel. Topics in Quantum Electron. **4**, pp. 426–429 (1998). (Cit. on p. 91)

[Buc05] J. R. Buckley, F. W. Wise, F. Ö. Ilday, and T. Sosnowski. *Femtosecond fiber lasers with pulse energies above 10 nJ*. Opt. Lett. **30**, pp. 1888–1890 (2005). (Cit. on p. 11)

[Cau97] V. Cautaerts, D. J. Richardson, R. Paschotta, and D. C. Hanna. *Stretched pulse* Yb^{3+} *silica fiber laser*. Opt. Lett. **22**, pp. 316–318 (1997). (Cit. on p. 23)

[Cha06] G. Chang, C. J. Divin, C.-H. Liu, S. L. Williamson, A. Galvanauskas, and T. B. Norris. *Power scalable compact THz system based on an ultrafast Yb-doped fiber amplifier*. Opt. Express **14**, pp. 7909–7913 (2006). (Cit. on p. 1)

[Cha09] G. Chang, M. Rever, V. Smirnov, L. Glebov, and A. Galvanauskas. *Femtosecond Yb-fiber chirped-pulse-amplification system based on chirped-volume Bragg gratings*. Opt. Lett. **34**, pp. 2952–2954 (2009). (Cit. on p. 14)

[Cha10] V. Chauhan, P. Bowlan, J. Cohen, and R. Trebino. *Single-diffraction-grating and grism pulse compressors*. J. Opt. Soc. Am. B **27**, pp. 619–624 (2010). (Cit. on pp. 19, 25, 75, 90)

[Che96] G. Cheriaux, P. Rousseau, F. Salin, J. P. Chambaret, B. Walker, and L. F. Dimauro. *Aberration-free stretcher design for ultrashort-pulse amplification*. Opt. Lett. **21**, pp. 414–416 (1996). (Cit. on p. 14)

[Chi10] N. B. Chichkov, K. Hausmann, D. Wandt, U. Morgner, J. Neumann, and D. Kracht. *50 fs pulses from an all-normal dispersion erbium fiber oscillator*. Opt. Lett. **35**, pp. 3081–3083 (2010). (Cit. on pp. 12, 38, 50)

[Chi11] N. B. Chichkov, C. Hapke, K. Hausmann, T. Theeg, D. Wandt, U. Morgner, J. Neumann, and D. Kracht. *0.5 µJ pulses from a giant-chirp ytterbium fiber oscillator*. Opt. Express **19**, pp. 3647–3650 (2011). (Cit. on pp. 31, 47, 82)

[Chi12] N. B. Chichkov, C. Hapke, J. Neumann, D. Kracht, D. Wandt, and U. Morgner. *Pulse duration and energy scaling of femtosecond all-normal dispersion fiber oscillators*. Opt. Express **20**, pp. 3844–3852 (2012). (Cit. on pp. 12, 47, 82)

[Chi96] B. N. Chichkov, C. Momma, S. Nolte, F. von Alvensleben, and A. Tünnermann. *Femtosecond, picosecond and nanosecond laser ablation of solids*. Appl. Phys. A **63**, pp. 109–115 (1996). (Cit. on p. 1)

[Cho06] A. Chong, J. Buckley, W. Renninger, and F. Wise. *All-normal-dispersion femtosecond fiber laser*. Opt. Express **14**, pp. 10095–10100 (2006). (Cit. on p. 12)

[Cho07] A. Chong, W. H. Renninger, and F. W. Wise. *All-normal-dispersion femtosecond fiber laser with pulse energy above 20 nJ*. Opt. Lett. **32**, pp. 2408–2410 (2007). (Cit. on pp. 23, 31, 40)

[Cho08a] A. Chong, W. H. Renninger, and F. W. Wise. *Properties of normal-dispersion femtosecond fiber lasers*. J. Opt. Soc. Am. B **25**, pp. 140–148 (2008). (Cit. on pp. 38, 50)

[Cho08b] A. Chong, W. H. Renninger, and F. W. Wise. *Route to the minimum pulse duration in normal-dispersion fiber lasers*. Opt. Lett. **33**, pp. 2638–2640 (2008). (Cit. on p. 50)

[Cho08c] C. Y. Chong. *Femtosecond fiber lasers and amplifiers based on the pulse propagation at normal dispersion*. PhD thesis. Cornell University (2008). (Cit. on pp. 38, 50)

[Cla03] T. Clausnitzer, J. Limpert, K. Zöllner, H. Zellmer, H.-J. Fuchs, E.-B. Kley, A. Tünnermann, M. Jupé, and D. Ristau. *Highly efficient transmission gratings in fused silica for chirped-pulse amplification systems*. Appl. Opt. **42**, pp. 6934–6938 (2003). (Cit. on p. 14)

[Cla08] T. Clausnitzer, T. Kämpfe, E.-B. Kley, A. Tünnermann, A. V. Tishchenko, and O. Parriaux. *Highly-dispersive dielectric transmission gratings with 100% diffraction efficiency*. Opt. Express **16**, pp. 5577–5584 (2008). (Cit. on p. 14)

[Cla09] T. Clausnitzer. *Personal communication*. Apr. 2009 (cit. on p. 75).

[Cor93] P. B. Corkum. *Plasma perspective on strong-field multiphoton ionization*. Phys. Rev. Lett. **71**, 1994–1997 (1993). (Cit. on p. 1)

[Cry11] Crystal Fibre / NKT Photonics. *HC-1060-02 hollow core photonic bandgap fiber for 1060 nm range applications*. Datasheet. http://www.nktphotonics.com/ (2011). (Cit. on p. 15)

[Des94] E. Desurvire. *Erbium-doped fiber amplifiers*. John Wiley & Sons (1994). (Cit. on p. 8)

[Die06] J.-C. Diels and W. Rudolph. *Ultrashort laser pulse phenomena*. Academic Press (2006). (Cit. on pp. 14, 62, 64)

[Die83] W. Dietel, J. J. Fontaine, and J.-C. Diels. *Intracavity pulse compression with glass: a new method of generating pulses shorter than 60 fsec*. Opt. Lett. **8**, pp. 4–6 (1983). (Cit. on p. 14)

[Dom99] V. Dominic, S. MacCormack, R. Waarts, S. Sanders, S. Bicknese, R. Dohle, E. Wolak, P. Yeh, and E. Zucker. *110 W fibre laser*. Electron. Lett. **35**, pp. 1158–1160 (1999). (Cit. on p. 43)

[Dru08] F. Druon, M. Hanna, G. Lucas-Leclin, Y. Zaouter, D. Papadopoulos, and P. Georges. *Simple and general method to calculate the dispersion properties of complex and aberrated stretchers-compressors*. J. Opt. Soc. Am. B **25**, pp. 754–762 (2008). (Cit. on p. 19)

[Dur08] C. G. Durfee, J. A. Squier, and S. Kane. *A modular approach to the analytic calculation of spectral phase for grisms and other refractive/diffractive structures*. Opt. Express **16**, pp. 18004–18016 (2008). (Cit. on p. 17)

[Eva49a] J. W. Evans. *The birefringent filter*. J. Opt. Soc. Am. **39**, pp. 229–237 (1949). (Cit. on p. 31)

[Eva49b] J. W. Evans. *The birefringent filter; a correction*. J. Opt. Soc. Am. **39**, p. 412 (1949). (Cit. on p. 31)

[Fek09] J. Fekete, A. Cserteg, and R. Szipocs. *All-fiber, all-normal dispersion ytterbium ring oscillator*. Laser Phys. Lett. **6**, pp. 49–53 (2009). (Cit. on p. 49)

[Fer00] M. E. Fermann, V. I. Kruglov, B. C. Thomsen, J. M. Dudley, and J. D. Harvey. *Self-similar propagation and amplification of parabolic pulses in optical fibers*. Phys. Rev. Lett. **84**, pp. 6010–6013 (2000). (Cit. on p. 11)

[Fer01] M. Fermann, M. Stock, A. Galvanauskas, G. Cho, and B. Thomsen. *Third-order dispersion control in ultrafast Yb fiber amplifiers*. Advanced Solid-State Lasers, Optical Society of America, TuA3 (2001). (Cit. on p. 59)

[Fer09] A. Fernández, L. Zhu, A. J. Verhoef, D. Sidorov-Biryukov, A. Pugžlys, A. Baltuška, K.-H. Liao, C.-H. Liu, A. Galvanauskas, S. Kane, R. Holzwarth, and F. Ö. Ilday. *Broadly tunable carrier envelope phase stable optical parametric amplifier pumped by a monolithic ytterbium fiber amplifier*. Opt. Lett. **34**, pp. 2799–2801 (2009). (Cit. on p. 59)

[Fon07] K. H. Fong, K. Kikuchi, and S. Y. Set. *High-energy ultrashort pulse generation from a fundamentally mode-locked fiber laser at 1.7 MHz*. Optical Fiber Communication Conference and Exposition and The National Fiber Optic Engineers Conference, Optical Society of America, OTuF2 (2007). (Cit. on p. 23)

[For84] R. L. Fork, O. E. Martinez, and J. P. Gordon. *Negative dispersion using pairs of prisms*. Opt. Lett. **9**, pp. 150–152 (1984). (Cit. on p. 14)

[For87] R. L. Fork, C. H. B. Cruz, P. C. Becker, and C. V. Shank. *Compression of optical pulses to six femtoseconds by using cubic phase compensation*. Opt. Lett. **12**, pp. 483–485 (1987). (Cit. on p. 17)

[Gau04] D. M. Gaudiosi, A. L. Lytle, P. Kohl, M. M. Murnane, H. C. Kapteyn, and S. Backus. *11-W average power Ti:sapphire amplifier system using downchirped pulse amplification*. Opt. Lett. **29**, pp. 2665–2667 (2004). (Cit. on p. 14)

[Gau06] D. M. Gaudiosi, E. Gagnon, A. L. Lytle, J. L. Fiore, E. A. Gibson, S. Kane, J. Squier, M. M. Murnane, H. C. Kapteyn, R. Jimenez, and S. Backus. *Multi-kilohertz repetition rate Ti:sapphire amplifier based on down-chirped pulse amplification*. Opt. Express **14**, pp. 9277–9283 (2006). (Cit. on p. 14)

[Gho99] G. Ghosh. *Dispersion-equation coefficients for the refractive index and birefringence of calcite and quartz crystals*. Opt. Comm. **163**, pp. 95–102 (1999). (Cit. on p. 32)

[Gib06] E. A. Gibson, D. M. Gaudiosi, H. C. Kapteyn, R. Jimenez, S. Kane, R. Huff, C. Durfee, and J. Squier. *Efficient reflection grisms for pulse compression and dispersion compensation of femtosecond pulses*. Opt. Lett. **31**, pp. 3363–3365 (2006). (Cit. on p. 17)

[Glo71] D. Gloge. *Weakly guiding fibers*. Appl. Opt. **10**, pp. 2252–2258 (1971). (Cit. on p. 7)

[Grü00] L. Grüner-Nielsen, S. N. Knudsen, B. Edvold, T. Veng, D. Magnussen, C. C. Larsen, and H. Damsgaard. *Dispersion compensating fibers*. Optical Fiber Technology **6**, pp. 164–180 (2000). (Cit. on pp. 14, 20)

[Grü05] L. Grüner-Nielsen, M. Wandel, P. Kristensen, C. Jorgensen, L. V. Jorgensen, B. Edvold, B. Pálsdóttir, and D. Jakobsen. *Dispersion-compensating fibers*. J. Lightwave Technol. **23**, pp. 3566–3579 (2005). (Cit. on p. 20)

[Grü10] L. Grüner-Nielsen, D. Jakobsen, K. G. Jespersen, and B. Pálsdóttir. *A stretcher fiber for use in fs chirped pulse Yb amplifiers*. Opt. Express **18**, pp. 3768–3773 (2010). (Cit. on pp. 14, 21, 60, 61, 83)

[Han05] P. Hannaford. *Femtosecond Laser Spectroscopy*. Springer (2005). (Cit. on p. 1)

[Hap10] C. Hapke. *Untersuchung von Ytterbium-dotierten Ultrakurzpulsfaserlasern ohne Dispersionskompensation mit niedriger Repetitionsrate*. Diploma thesis. Leibniz Universität Hannover (2010). (Cit. on p. 31)

[Hau00] H. Haus. *Mode-locking of lasers*. IEEE Journ. of Sel. Topics in Quantum Electron. **7**, pp. 1173–85 (2000). (Cit. on p. 9)

[Hau95] H. A. Haus, K. Tamura, L. E. Nelson, and E. P. Ippen. *Stretched-pulse additive pulse mode-locking in fiber ring lasers: theory and experiment*. IEEE Journ. of Quantum Electron. **31**, pp. 591–598 (1995). (Cit. on p. 10)

[Hua11] J. J. Huang, L. Y. Zhang, and Y. Q. Yang. *Reinvestigation on the frequency dispersion of a grating-pair compressor*. Opt. Express **19**, pp. 814–819 (2011). (Cit. on p. 18)

[Ild04a] F. Ö. Ilday. *Theory and practice of high-energy femtosecond fiber lasers*. PhD thesis. Cornell University (2004). (Cit. on p. 36)

[Ild04b] F. Ö. Ilday, J. R. Buckley, W. G. Clark, and F. W. Wise. *Self-similar evolution of parabolic pulses in a laser*. Phys. Rev. Lett. **92**, pp. 213902–213905 (2004). (Cit. on p. 11)

[Ime04] G. Imeshev, I. Hartl, and M. E. Fermann. *Chirped pulse amplification with a nonlinearly chirped fiber Bragg grating matched to the Treacy compressor*. Opt. Lett. **29**, pp. 679–681 (2004). (Cit. on pp. 14, 17)

[Jia02] J. Jiang, Z. Zhang, and T. Hasama. *Evaluation of chirped-pulse-amplification systems with Offner triplet telescope stretchers*. J. Opt. Soc. Am. B **19**, pp. 678–683 (2002). (Cit. on p. 14)

[Kal10] H. Kalaycioglu, B. Oktem, Ç. Şenel, P. P. Paltani, and F. Ilday. *Microjoule-energy, 1 MHz repetition rate pulses from all-fiber-integrated nonlinear chirped-pulse amplifier*. Opt. Lett. **35**, pp. 959–961 (2010). (Cit. on p. 60)

[Kan94] S. Kane, J. Squier, J. V. Rudd, and G. Mourou. *Hybrid grating-prism stretcher-compressor system with cubic phase and wavelength tunability and decreased alignment sensitivity*. Opt. Lett. **19**, pp. 1876–1878 (1994). (Cit. on pp. 17, 59)

[Kan95] S. Kane and J. Squier. *Grating compensation of third-order material dispersion in the normal dispersion regime: Sub-100-fs chirped-pulse amplification using a fiber stretcher and grating-pair compressor*. IEEE Journ. of Quantum Electron. **31**, pp. 2052–2057 (1995). (Cit. on pp. 17, 59)

[Kan97] S. Kane and J. Squier. *Grism-pair stretcher–compressor system for simultaneous second- and third-order dispersion compensation in chirped-pulse amplification*. J. Opt. Soc. Am. B **14**, pp. 661–665 (1997). (Cit. on pp. 17, 25)

[Kie08] K. Kieu and F. W. Wise. *All-fiber normal-dispersion femtosecond laser*. Opt. Express **16**, pp. 11453–11458 (2008). (Cit. on p. 49)

[Kie09] K. Kieu, W. H. Renninger, A. Chong, and F. W. Wise. *Sub-100 fs pulses at watt-level powers from a dissipative-soliton fiber laser*. Opt. Lett. **34**, pp. 593–595 (2009). (Cit. on p. 43)

[Kob08] S. Kobtsev, S. Kukarin, and Y. Fedotov. *Ultra-low repetition rate mode-locked fiber laser with high-energy pulses*. Opt. Express **16**, pp. 21936–21941 (2008). (Cit. on p. 23)

[Kob92] S. M. Kobtsev and N. A. Sventsitskaya. *Application of birefringent filters in continuous-wave tunable lasers: a review*. Opt. Spectrosc. **73**, pp. 114–123 (1992). (Cit. on p. 32)

[Kop00] J. P. Koplow, D. A. V. Kliner, and L. Goldberg. *Single-mode operation of a coiled multimode fiber amplifier*. Opt. Lett. **25**, pp. 442–444 (2000). (Cit. on p. 6)

[Kuz07] L. Kuznetsova and F. W. Wise. *Scaling of femtosecond Yb-doped fiber amplifiers to tens of microjoule pulse energy via nonlinear chirped pulse amplification*. Opt. Lett. **32**, pp. 2671–2673 (2007). (Cit. on p. 60)

[Lai94] M. Lai, S. T. Lai, and C. Swinger. *Single-grating laser pulse stretcher and compressor*. Appl. Opt. **33**, pp. 6985–6987 (1994). (Cit. on p. 19)

[Lam80] G. L. Lamb, Jr. *Elements of soliton theory*. John Wiley and Sons, New York (1980). (Cit. on p. 10)

[Li11] L. Li, M. Hong, M. Schmidt, M. Zhong, A. Malshe, B. Huis in 't Veld, and V. Kovalenko. *Laser nano-manufacturing - State of the art and challenges*. CIRP Annals - Manufacturing Technology **60**, pp. 735–755 (2011). (Cit. on p. 1)

[Li90] G. Li and Y. Li. *Tuning sensitivity of dye laser birefringent filters*. Appl. Opt. **29**, pp. 3462–3463 (1990). (Cit. on p. 31)

[Lia07] K.-H. Liao, M.-Y. Cheng, E. Flecher, V. I. Smirnov, L. B. Glebov, and A. Galvanauskas. *Large-aperture chirped volume Bragg grating based fiber CPA system*. Opt. Express **15**, pp. 4876–4882 (2007). (Cit. on p. 14)

[Lim03] H. Lim, F. Ö. Ilday, and F. W. Wise. *Generation of 2-nJ pulses from a femtosecond ytterbium fiber laser*. Opt. Lett. **28**, pp. 660–662 (2003). (Cit. on p. 11)

[Mar77] D. Marcuse. *Loss analysis of single-mode fiber splices*. Bell Syst. Tech. J. **56**, pp. 703–718 (1977). (Cit. on p. 7)

[Mar87] O. E. Martinez. *3000 times grating compressor with positive group velocity dispersion: application to fiber compensation in 1.3 - 1.6 μm region*. IEEE Journ. of Quantum Electron. **23**, pp. 59–64 (1987). (Cit. on pp. 14, 59)

[Mar88] O. E. Martinez. *Matrix formalism for pulse compressors*. IEEE Journ. of Quantum Electron. **12**, pp. 2530 –2536 (1988). (Cit. on p. 19)

[Mit05] F. Mitschke. *Glasfasern*. Elsevier (2005). (Cit. on pp. 5, 7)

[Mit87] F. Mitschke and L. Mollenauer. *Ultrashort pulses from the soliton laser*. Opt. Lett. **12**, pp. 407–9 (1987). (Cit. on p. 10)

[Mol84] L. F. Mollenauer and R. H. Stolen. *The soliton laser*. Opt. Lett. **9**, pp. 13–15 (1984). (Cit. on p. 10)

[Mor10] D. Mortag, C. Hapke, D. Wandt, U. Morgner, D. Kracht, and J. Neumann. *Low repetition rate high-energy fiber oscillator*. Conference on Lasers and Electro-Optics, Optical Society of America, JTuD37 (2010). (Cit. on p. 31)

[Mor11] D. Mortag, D. Wandt, U. Morgner, D. Kracht, and J. Neumann. *Sub-80-fs pulses from an all-fiber-integrated dissipative-soliton laser at 1 μm*. Opt. Express **19**, pp. 546–551 (2011). (Cit. on p. 50)

[Mor12] D. Mortag, T. Theeg, K. Hausmann, L. Grüner-Nielsen, K. G. Jespersen, U. Morgner, D. Wandt, D. Kracht, and J. Neumann. *Sub-200 fs microjoule pulses from a monolithic linear fiber CPA system*. Opt. Comm. **285**, pp. 706–709 (2012). (Cit. on pp. 49, 60)

[Muk09] P. K. Mukhopadhyay, K. Özgören, I. L. Budunoglu, and F. Ö. Ilday. *All-fiber low-noise high-power femtosecond Yb-fiber amplifier system seeded by an all-normal dispersion fiber oscillator*. IEEE J. Sel. Top. Quantum Electron. **15**, pp. 145–152 (2009). (Cit. on p. 60)

[Nel96] L. E. Nelson, S. B. Fleischer, G. Lenz, and E. P. Ippen. *Efficient frequency doubling of a femtosecond fiber laser*. Opt. Lett. **21**, pp. 1759–1761 (1996). (Cit. on p. 11)

[Nie07] C. K. Nielsen and S. R. Keiding. *All-fiber mode-locked fiber laser*. Opt. Lett. **32**, pp. 1474–1476 (2007). (Cit. on p. 49)

[Nij98] J. H. B. Nijhof, W. Forysiak, and N. J. Doran. *Dispersion-managed solitons in the normal dispersion regime: a physical interpretation*. Opt. Lett. **23**, pp. 1674–1676 (1998). (Cit. on p. 10)

[Nuf06] Nufern. *980/1060 nm select cutoff single-mode fiber 1060-XP*. Datasheet. http://www.nufern.com/ (2006). (Cit. on pp. 5, 7, 14)

[Oue87] F. Ouellette. *Dispersion cancellation using linearly chirped Bragg grating filters in optical waveguides*. Opt. Lett. **12**, pp. 847–849 (1987). (Cit. on pp. 14, 16)

[Özg10] K. Özgören and F. Ö. Ilday. *All-fiber all-normal dispersion laser with a fiber-based Lyot filter*. Opt. Lett. **35**, pp. 1296–1298 (2010). (Cit. on p. 49)

[Pal05] C. Palmer. *Diffraction grating handbook*. Newport Corporation (2005). (Cit. on p. 18)

[Pap03] D. N. Papadopoulos, S. Forget, M. Delaigue, F. Druon, F. Balembois, and P. Georges. *Passively mode-locked diode-pumped Nd:YVO$_4$ oscillator operating at an ultralow repetition rate*. Opt. Lett. **28**, pp. 1838–1840 (2003). (Cit. on p. 23)

[Pap09] D. N. Papadopoulos, F. Druon, J. Boudeile, I. Martial, M. Hanna, P. Georges, P. O. Petit, P. Goldner, and B. Viana. *Low-repetition-rate femtosecond operation in extended-cavity mode-locked Yb:CALGO laser*. Opt. Lett. **34**, pp. 196–198 (2009). (Cit. on p. 23)

[Pas95] H. Pask, R. Carman, D. C. Hanna, A. Tropper, C. Mackechnie, P. Barber, and J. Dawes. *Ytterbium-doped silica fiber lasers: versatile sources for the 1-1.2 μm region*. IEEE Journ. of Quantum Electron. **1**, pp. 2–13 (1995). (Cit. on p. 9)

[Pes87] M. Pessot, P. Maine, and G. Mourou. *1000 times expansion/compression of optical pulses for chirped pulse amplification*. Opt. Commun. **62**, pp. 419–421 (1987). (Cit. on pp. 14, 59)

[Pes89] M. Pessot, J. Squier, G. Mourou, and D. J. Harter. *Chirped-pulse amplification of 100-fsec pulses*. Opt. Lett. **14**, pp. 797–799 (1989). (Cit. on p. 17)

[Pla10] K. Plamann, F. Aptel, C. L. Arnold, A. Courjaud, C. Crotti, F. Deloison, F. Druon, P. Georges, M. Hanna, J.-M. Legeais, F. Morin, E. Mottay, V. Nuzzo, D. A. Peyrot, and M. Savoldelli. *Ultrashort pulse laser surgery of the cornea and the sclera*. J. Opt. **12**, 084002 (30pp) (2010). (Cit. on p. 1)

[Pro07] O. Prochnow, A. Ruehl, M. Schultz, D. Wandt, and D. Kracht. *All-fiber similariton laser at 1 μm without dispersion compensation*. Opt. Express **15**, pp. 6889–6893 (2007). (Cit. on p. 49)

[Ram06] S. Ramachandran, S. Ghalmi, J. W. Nicholson, M. F. Yan, P. Wisk, E. Monberg, and F. V. Dimarcello. *Anomalous dispersion in a solid, silica-based fiber*. Opt. Lett. **31**, pp. 2532–2534 (2006). (Cit. on p. 14)

[Ren08] W. H. Renninger, A. Chong, and F. W. Wise. *Giant-chirp oscillators for short-pulse fiber amplifiers*. Opt. Lett. **33**, pp. 3025–3027 (2008). (Cit. on pp. 23, 31)

[Ric10] D. J. Richardson, J. Nilsson, and W. A. Clarkson. *High power fiber lasers: current status and future perspectives [Invited]*. J. Opt. Soc. Am. B **27**, B63–B92 (2010). (Cit. on p. 2)

[Rip95] D. J. Ripin and L. Goldberg. *High efficiency side-coupling of light into optical fibres using imbedded v-grooves*. Electron. Lett. **31**, pp. 2204–2205 (1995). (Cit. on p. 43)

[Rob05] P. Roberts, F. Couny, H. Sabert, B. Mangan, D. Williams, L. Farr, M. Mason, A. Tomlinson, T. Birks, J. Knight, and P. S. J. Russell. *Ultimate low loss of hollow-core photonic crystal fibres*. Opt. Express **13**, pp. 236–244 (2005). (Cit. on p. 15)

[Rot89] J. E. Rothenberg and D. Grischkowsky. *Observation of the formation of an optical intensity shock and wave breaking in the nonlinear propagation of pulses in optical fibers*. Phys. Rev. Lett. **62**, pp. 531–534 (1989). (Cit. on p. 11)

[Rue10] A. Ruehl, A. Marcinkevicius, M. E. Fermann, and I. Hartl. *80 W, 120 fs Yb-fiber frequency comb*. Opt. Lett. **35**, pp. 3015–3017 (2010). (Cit. on p. 59)

[Say09] H. Sayinç, D. Mortag, D. Wandt, J. Neumann, and D. Kracht. *Sub-100 fs pulses from a low repetition rate Yb-doped fiber laser*. Opt. Express **17**, pp. 5731–5735 (2009). (Cit. on pp. 11, 24)

[Sch07] Schott AG. *Optical glass catalogue*. http://www.schott.com/ (2007). (Cit. on p. 7)

[Sch08] M. Schultz, H. Karow, O. Prochnow, D. Wandt, U. Morgner, and D. Kracht. *All-fiber ytterbium femtosecond laser without dispersion compensation*. Opt. Express **16**, pp. 19562–19567 (2008). (Cit. on p. 49)

[Sho10] F. Shohda, Y. Hori, M. Nakazawa, J. Mata, and J. Tsukamoto. *131 fs, 33 MHz all-fiber soliton laser at 1.07 μm with a film-type SWNT saturable absorber coated on polyimide*. Opt. Express **18**, pp. 11223–11229 (2010). (Cit. on p. 49)

[Smi03] C. M. Smith, N. Venkataraman, M. T. Gallagher, D. Müller, J. A. West, N. F. Borrelli, D. C. Allan, and K. W. Koch. *Low-loss hollow-core silica/air photonic bandgap fibre*. Nature **424**, pp. 657–659 (2003). (Cit. on p. 15)

[Smi70] P. W. Smith. *Mode-locking of lasers*. Proceedings of the IEEE **58**, pp. 1342–1356 (1970). (Cit. on p. 9)

[Sni88] E. Snitzer, H. Po, F. Hakimi, R. Tumminelli, and B. C. McCollum. *Double clad, offset core Nd fiber laser*. Optical Fiber Sensors, Optical Society of America, PD5 (1988). (Cit. on p. 43)

[Squ98] J. Squier, C. P. J. Barty, F. Salin, C. L. Blanc, and S. Kane. *Use of mismatched grating pairs in chirped-pulse amplification systems*. Appl. Opt. **37**, pp. 1638–1641 (1998). (Cit. on p. 14)

[Str85] D. Strickland and G. Mourou. *Compression of amplified chirped optical pulses*. Opt. Commun. **55**, pp. 447 –449 (1985). (Cit. on pp. 13, 59)

[Sug02] A. Sugar. *Ultrafast (femtosecond) laser refractive surgery*. Curr. Opin. in Ophtalmol. **13**, pp. 246–249 (2002). (Cit. on p. 1)

[Tom85] W. J. Tomlinson, R. H. Stolen, and A. M. Johnson. *Optical wave breaking of pulses in nonlinear optical fibers*. Opt. Lett. **10**, pp. 457–459 (1985). (Cit. on p. 11)

[Tou93] P. Tournois. *New diffraction grating pair with very linear dispersion for laser pulse compression*. Electron. Lett. **29**, pp. 1414 –1415 (1993). (Cit. on p. 17)

[Tre69] E. Treacy. *Optical pulse compression with diffraction gratings*. IEEE Journ. of Quantum Electron. **5**, pp. 454 –458 (1969). (Cit. on pp. 14, 18, 59)

[Ude99] T. Udem, J. Reichert, R. Holzwarth, and T. Hänsch. *Absolute optical frequency measurement of the cesium D1 line with a mode-locked laser*. Phys. Rev. Lett. **82**, pp. 3568–71 (1999). (Cit. on p. 1)

[Wis08] F. Wise, A. Chong, and W. Renninger. *High-energy femtosecond fiber lasers based on pulse propagation at normal dispersion*. Laser & Photonics Reviews **2**, pp. 58–73 (2008). (Cit. on pp. 11, 12, 49)

[Zao07] Y. Zaouter, D. N. Papadopoulos, M. Hanna, F. Druon, E. Cormier, and P. Georges. *Third-order spectral phase compensation in parabolic pulse compression*. Opt. Express **15**, pp. 9372–9377 (2007). (Cit. on pp. 17, 25)

[Zao08] Y. Zaouter, J. Boullet, E. Mottay, and E. Cormier. *Transform-limited 100 μJ, 340 MW pulses from a nonlinear-fiber chirped-pulse amplifier using a mismatched grating stretcher-compressor*. Opt. Lett. **33**, pp. 1527–1529 (2008). (Cit. on p. 60)

[Zho06] S. Zhou, D. G. Ouzounov, C. Sinclair, and F. W. Wise. *Generation of 400-fs solitons with 2-MHz repetition rate by a Yb-fiber laser*. 19th Annual Meeting of the IEEE, Lasers and Electro-Optics Society (LEOS), pp. 209–2010 (2006). (Cit. on p. 23)

[Zho08] X. Zhou, D. Yoshitomi, Y. Kobayashi, and K. Torizuka. *Generation of 28-fs pulses from a mode-locked ytterbium fiber oscillator*. Opt. Express **16**, pp. 7055–7059 (2008). (Cit. on p. 23)

[Zhu90] S. Zhu. *Birefringent filter with tilted optic axis for tuning dye lasers: theory and design*. Appl. Opt. **29**, pp. 410–415 (1990). (Cit. on p. 31)

List of publications

Conference contributions

1. D. Mortag, H. Sayinç, D. Wandt, U. Morgner, D. Kracht, and J. Neumann. *93 fs pulses from a low repetition rate fiber laser.* CLEO/Europe and EQEC 2009 Conference Digest (Optical Society of America, 2009), CF2.3 (2009).

2. H. Sayinç, D. Mortag, O. Prochnow, M. Schultz, D. Wandt, and D. Kracht. *Pulsenergie Skalierung in gänzlich normal dispersiven Faserlasern durch Reduktion der Repetitionsrate.* DPG Spring Meeting 2010, Q 19.3 (2010).

3. C. Hapke, D. Mortag, D. Wandt, U. Morgner, D. Kracht, and J. Neumann. *Passiv modengekoppelter Ytterbium-Faser-Oszillator mit hoher Pulsenergie bei einer Repetitionsrate von 2 MHz.* DPG Spring Meeting 2010, Q 19.6 (2010).

4. D. Mortag, D. Wandt, U. Morgner, D. Kracht, and J. Neumann. *Ytterbium-dotierter Femtosekunden-Faser-Oszillator mit einer mittleren Ausgangsleistung von 1,5 W.* DPG Spring Meeting 2010, Q 19.7 (2010).

5. D. Mortag, C. Hapke, D. Wandt, U. Morgner, D. Kracht, and J. Neumann. *Low repetition rate high-energy fiber oscillator.* Conference on Lasers and Electro-Optics OSA Technical Digest (CD) (Optical Society of America, 2010), JTuD37 (2010).

6. D. Mortag, D. Wandt, U. Morgner, D. Kracht, and J. Neumann. *All-fiber ytterbium femtosecond dissipative-soliton laser.* 4th EPS-QEOD Europhoton Conference 2010 Digest (CD), paper ThC5 (2010).

7. D. Mortag, T. Theeg, K. Hausmann, L. Grüner-Nielsen, K. G. Jespersen, D. Wandt, U. Morgner, D. Kracht, and J. Neumann. *Sub-200-fs microjoule pulses from an all-fiber CPA system.* CLEO/Europe and EQEC 2011 Conference Digest (Optical Society of America, 2011), CJ4.1 (2011).

8. D. Mortag, T. Theeg, K. Hausmann, L. Grüner-Nielsen, K. G. Jespersen, D. Wandt, U. Morgner, D. Kracht, and J. Neumann. *Generation of sub-200-fs microjoule pulses from an all-fiber CPA system.* OSA Topical Meeting on Specialty Optical Fibers (SOF) 2011 Conference Digest (Optical Society of America, 2011), SOWA2 (2011).

Reviewed journal articles

1. H. Sayinç, D. Mortag, D. Wandt, J. Neumann, and D. Kracht. *Sub-100 fs pulses from a low repetition rate Yb-doped fiber laser.* Opt. Express **17**, pp. 5731-5735 (2009).

2. D. Mortag, D. Wandt, U. Morgner, D. Kracht, and J. Neumann. *Sub-80-fs pulses from an all-fiber-integrated dissipative-soliton laser at 1 µm.* Opt. Express **19**, pp. 546-551 (2011).

3. D. Mortag, T. Theeg, K. Hausmann, L. Grüner-Nielsen, K. G. Jespersen, U. Morgner, D. Wandt, D. Kracht, and J. Neumann. *Sub-200 fs microjoule pulses from a monolithic linear fiber CPA system.* Opt. Comm. **285**, pp. 706-709 (2012).

Other publications

1. D. Mortag. *Aufbau und Untersuchung eines Ultrakurzpuls-Faserverstärkers. Diploma thesis.* Prof. René Beigang, Ultrafast Photonics and THz Physics Group, Physics Department, University of Kaiserslautern, Germany (2007).

Curriculum vitae

Personal data

Name	Dirk Mortag
Date of birth	17 August 1980
Place of birth	Celle, Germany
Nationality	German

School education

08/1987 - 07/1991	Grundschule Blumlage, Celle
08/1991 - 06/1993	Orientierungsstufe Schulzentrum Burgstraße, Celle
08/1993 - 06/2000	Gymnasium Ernestinum, Celle
06/2000	Allgemeine Hochschulreife

Community service

09/2000 - 07/2001	Sonderpädagogischer Kindergarten "Spunk", Celle (GiB Hannover)

University education

10/2000 - 09/2001	Distance physics studies "Früheinstieg in das Physikstudium (FiPS)", University of Kaiserslautern, Germany
10/2001 - 06/2007	Physics studies, University of Kaiserslautern, Germany
07/2004 - 12/2004	Physics and mathematics studies, University of Sydney, Australia
06/2007	Diploma degree in physics (Diplom-Physiker), University of Kaiserslautern, Germany. Thesis title: "Aufbau und Untersuchung eines Ultrakurzpuls-Faserverstärkers"

Professional affiliations

02/2006 - 03/2007	Research assistant, Fraunhofer-Institut für Physikalische Messtechnik IPM, Ultrafast Photonics and THz Physics Group, Außenstelle Kaiserslautern, Germany
08/2007 - 01/2012	Research scientist / Ph.D. student, Laser Zentrum Hannover e.V., Laser Development Department, Ultrafast Photonics Group, Germany
03/2012 - 07/2012	Research scientist, Laser Zentrum Hannover e.V., Laser Development Department, Ultrafast Photonics Group, Germany
08/2012 - present	Research scientist, ROFIN-SINAR Laser GmbH, Germany

Acknowledgment

First of all, I would like to thank everybody who directly or indirectly contributed and helped to make this work possible even though not everybody is mentioned explicitly.

I would like to thank Prof. Dr. Uwe Morgner for supervising and supporting my work. I would also like to thank Prof. Dr. Detlev Ristau and Prof. Dr. Thomas Hauf for serving as committee members.

I would like to thank the former and the actual head of the Laser Development Department Dr. Dietmar Kracht and Dr. Jörg Neumann for the possibility to work on this topic as well as the head of the ultrafast photonics group Dr. Dieter Wandt for helpful discussions.

I would like to thank Dr. Lars Grüner-Nielsen and Dr. Kim Giessmann Jespersen from OFS Denmark for providing several spools of the stretcher fiber with anomalous third-order dispersion.

I am very thankful to Hakan Sayinç and Christian Hapke for their help on the stretched-pulse and dissipative-soliton low-repetition rate laser, respectively, as well as Thomas Theeg and Katharina Hausmann for providing specialty fiber couplers. I am also grateful to Dr. Peter Weßels and Udo Bünting for their help concerning the grism compressor. I also like to thank Marc Priehs for several technical drawings. I would like to thank the Optical Coatings Group and especially Dr. Stefan Günster for providing specialty coatings on gratings, prisms, and mirrors.

I thank all members of the Laser Development Department for the great cooperativeness and the good working environment. For proofreading I would like to thank Dr. Jörg Neumann and Dr. Dieter Wandt.

Last but not least I would like to thank my parents and my family for giving me great support during my studies.